SYNTHETIC ROUTES TO NEW CORE/SHELL NANOGELS:

DESIGN AND APPLICATIONS IN BIOMATERIALS

A Dissertation
Presented to
The Academic Faculty

by

Neetu Singh

In Partial Fulfillment
of the Requirements for the Degree
Doctor of Philosophy in the
School of Chemistry and Biochemistry
& Petit Institute of Bioengineering and Bioscience

Georgia Institute of Technology
April 2008

SYNTHETIC ROUTES TO NEW CORE/SHELL NANOGELS:

DESIGN AND APPLICATIONS IN BIOMATERIALS

Approved by:

Dr. L. Andrew Lyon, Advisor
School of Chemistry and Biochemistry &
Petit Institute of Bioengineering and
Bioscience
Georgia Institute of Technology

Dr. Laren Tolbert
School of Chemistry and Biochemistry
Georgia Institute of Technology

Dr. Seth Marder
School of School of Chemistry and
Biochemistry
Georgia Institute of Technology

Dr. Marcus Weck
School of School of Chemistry and
Biochemistry
Georgia Institute of Technology

Dr. Niren Murthy
Wallace H. Coulter Department of
Biomedical Engineering
Georgia Institute of Technology

Date Approved: March 06, 2008

Dedicated to Mummy, Papa, and Montu

ACKNOWLEDGEMENTS

I wish to begin by thanking my advisor Prof. Andrew Lyon, without whose vision and guidance this dissertation would not have been possible. His passion for research, his ideas and his mentorship will continue to inspire me for years. I also want to thank him for supporting me through the ebb and flow of my life during the last four years of my stay here at Georgia Tech. He has given me independence to think and to carry out research in many diverse areas, which I believe has made me a mature researcher and person. Everything I have learned about being a scientist I owe to him.

I wish to thank all Lyon research group members former and present especially, Mike Serpe, Stella, Satish, Christine, Jongseong, Daisuke, Jon, Bart, Ashlee, Toni, Grant, Courtney, Zhiyong and the newest member Mike, who not only made the work place lively but also taught me valuable techniques, provided critique, and helped me see beyond my own projects. The high quality of work my peers produced was a constant source of inspiration. They have not only been great colleagues but also wonderful friends. I also want to thank all the undergraduates who worked with me.

I wish to thank my collaborators Amanda Bridges and Prof. Andres Garcia whose expertise and willingness to share thoughts has been instrumental in the success of my projects.

I wish to express my gratitude to my family, my father, mother, and brother for inspiring me, encouraging me to explore, and for their unconditional support and love. I am grateful to my parents for letting me pursue my dreams against all odds. Even being far away they were always morally, mentally and spiritually with me, supporting and

encouraging every step of this long trip. I would not be where I am, were it not for their constant encouragement.

This section will not be complete without acknowledging the love and support of my friends here in Atlanta, especially Prashant, Mita, Sameer, and Annie who always believed in me and encouraged me to do better than I thought was possible and provided me with a family away from home. I would like to acknowledge Prashant for long scientific discussions and his help with suggestions for my research and also for reading my manuscripts.

Last but not the least, I would like to acknowledge my husband Ravi and his family. Ravi helped me remain motivated, focused and determined in the pursuit of my goals.

TABLE OF CONTENTS

LIST OF TABLES

LIST OF FIGURES

LIST OF SCHEMES

LIST OF SYMBOLS AND ABBREVIATIONS

SFEP	Surfactant Free Emulsion Polymerization
RAFT	Reversible Addition-Fragmentation Chain Transfer
ATRP	Atom Transfer Radical Polymerization
THF	Tetrahydrofuran
DSC	Differential Scanning Calorimeter
NIPAm	*N*-isopropylacrylamide
NIPMAm	*N*-isopropylmethacrylamide
HEMA	2-hydroxyethyl methacrlate
BIS	*N,N'*-Methylene(bisacrylamide)
TBA	*N-tert*-butylacrylamide
AAc	Acrylic Acid
pNIPAm	Poly(*N*-isopropylacrylamide)
VPT	Volume Phase Transition
LCST	Lower Critical Solution Temperature
pNIPAm-co-AAc	Poly(*N*-isopropylacrylamide-*co*-acrylic acid)
VPTT	Volume Phase Transition Temperature
SDS	Sodium Dodecyl Sulfate
DMF	Dimethylformamide
KPS	Potassium Persulfate
APS	Ammonium Persulfate
RI	Refractive Index

PCS	Photon Correlation Spectroscopy
CPS	Counts Per Second
HCl	Hydrochloric Acid
NMR	Nuclear Magnetic Resonance
D_2O	Deuterium Oxide
APTMS	3-Aminopropyltrimethoxysilane
AFA	4-Aminofluorescein Acrylamide
DIC	Differential Image Contrast
PEG	Poly(ethylene glycol)
PEO	Poly(Ethylene Oxide)
Au	Gold
AFM	Atomic force microscopy
°C	Degrees Celsius
IR	Infrared spectroscopy
MALLS	Multi-angle Laser Light Scattering
mM	Milli-molar
R_g	Radius of Gyration
R_h	Hydrodynamic Radius
T	Temperature
TEM	Transmission Electron Microscopy
UV	Ultraviolet Spectroscopy
VIS	Visible Spectroscopy
CMC	Critical Micelle Concentration
DHEA	*N,N'*-(1,2-Dihydroxyethylene)-bisacrylamide

DLS	Dynamic Light Scattering
MWCO	Molecular Weight Cut Off
NaIO$_4$	Sodium Periodate
EDC	1-ethyl-3-(3-dimethylaminopropyl)carbodiimide
DMSO	Dimethyl Sulfoxide
DCC	*N,N'*-dicyclohexylcarbodiimide
BP	Benzophenone
ABP	4-Aminobenzophenone
PBS	Phosphate Buffered Saline
HRP-Avidin	Avidin-Horseradish Peroxidase Conjugate
HABA	2-(4'-hydroxyazobenzene) Benzoic Acid
FITC-BSA	Fluorescein Isothiocyanate labeled Bovine Serum Albumin
XPS	X-ray Photoelectron Spectroscopy
Fmoc	Fluorenyl-methoxy-carbonyl
TAMRA-SE	5-carboxytetramethyl Rhodamine Succinimydyl Eester
APMA	*N*-(3-aminopropyl)methacrylamide
NHS	N-Hydroxysuccinimide
AFFF	Asymmetric Field Flow Fractionation
MES	2-(*N*-morpholino)ethanesulfonic acid
PET	poly(ethylene terephthalate)
OD	Optical Density
EG$_3$	Tri(ethylene glycol)
SAM	Self Assembeled Monolayer
TCPS	Tissue Culture Polystyrene
IP	Intraperitoneal

ECM	Extracellular Matrix
MCP-1	Monocyte Chemotactic Protein-1
TNF-α	Tumor Necrosis Factor- α
IL-1β	Interleukine-1β

SUMMARY

Nanomaterials are showing great potential in the fields of biomedicine and biology not only due to their unique size-dependent properties but also since their size is on a similar scale as that of proteins and other biomolecules. A very interesting class of nanoparticles extensively used for bio-applications is that of hydrogel particles, also called nanogels. There is an increasing interest in the design of hydrogel nanoparticles that have biofunctionality for applications in cell targeting, drug delivery, and biomedicine. In order to interact with a biological target, the nanoparticles have to be furnished with a biological or molecular coating, which acts as an active biointerface. It is desirable to chemically modify the nanoparticles to provide them with the appropriate biofunctionality. Thus, there is an ever-increasing need to identify synthetic strategies and chemoligation strategies for the facile incorporation of bioactive moieties.

This dissertation focuses on developing synthetic strategies for making diverse hydrogel nanoparticles customized to have desirable properties for various bio-applications. We have also investigated the potential of such nanoparticles as coatings for biomedical implants.

Chapter 1 gives a brief introduction to hydrogel nanoparticles and the properties that make them attractive for various applications. The details of the syntheses of well defined, stable nanoparticles, commonly used in literature, are described in Chapter 2. Chapter 3 describes our synthesis of hollow sub-50 nm nanogels, which are otherwise difficult to synthesize based on the strategy discussed in Chapter 2. Chapter 4 also demonstrates how simple strategies borrowed from organic chemistry help in producing

nanogels with multiple functionalities that are otherwise difficult to obtain, which also is an important advance over the synthetic methods discussed in Chapter 2. Chapter 5 describes how a general strategy based on photoaffinity labeling can yield materials with many applications ranging from optical materials, drug delivery, to biosensing.

The latter part of the dissertation describes applications of various nanogels in biology especially as coatings that can control inflammation caused by biomaterials. Chapter 1 also, briefly introduces the importance of developing materials for reducing rejection and directing inflammation towards healing when medical implants are implanted in the body. Chapter 6 describes a method to functionalize flexible biomaterials with the nanogels, thus enabling *in vivo* investigations of the nanogels as potential coatings for controlling inflammation. Chapter 6 describes the biological studies performed (in collaboration with Garcia Group in the School of Mechanical Engineering at Georgia Tech) on various nanogels, aimed towards obtaining the most functional and efficient materials for implant applications. Chapter 8 describes application of hollow nanogels for covalently immobilizing biomolecules. This chapter also demonstrates how simple non-functional materials can be made unique and functional by means of traditional organic reactions. Finally, in order to broaden the applications of nanogel based materials, Chapter 9 suggests some extensions to the work described in this dissertation for further development of more complex materials based on the new synthetic strategies developed in this work.

CHAPTER 1

INTRODUCTION

This chapter gives a brief introduction to hydrogel nanoparticles and the properties that make them attractive for various bio-applications, in particular as potential materials for controlling inflammation due to medical implants. It briefly describes the importance of developing materials for reducing rejection and directing inflammation towards healing when medical implants are implanted in the body.

1.1 Smart Polymers and Hydrogels

Considerable research attention has been focused recently on materials that change their structure and properties in response to external chemical and / or physical stimuli. These materials are called "intelligent" or "smart" materials. They are also named as "stimuli-responsive" polymers. Hydrogels, as the name implies, are gels that swell in aqueous media. They are composed of a hydrophilic polymer component that is cross-linked into a network by either covalent or non-covalent interactions.[1-3]

Stimulus-responsive or "smart" polymers and hydrogels can be classified according to the stimuli they respond to, for example temperature,[4] pH,[5,6] ionic strength,[7-9] light,[10-14] electric field[15] and biomolecules-sensitive.[16-20] They undergo fast, reversible changes in their microstructure from a hydrophilic to a hydrophobic state.[21] These changes are apparent at the macroscopic level as precipitate formation from a solution or order-of magnitude changes in the size and water content of hydrogels.[22] An appropriate

proportion of hydrophobicity and hydrophilicity in the molecular structure of the polymer is believed to be required for the phase transition to occur. The responsive behavior of the hydrogels is dictated by the type of the polymer used in making the gel and/or any modifications made post-polymerization.

As the stimulus-responsive behavior occurs in aqueous solutions, these polymers and hydrogels are becoming increasingly attractive for biotechnology and medicine, for their use, among others, as basic components drug delivery,[23,24] sensors,[25-27] nanophotonics,[28-30] catalysis[31] and separations.[32-35] immobilization of enzymes[36] and tissue engineering[37].

The use of stimuli-sensitive polymers in fabricating hydrogels has led to many interesting applications. One of the most widely studied stimuli-sensitive polymers is poly(*N*-isopropylacrylamide) (pNIPAm) formed from the monomer *N*-isopropylacrylamide. Since most of our group's work is based on pNIPAm, and also to facilitate the understanding of some of the later parts of this chapter, it is appropriate to provide a brief background on this polymer.

1.2 Thermoresponsive Polymers and the Phase Transition Phenomenon

Temperature-sensitive polymers like pNIPAm, exhibit critical solution temperature behavior where phase separation is induced on going above a certain temperature. Polymers of this type can undergo a thermally induced, reversible phase transition; they are soluble in a solvent (water) at low temperatures but become insoluble as the temperature rises above the critical solution temperature.

The liquid-liquid phase diagram at constant pressure of binary polymer solutions is usually determined by plotting the temperature of incipient phase separation as a function of the overall polymer concentration. Although the solution is homogeneous at low temperature, a macroscopic phase separation appears when the temperature exceeds a critical value called the critical solution temperature or the cloud point of the mixture.[38] The minimum in the phase diagram (known also as cloud point curve) is called the precipitation threshold, or the lower critical solution temperature (LCST), since it denotes the extreme temperature at which phase separation can occur.[39]

For a linear flexible polymer chain in solution, there has been much debate concerning the major determinant of the coil-to-globule transition, whether "hydrophobic effects" and / or "hydrogen bonding effects" are dominant in general in aqueous solutions. [40] The critical solution temperature of the thermoresponsive polymers is associated with changes in both "hydrogen bonding" and "hydrophobic interactions" within the interacting polymer solvent system. At the molecular level the phase transition of temperature-sensitive polymers is a change from hydrated random coil to hydrophobic globule. As the temperature rises and approaches the phase transition point, the first step of the phase separation is the breaking up of the relatively strong hydrogen bonds, formed around the polymer coil between water molecules and the NH or C=O groups of the temperature-sensitive polymers, followed by the collapse of the polymer molecule into a hydrophobic globule. Polymer-polymer interactions responsible for the aggregation and the subsequent precipitation of the polymer out of solution takes place since the hydrogen bonding becomes weaker and breaks as the temperature is raised.[39,41]
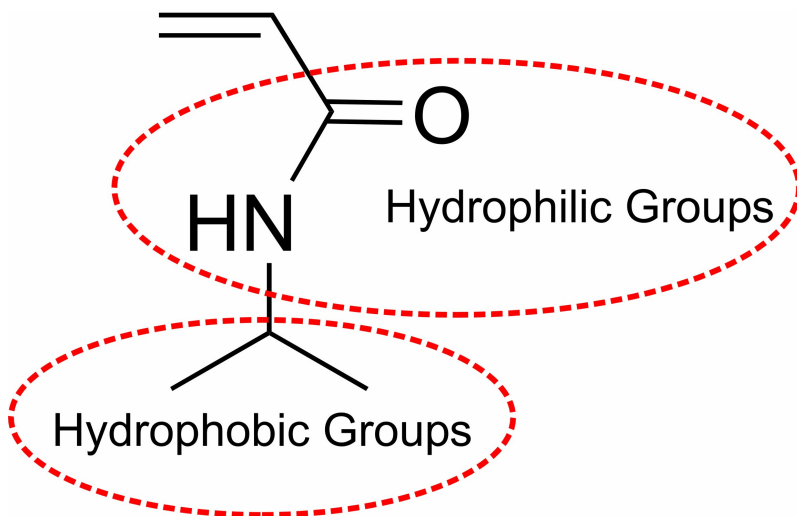
Figure 1.1. Molecular structures of monomer NIPAm and identification of the hydrophilic and hydrophobic regions.

1.3. Thermodynamics of Polymer Solutions

Specific interactions between solute and solvent are required for the occurrence of the phase transition, which result in negative values for the changes in both the enthalpy, and the entropy of mixing (hydrophobic effect). In more detail, the water molecules trapped by hydrogen bonds between the side chain amide groups and water form a thin shell of ordered structure around the hydrophilic part (Figure 1.1) of the polymer.[42] Formation of this hydration shell gives a negative enthalpy for the solution process at a lower temperature, at which the hydrogen bonds stay substantially unbroken. At the same time, water molecules also form a hydrated shell of ordered ice-like structure upon the hydrogen bonds between water molecules themselves around the hydrophobic part of the

polymer (Figure 1.2).[42] This structured water leads to entropically-driven polymer-polymer interactions via the hydrophobic effect.[40] Increasing temperature tends to break the hydrogen bonds and as a result, the hydrated shells around the polymers are disordered and entropically-favored release of bound and structured water molecules results, leading to the formation of a globular polymer conformation. Now, the polymer-polymer hydrophobic interactions become stronger than the polymer-solvent interactions, and the polymer phase separates. Hydrophobic interactions can take place between the same and different polymer chains and this process is manifested as single chain collapse and intermolecular aggregation, suppressing conformation changes of the polymer.
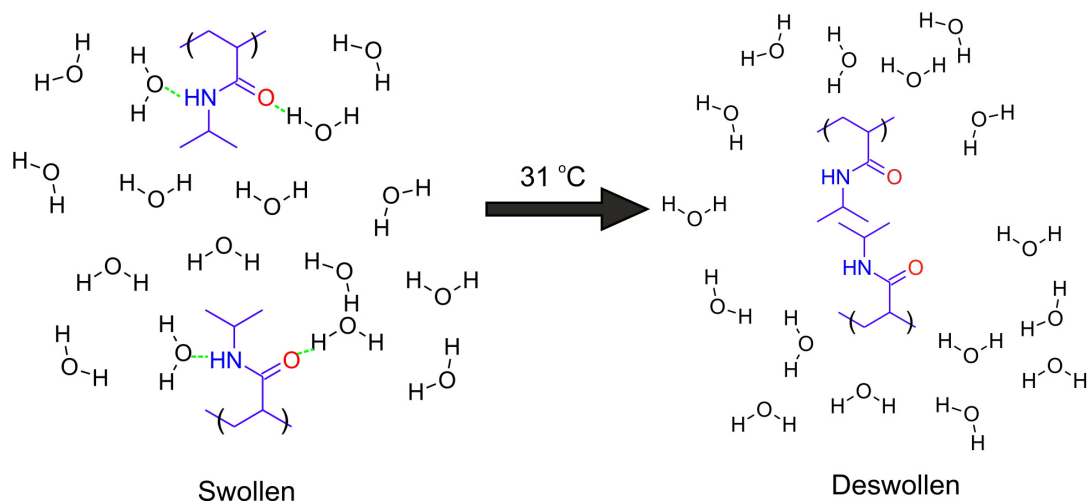
Figure 1.2 Water dissociation process that occurs when pNIPAm hydrogel networks deswell at temperature above the LCST. The hydrogen bonding is depicted by a green dashed line.

1.4 Nanogels

The most typical form of a hydrogel is in a macroscopic form.[4,43,44] These "bulk" gels can be anywhere from millimeters in dimension or larger. The material used in the work described in this dissertation is largely related to smaller entities, which are typically called nanogels.[5,45] Nanogels are colloidally stable hydrogels whose size can vary from tens of nanometers to micrometers. Perhaps the earliest report of nanogel synthesis was by Staudinger in 1935,[46] but interest in such materials for biotechnology applications has only flourished recently. For recent reviews on the subject of colloidal hydrogels, the reader is referred to excellent compilations of Pelton[47] and Vincent.[48]

These colloidally stable nanogels, have similar properties as their macrogel counterparts *i.e.* a pNIPAm nanogel, like the bulk gel, will also undergo a VPTT near the LCST of the parent polymer.[48,49] In addition to these properties, nanogels have other characteristics of colloidal dispersions such as zeta potentials,[48,50,51] and can also form ordered phases when prepared as a highly monodispersed sol.[52-55]

Some very important studies have focused on the differences between macro- and nanogels with respect to their phase behavior. For example, Wu *et al.* have shown that the VPTT of the nanogels is slightly higher than the LCST of pNIPAm, and also that the transition region is less sharp than that of bulk gels.[56] The reason for this continuous transition is due to a greater heterogeneity in the subchain lengths of the nanogels as compared to traditionally prepared macrogels. When the nanogels are subjected to T > VPTT, the regions of the particle with longer subchain lengths collapse at a lower temperature than the regions with shorter subchains. Thus one can think of the observed phase transition for a nanogel as being the summation of the phase transitions of the

different sub-networks in the particle. We have also observed this behavior in core/shell structured nanogels using fluorescent probes to interrogate cross-linker gradients.[57]

Chemical functionalization of nanogels not only facilitates control over the volume phase transition but also allows post-polymerization modifications and provides handles to trigger response to external stimuli like pH, ionic strength or light. However, to achieve efficient design of functional nanogels based on chemical modification, it is important to understand how the functional groups are distributed in the polymer network. A recent report by Hoare and Pelton gives an insight into this aspect. The researchers describe two different methods of obtaining controllable distribution of the functional groups in the system.[58] As the first method, acrylic acid groups were incorporated in acrylamide/NIPAm nanogels by hydrolyzing the acrylamide blocks. The second method involved direct copolymerization of methacrylic acid (MAA) with NIPAm. The distribution of the acid functional groups obtained by the two methods had different topochemical distributions. Another factor that influenced the distribution is the temperature of AM hydrolysis i.e. above or below the LCST of the nanogel. Based on potentiometric and conductometric titrations as well as electrophoretic mobility evaluations of the nanogels, it was found that at a temperature below the LCST, most of the carboxyl groups were located throughout the nanogel, whereas at a temperature above the LCST, a high percentage of carboxyl groups was found to be located at or near the surface of the nanogels. In case of *p*MAA-*co*-*p*NIPAm nanogels, there exists a core-shell kind of a structure with MAA mostly forming the shell. This difference in the distribution of the carboxyl groups in the nanogels produced by the two different comonomers is because of the difference in the polymerization kinetics due to different reactivity ratio of

the monomers. The copolymer of acrylamide and NIPAm is expected to have random incorporation of the monomers resulting in acrylamide and hence carboxyl groups on hydrolysis, throughout the bulk of the nanogel. On the other hand, the reactivity ratios of MAA and NIPAm suggest that there is greater affinity for the homopolymerization of NIPAm, which is followed by MAA monomer polymerization resulting in the core-shell-like structure.

1.5 Post-Polymerization Modification of Hydrogels

For certain applications, not all of the desired hydrogel functionalities can be added during the polymerization step. There are several reasons for this: the desired functionalities may not be stable during the polymerization step or the molecules are simply not polymerizable. This is especially true for most biomolecular structures from which hybrid gels would be prepared. To allow further functionalization of hydrogels, most often a small amount of comonomer with acidic or basic functionality is copolymerized during the polymerization step. These functional groups are then used for attachment of molecules that could not be directly incorporated by polymerization.

The group of Haruma Kawaguchi has used post polymerization modifications extensively for making particles with variety of functions.[59] For example, to synthesize a tetra-functional particle, they first synthesized standard nanogels using acrylamide, BIS, methacrylic acid and *p*-nitrophenyl acrylate as the co-monomers. The thus introduced ester side chain can be hydrolyzed to give acidic particles, or after hydrolysis can be reacted with ethylene diamine to give amphoteric particles. The acid groups were also coupled with a long chain alkyl amine to form hydrophobic particles. Finally the acid

8

groups were coupled to an IgG to form bio-functionalized nanogels. This particular report illustrates the tremendous versatility in nanogel structure and function that is offered by post polymerization modification.

Another interesting system involved the synthesis of pNIPAm chains bearing terminal carboxyl groups, which were then grafted to nanogels. The carboxy termini were then used to attach the enzyme trypsin, resulting into a particle having two different kinds of pNIPAm chains on the surface; one with trypsin and the other without it. Surprisingly, it was found that the two chains had different transition temperatures. The free chains collapsed at a lower temperature than the trypsin conjugated chains, thereby exposing the enzyme for substrate binding. Hence by this simple construct they were able to control the enzyme activity by controlling the temperature.[60]

In a report by Delair, *et al.*, the immobilization of DNA on nanogels by post polymerization modification was described. PNIPAm nanogels with an amine comonomer were synthesized. Single stranded DNA with an amine group at the 5' end was reacted with 1,4-phenylene diisocyanate in 1:2 ratio so that one of the isocyanates was coupled to the DNA, while the other one remained free. After purification, the DNA was coupled to the pNIPAm nanogels by reacting the free isocyanate with the amines on the surface of the particles. The DNA particles were then used for detection of viral DNA and also for formation of two dimensional arrays on planar substrates.[61]

Depending on the application of the nanogels, they can be modified by post-polymerization modification. In this method, the polymerized functional group on the nanogels is used to attach further functionalities by a chemical reaction. These functionalities can range from small ligand molecules to large proteins.[84-94]

Post polymerization modification can be not only used for coupling biomolecules but also for grafting synthetic polymer chains. Hu *et al.* synthesized pNIPAm nanogels and grafted pNIPAm chains on these particles by reversible addition-fragmentation chain transfer (RAFT).[62] They then used these particles to study thermal behavior of the grafted polymer. In another example Hu and Wu grafted poly(ethylene oxide) (PEO) chains on the nanogel particles. The hydrophilic PEO chains were observed to stretch from the particle surface as the particles size decreased with the increase in temperature.[63]

With the recent explosion of the fields of nanotechnology and biotechnology, polymer bioconjugates have gained increased attention in materials science.[2] Consequently, the construction of hybrids of biological and synthetic macromolecules became in the last few years an important trend in polymer chemistry. Given all the progress made in the field of nanogel synthesis (described in detail in Chapter 2) and their post-polymerization modification, there still remains scope to design synthetic strategies for producing materials that can be interfaced with biologically relevant molecules easily and used for various applications. Thus the focus of the projects described in this dissertation was broadly upon the design, synthesis and characterization of unique nanogels, with emphasis upon the development of synthetic strategies that will yield well-defined complex nano-structured materials. The nanogels synthesized have potential for studying molecular-level behavior at interfaces, in thin films, and in solution, while also enabling the development of encapsulation, drug-delivery, and nanoscale-patterning technologies.

1.6 Application of Nanogels in Biomaterials

One of the top demands in the fields of medicine and biotechnology is the ability to engineer the interactions of cells with surfaces. Such ability would be extremely useful in the field of biomaterials, for instance for developing an implant or surgical device that is highly biocompatible or minimally damaging to the body. Proteins and cells are known to uncontrollably attach onto medical implant surfaces, resulting in undesirable fibrous encapsulation, detrimental clinical complications, an increased risk of infection, and poor device performance.[64-67] To develop a material that is highly "bio-inert", one would need to reduce any nonspecific physiological responses to the material. In fact, a truly bioactive system can be achieved by reintroducing the attachment of only desired cells in a predictable fashion by using specific cell signaling molecules or adhesion ligands, often presented in precisely engineered geometries.[68-70] Thus, it is important to evaluate the fouling of biomaterials as well as to design effective strategies for mediating cellular recruitment at engineered surfaces.[65,71,72]

1.7 Response to Implanted Materials

One must understand the response of the host system (known as healing) to an implanted material not only to characterize the performance of existing biomaterials but also to aid in the design of new biomaterials with improved host response.

The normal healing response following a tissue injury is initiated through a series of complex events that include acute inflammation, the formation of granulation tissue, and finally scar formation.[66,67] The immediate response to an injury is the flooding of the injured area with blood. Fibrinogen within the blood is cleaved into fibrin to form a blood

clot that promotes platelet adhesion and aggregation. Cytokines and growth factors are released to recruit white blood cells, mainly neutrophils. Monocytes are then called to the wound site where they differentiate into macrophages, which clean up the wound site from foreign materials, bacteria, and dead cells, and also recruit cells such as fibroblasts and endothelial cells, which convert the fibrin clot into a highly vascularized granulation tissue. The formation of blood vessels is essential to the healing wound. The granulation tissue is subsequently replaced by an extracellular matrix (ECM) deposited primarily by fibroblasts. The degree of ECM remodeling depends on the extent and location of the injury. In some cases, complete restoration of the tissue architecture is possible; however, in most cases the granulation tissue is remodeled into scar tissue.

A biomaterial implanted into the body, however, induces a different response, termed the foreign body reaction. Briefly; a biomaterial immediately upon implantation induces nonspecific protein adsorption on to its surface.[67,73] Non-specific protein adsorption, however, never occurs in the normal physiological process of wound healing discussed in the preceding paragraph. Thus, nonspecific protein adsorption is possibly the primary instigator in the foreign body reaction. A number of different cells that play important roles in normal wound healing, such as monocytes, leukocytes, and platelets, adhere to the biomaterial surface resulting in the upregulation of cytokines and subsequent pro-inflammatory processes.[74] Since the implant is significantly larger than the adhered macrophages, from the latter cannot phagocytose the foreign body. The frustrated macrophages fuse together to form multinucleated foreign body giant cells that often persist for the lifetime of the implant.[75] Thus the implant is walled off by an

12

avascular, collagenous fibrous tissue, typically 50–200 μm thick. This is the last step in the foreign body reaction.

1.8 Non-Fouling Materials

The ability of poly(ethylene glycol) (PEG) to reduce or eliminate protein adsorption is well known, and extensively used in both fundamental research and biomedical applications.[76] There have been many approaches, such as covalent immobilization and adsorption to attach PEG on materials to render them non-fouling. While polymeric or oligomeric ethylene glycol is ideal as a bio-inert background material, it is prone to auto-oxidation and hydrolytic degradation over time and thus has poor stability in long-term clinical applications.[77-80] As an alternative, Lopez *et al.* have investigated PEG-like surfaces prepared by radio frequency plasma deposition of tetraethyleneglycol dimethylether (tetraglyme), which forms a highly non-fouling cross-linked structure.[81] When studied *in vitro* these surfaces exhibited little protein adsorption and significantly reduced blood platelet and monocyte adhesion.[81-84] However, in an *in vivo* study the response of the tetraglyme treated biomaterials was not found to better than the untreated biomaterial.[85] After 4 weeks, a fibrous capsule was observed for all the implants, whether treated or untreated. The capsule thickness was similar regardless of treatment. Also, when the implants were analyzed for the density of the macrophages adhering, the tetraglyme-treated samples had much higher macrophage adhesion in comparison with the untreated samples. Although the reason for this difference between

in vitro and *in vivo* studies is not clearly known, the degradation of the tetraglyme surface *in vivo*, and subsequent loss of the non-fouling character is considered as a possibility.

Consequently, other materials, including PEG-based hydrogels, dextran, mannitol, or phosphorylcholine, have been explored as viable bio-inert alternatives. [86-90] Typically, self assembled monolayers (SAMs) chemical grafting, or other polymerization methods have been employed to present these resistant materials onto a desired surface. [70,90-102] However, potential problems include incomplete, non-uniform surface coverage and possible multiple synthetic steps, which greatly limit the use of these techniques for creating bioinert coatings. Besides, SAMs are restricted to silicon oxide or gold substrates.

Although several methods and coatings based on PEG have been developed, the mechanisms by which proteins and cells interact with these surfaces remain unclear. Previous studies have demonstrated that the adhesion resistance of PEG-coated surfaces increases with chain packing density and increasing length of the polymer chains.[103] It has also been suggested that PEG molecular weight, PEG chain density, and polymer chain architecture, are important parameters that can affect the non-fouling performance of PEG-containing coatings. It was recently observed that the non-fouling property of PEG-containing coatings increased with an increasing PEG chain density.

One approach that is attractive and perhaps complementary to the SAM-modified surfaces, involves coating with hydrogel substrates and matrices, which more accurately represent the mechanical and structural properties of the extracellular matrices in which cells grow *in vivo*. Research has been carried out in the area of hydrogel-based materials as non-fouling substrates, generally focused on the use of bulk polymer gels for coating

of the surface of the implants or devices. Hydrogel-based coatings are attractive because the substrate-deposited hydrogel can be further elaborated upon synthetically to incorporate the necessary functionalities.[87,104,105] A number of bio-functionalized hydrogel matrices for directed cell growth have been developed,[105-114] including those based on proteolytically degradable cross-links.[115-120]

Since nanogels essentially have the same properties as bulk gels, coatings based on nanogels offer a unique and versatile approach to surface functionalization and modification. These coatings combine, and enhance the best properties of both the SAM and bulk hydrogel based approaches. The reason being, ease of synthesizing nanogels that contain multiple chemically orthogonal functionalities, thereby allowing each particle to contain multiple handles for bioconjugate synthesis. Also, all bioconjugation reactions can be performed in solution, after which the particles can be attached to the substrate. This overcomes many of the common problems associated with performing multiple chemical transformations on surfaces as in the case of SAMs.

Our group has synthesized particles in which the adsorption of the proteins to the particles is reduced by using PEG grafting.[121] In this work, pNIPAm-core/pNIPAm-shell particles were employed and PEG was attached either to the core or to the shell by co-polymerization of PEG-monomethacrylate. Reduced protein adsorption was observed for both the core and shell-grafted PEG particles. It was further observed by NMR and protein adsorption measurements that at high temperature the PEG chains phase-separate to the particle surface, thus presenting a hydrophilic polymer surface that resists protein adsorption. In case of the particles in which the PEG is attached to the core, the PEG

chains are able to penetrate the shell and phase separate to the surface, thus reducing the surface energy of the deswollen particles.

Cell adhesion to adsorbed proteins is mediated through integrin and other receptors located within the cell membrane.[122] Following the adherence of cells to the protein film, a series of intracellular signaling events is triggered. Therefore, controlling protein adsorption on the surface of biomaterials may be critical to controlling and directing cell responses to biomaterials. Our approach involved first reducing any nonspecific protein adsorption and then creating a bioactive system by reintroducing the attachment of only desired cells in a predictable fashion by using specific cell signaling molecules or adhesion ligands. We hypothesize that such an approach can provide a better material for controlling the cascade of inflammatory events. The efforts to synthesize complex microgels, which can be further used for such bio-inert and selectively bio-active interfaces, are described in Chapter 6 and 7.

1.9 References and Notes

[1]   Gehrke, S. H. In *Adv. Polym. Sci.*; Springer-Verlag: Berlin, 1993; Vol. 110, p 82-144.

[2]   Hoffman, A. S. Hydrogels for biomedical applications. *Adv. Drug Deliv. Rev.* **2002**, *54*, 3-12.

[3]   Yeomans, K. Hydrogels - very versatile materials. *Chem. Rev.* **2000**, *10*, 2-5.

[4]   Li, Y.; Tanaka, T. Kinetics of Swelling and Shrinking of Gels. *J. Chem. Phys.* **1990**, *92*, 1365-1371.

[5]   Jones, C. D.; Lyon, L. A. Synthesis and Characterization of Multiresponsive Core-Shell Microgels. *Macromolecules* **2000**, *33*, 8301-8306.

[6]   Moselhy, J.; Wu, X. Y.; Nicholov, R.; Kodaria, K. In vitro studies of the interaction of poly(NIPAm/MAA) nanoparticles with proteins and cells. *J. Biomater. Sci., Polym. Ed.* **2000**, *11*, 123-147.

[7]   Duracher, D.; Sauzedde, F.; Elaissari, A.; Perrin, A.; Pichot, C. Cationic amino-containing N-isopropylacrylamide-styrene copolymer latex particles: 1 - Particle size and morphology vs. polymerization process. *Colloid and Polymer Science* **1998**, *276*, 219-231.

[8]   Duracher, D.; Sauzedde, F.; Elaissari, A.; Pichot, C.; Nabzar, L. Cationic amino-containing N-isopropyl-acrylamide-styrene copolymer particles: 2-surface and colloidal characteristics. *Colloid and Polymer Science* **1998**, *276*, 920-929.

[9]   Snowden, M. J.; Chowdhry, B. Z.; Vincent, B.; Morris, G. E. Colloidal copolymer microgels of N-isopropylacrylamide and acrylic acid: pH, ionic strength and temperature effects. *Journal of the Chemical Society-Faraday Transactions* **1996**, *92*, 5013-5016.

[10]   Sershen, S. R.; Westcott, S. L.; Halas, N. J.; West, J. L. Temperature-sensitive polymer-nanoshell composites for photothermally modulated drug delivery. *J. Biomed. Mater. Res* **2000**, *51*, 293-298.

[11]   Sershen, S. R.; Westcott, S. L.; Halas, N. J.; West, J. L. Independent optically addressable nanoparticle-polymer optomechanical composites. *Appl. Phys. Lett.* **2002**, *80*, 4609-4611.

[12]   Sershen, S. R.; Westcott, S. L.; West, J. L.; Halas, N. J. An opto-mechanical nanoshell-polymer composite. *Appl. Phys. B* **2001**, *73*, 379-381.

[13]   Suzuki, A.; Ishii, T.; Maruyama, Y. Optical switching in polymer gels. *Journal of Applied Physics* **1996**, *80*, 131-136.

[14]   Suzuki, A.; Tanaka, T. Phase-Transition in Polymer Gels Induced by Visible-Light. *Nature* **1990**, *346*, 345-347.

[15]   Tanaka, T.; Nishio, I.; Sun, S. T.; Ueno-Nishio, S. Collapse of gels in an electric field. *Science* **1982**, *218*, 467-469.

[16]   Miyata, T.; Asami, N.; Uragami, T. A reversibly antigen-responsive hydrogel. *Nature* **1999**, *399*, 766-769.

[17]   Ogawa, K.; Nakayama, A.; Kokufuta, E. Preparation and characterization of thermosensitive polyampholyte nanogels. *Langmuir* **2003**, *19*, 3178-3184.

[18]   Ogawa, K.; Wang, B.; Kokufuta, E. Enzyme-Regulated Microgel Collapse for Controlled Membrane Permeability. *Langmuir* **2001**, *17*, 4704-4707.

[19]   Ogawa, Y.; Ogawa, K.; Wang, B.; Kokufuta, E. A biochemo-mechanical system consisting of polyampholyte gels with coimmobilized glucose oxidase and urease. *Langmuir* **2001**, *17*, 2670-2674.

[20]   Kim, J.; Nayak, S.; Lyon, L. A. Bioresponsive Hydrogel Microlenses. *J. Am. Chem. Soc.* **2005**, *127*, 9588-9592.

[21]   Galaev, I. Y.; Gupta, M. N.; Mattiasson, B. Use smart polymers for bioseparations. *CHEMTECH* **1996**, *26*, 19-25.

[22]   Galaev, I. Y.; Mattiasson, B. 'Smart' polymers and what they could do in biotechnology and medicine. *Trends Biotechnol.* **1999**, *17*, 335-340.

[23]   Katz, E.; Willner, I. Nanobiotechnology: integrated nanoparticle-biomolecule hybrid systems: Synthesis, properties, and applications. *Angew. Chem., Int. Ed.* **2004**, *43*, 6042-6108.

[24]   Langer, R. New methods of drug delivery. *Science* **1990**, *249*, 1527-1533.

[25]   Holtz, J. H.; Asher, S. A. Polymerized colloidal crystal hydrogel films as intelligent chemical sensing materials. *Nature* **1997**, *389*, 829-832.

[26]   Ohko, Y.; Tatsuma, T.; Fujii, T.; Naoi, K.; Niwa, C.; Kubota, Y.; Fujishima, A. Multicolor photochromism of TiO2 films loaded with silver nanoparticles. *Nat. Mater.* **2003**, *2*, 29-31.

[27]   Kim, J.; Singh, N.; Lyon, L. A. Label-free biosensing with hydrogel microlenses. *Angew. Chem., Int. Ed.* **2006**, *45*, 1446-1449.

[28]   Debord, J. D.; Eustis, S.; Debord, S. B.; Lofye, M. T.; Lyon, L. A. Color-tunable colloidal crystals from soft hydrogel nanoparticles. *Adv. Mater.* **2002**, *14*, 658-662.

[29]   Lyon, L. A.; Debord, J. D.; Debord, S. B.; Jones, C. D.; McGrath, J. G.; Serpe, M. J. Microgel Colloidal Crystals. *J. Phys. Chem. B* **2004**, *108*, 19099-19108.

[30]   Niemeyer, C. M. Functional hybrid devices of proteins and inorganic nanoparticles. *Angew. Chem., Int. Ed.* **2003**, *42*, 5796-5800.

[31]   Bergbreiter, D. E.; Case, B. L.; Liu, Y.-S.; Caraway, J. W. Poly(N-isopropylacrylamide) Soluble Polymer Supports in Catalysis and Synthesis. *Macromolecules* **1998**, *31*, 6053-6062.

[32]   Anastase-Ravion, S.; Ding, Z.; Pelle, A.; Hoffman, A. S.; Letourneur, D. New antibody purification procedure using a thermally responsive poly(N-isopropylacrylamide)-dextran derivative conjugate. *J. Chromatogr., B: Biomed. Sci. Appl.* **2001**, *761*, 247-254.

[33]   Brugger, B.; Richtering, W. Magnetic, thermosensitive microgels as stimuli-responsive emulsifiers allowing for remote control of separability and stability of oil in water-emulsions. *Adv. Mater.* **2007**, *19*, 2973-2978.

[34]   Umeno, D.; Kawasaki, M.; Maeda, M. Water-soluble conjugate of double-stranded DNA and Poly(N-isopropylacrylamide) for one-pot affinity precipitation separation of DNA-binding proteins. *Bioconjug. Chem.* **1998**, *9*, 719-724.

[35]   Anastase-Ravion, S.; Ding, Z.; Pelle, A.; Hoffman, A. S.; Letourneur, D. New antibody purification procedure using a thermally responsive poly(N-isopropylacrylamide)-dextran derivative conjugate. *J. Chromatogr., B: Biomed. Sci. Appl.* **2001**, *761*, 247-254.

[36]   Ding, Z.; Chen, G.; Hoffman, A. S. Unusual properties of thermally sensitive oligomer-enzyme conjugates of poly(N-isopropylacrylamide)-trypsin. *J. Biomed. Mater. Res* **1998**, *39*, 498-505.

[37]   Ohya, S.; Nakayama, Y.; Matsuda, T. Thermoresponsive artificial extracellular matrix for tissue engineering: hyaluronic acid bioconjugated with poly[N-isopropylacrylamide) grafts. *Biomacromolecules* **2001**, *2*, 856-863.

[38]   Durand, A.; Lalot, T.; Brigodiot, M.; Marechal, E. Enzyme-mediated initiation of acrylamide polymerization: reaction mechanism. *Polymer* **2000**, *41*, 8183-8192.

[39]   Boutris, C.; Chatzi, E. G.; Kiparissides, C. Characterization of the LCST behavior of aqueous poly(N-isopropylacrylamide) solutions by thermal and cloud point techniques. *Polymer* **1997**, *38*, 2567-2570.

[40]   Schild, H. G. Poly(N-isopropylacrylamide): experiment, theory and application. *Prog. Polym. Sci.* **1992**, *17*, 163-249.

[41)   Fujishige, S.; Kubota, K.; Ando, I. Phase transition of aqueous solutions of poly(N-isopropylacrylamide) and poly(N-isopropylmethacrylamide). *J. Phys. Chem. B* **1989**, *93*, 3311-3313.

[42]   Horne, R. A.; Almeida, J. P.; Day, A. F.; Yu, N. T. Macromolecule hydration and the effect of solutes on the cloud point of aqueous solutions of polyvinyl methyl ether: a possible model for protein denaturation and temperature control in homeothermic animals. *J. Colloid Interface Sci.* **1971**, *35*, 77-84.

[43]   Li, Y.; Tanaka, T. Study of the universality class of the gel network system. *J. Chem. Phys.* **1989**, *90*, 5161-5166.

[44]   Tanaka, T. Kinetics of phase transition in polymer gels. *Physica A* **1986**, *140A*, 261-268.

[45]   Gan, D.; Lyon, L. A. Tunable Swelling Kinetics in Core-Shell Hydrogel Nanoparticles. *J. Am. Chem. Soc.* **2001**, *123*, 7511-7517.

[46]   Staudinger, H.; Husemann, E. *Ber. Dtsch. Chem. Ges.* **1935**, *68*, 1618.

[47]   Pelton, R. H. Temperature-sensitive aqueous microgels. *Adv. Colloid. Interface Sci.* **2000**, *85*, 1-33.

[48]   Saunders, B. R.; Vincent, B. Microgel particles as model colloids: theory, properties and applications. *Adv. Colloid Interface Sci.* **1999**, *80*, 1-25.

[49]   Pelton, R. Temperature-sensitive aqueous microgels. *Adv. Colloid. Interface Sci.* **2000**, *85*, 1-33.

[50]   Daly, E.; Saunders, B. R. Temperature-dependent electrophoretic mobility and hydrodynamic radius measurements of poly(N-isopropylacrylamide) microgel particles: structural insights. *Phys. Chem. Chem. Phys.* **2000**, *2*, 3187-3193.

[51]   Ohshima, H.; Makino, K.; Kato, T.; Fujimoto, K.; Kondo, T.; Kawaguchi, H. Electrophoretic Mobility of Latex-Particles Covered With Temperature-Sensitive Hydrogel Layers. *J. Colloid Interface Sci.* **1993**, *159*, 512-514.

[52]   Debord, J. D.; Lyon, L. A. Thermoresponsive Photonic Crystals. *J. Phys. Chem. B* **2000**, *104*, 6327-6331.

[53]   Senff, H.; Richtering, W. Temperature sensitive microgel suspensions: Colloidal phase behavior and rheology of soft spheres. *J. Chem. Phys.* **1999**, *111*, 1705-1711.

[54]   Hu, Z.; Lu, X.; Gao, J. Hydrogel opals. *Adv. Mater.* **2001**, *13*, 1708-1712.

[55]   Hellweg, T.; Dewhurst, C. D.; Bruckner, E.; Kratz, K.; Eimer, W. Colloidal crystals made of poly(N-isopropylacrylamide) microgel particles. *Colloid Polym. Sci.* **2000**, *278*, 972-978.

[56]   Wu, C.; Zhou, S. Volume Phase Transition of Swollen Gels: Discontinuous or Continuous? *Macromolecules* **1997**, *30*, 574-576.

[57]   Gan, D.; Lyon, L. A. Interfacial Nonradiative Energy Transfer in Responsive Core-Shell Hydrogel Nanoparticles. *J. Am. Chem. Soc.* **2001**, *123*, 8203-8209.

[58]   Hoare, T.; Pelton, R. Functional group distribution in carboxylic acid containing poly(*N*-isopropylacrylamide) microgels. *Langmuir* **2004**, *20*, 2123-2133

[59]   Kashiwabara, M.; Fujimoto, K.; Kawaguchi, H. Preparation of Monodisperse, Reactive Hydrogel Microspheres and Their Amphoterization. *Colloid Polym. Sci.* **1995**, *273*, 339-345.

[60]   Kawaguchi, H.; Kisara, K.; Takahashi, T.; Achiha, K.; Yasui, M.; Fujimoto, K. Versatility of thermosensitive particles. *Macromolecular Symposia* **2000**, *151*, 591-598.

[61]   Delair, T.; Meunier, F.; Elaissari, A.; Charles, M.-H.; Pichot, C. Amino-containing cationic latex-oligodeoxyribonucleotide conjugates: application to diagnostic test sensitivity enhancement. *Colloid. Surf. A* **1999**, *153*, 341-353.

[62]   Hu, T. J.; You, Y. Z.; Pan, C. Y.; Wu, C. The coil-to-globule-to-brush transition of linear thermally sensitive poly(N-isopropylacrylamide) chains grafted on a spherical microgel. *J. Phys. Chem. B* **2002**, *106*, 6659-6662.

[63]   Hu, T.; Wu, C. Grafting Density Induced Stretching and Collapse of Tethered Poly(ethylene oxide) Chains on a Thermally Sensitive Microgel. *Macromolecules* **2001**, *34*, 6802-6805.

[64]   Anderson, J. M.; Miller, K. M. Biomaterial biocompatibility and the macrophage. *Biomaterials* **1984**, *5*, 5-10.

[65]   Ratner, B. D. New ideas in biomaterials science--a path to engineered biomaterials. *J. Biomed. Mater. Res.* **1993**, *27*, 837-850.

[66]   Anderson, J. M. Biological responses to materials. *Annu. Rev. Mater. Res.* **2001**, *31*, 81-110.

[67]   Ratner, B. D.; Bryant, S. J. Biomaterials: Where we have been and where we are going. *Annu. Rev. Biomed. Eng.* **2004**, *6*, 41-75.

[68]   Hubbell, J. A. Bioactive biomaterials. *Curr. Opin. Biotechnol.* **1999**, *10*, 123-129.

[69]   Kao, W. J.; Hubbell, J. A.; Anderson, J. M. Protein-mediated macrophage adhesion and activation on biomaterials: a model for modulating cell behavior. *J. Mater. Sci.: Mater. Med.* **1999**, *10*, 601-605.

[70]   Lopez, G. P.; Albers, M. W.; Schreiber, S. L.; Carroll, R.; Peralta, E.; Whitesides, G. M. Convenient methods for patterning the adhesion of mammalian cells to surfaces using self-assembled monolayers of alkanethiolates on gold. *J. Am. Chem. Soc.* **1993**, *115*, 5877-5878.

[71]   Causa, F.; Netti, P. A.; Ambrosio, L. A multi-functional scaffold for tissue regeneration: The need to engineer a tissue analogue. *Biomaterials* **2007**, *28*, 5093-5099.

[72]   Furth, M. E.; Atala, A.; Van Dyke, M. E. Smart biomaterials design for tissue engineering and regenerative medicine. *Biomaterials* **2007**, *28*, 5068-5073.

[73]   Haycox, C. L.; Ratner, B. D. In vitro platelet interactions in whole human blood exposed to biomaterial surfaces: insights on blood compatibility. *J. Biomed. Mater. Res.* **1993**, *27*, 1181-1193.

[74]   Ziats, N. P.; Miller, K. M.; Anderson, J. M. In vitro and in vivo interactions of cells with biomaterials. *Biomaterials* **1988**, *9*, 5-13.

[75]   Salthouse, T. N. Some aspects of macrophage behavior at the implant interface. *J. Biomed. Mater. Res.* **1984**, *18*, 395-401.

[76]   Tziampazis, E.; Kohn, J.; Moghe, P. V. PEG-variant biomaterials as selectively adhesive protein templates: model surfaces for controlled cell adhesion and migration. *Biomaterials* **2000**, *21*, 511-520.

[77]   Wieland, B.; Lancaster, J. P.; Hoaglund, C. S.; Holota, P.; Tornquist, W. J. Electrochemical and Infrared Spectroscopic Quantitative Determination of the Platinum-Catalyzed Ethylene Glycol Oxidation Mechanism at CO Adsorption Potentials. *Langmuir* **1996**, *12*, 2594-2601.

[78]   Collier, T. O.; Anderson, J. M. Protein and surface effects on monocyte and macrophage adhesion, maturation, and survival. *J. Biomed. Mater. Res.* **2002**, *60*, 487-496.

[79]   Behling, C. A.; Spector, M. Quantitative characterization of cells at the interface of long-term implants of selected polymers. *J. Biomed. Mater. Res.* **1986**, *20*, 653-666.

[80]   Johansson, C. B.; Albrektsson, T.; Ericson, L. E.; Thomsen, P. A quantitative comparison of the cell response to commercially pure titanium and Ti-6Al-4V implants in the abdominal wall of rats. *J. Mater. Sci.: Mater. Med.* **1992**, *3*, 126-136.

[81]   Lopez, G. P.; Ratner, B. D.; Tidwell, C. D.; Haycox, C. L.; Rapoza, R. J.; Horbett, T. A. Glow discharge plasma deposition of tetraethylene glycol dimethyl ether for fouling-resistant biomaterial surfaces. *J. Biomed. Mater. Res.* **1992**, *26*, 415-439.

[82]   Shen, M.; Horbett, T. A. The effects of surface chemistry and adsorbed proteins on monocyte/macrophage adhesion to chemically modified polystyrene surfaces. *J. Biomed. Mater. Res.* **2001**, *57*, 336-345.

[83]   Shen, M.; Pan, Y. V.; Wagner, M. S.; Hauch, K. D.; Castner, D. G.; Ratner, B. D.; Horbett, T. A. Inhibition of monocyte adhesion and fibrinogen adsorption on glow discharge plasma deposited tetraethylene glycol dimethyl ether. *J. Biomater. Sci. Polym.* **2001**, *12*, 961-978.

[84]   Tsai, W.-B.; Grunkemeier, J. M.; McFarland, C. D.; Horbett, T. A. Platelet adhesion to polystyrene-based surfaces preadsorbed with plasmas selectively depleted in fibrinogen, fibronectin, vitronectin, or von Willebrand's factor. *J. Biomed. Mater. Res.* **2002**, *60*, 348-359.

[85]   Shen, M.; Martinson, L.; Wagner, M. S.; Castner, D. G.; Ratner, B. D.; Horbett, T. A. PEO-like plasma polymerized tetraglyme surface interactions with leukocytes and proteins: in vitro and in vivo studies. *J. Biomater. Sci., Polym. Ed.* **2002**, *13*, 367-390.

[86]   Ma, Z.; Mao, Z.; Gao, C. Surface modification and property analysis of biomedical polymers used for tissue engineering. *Colloids Surf., B* **2007**, *60*, 137-157.

[87]   Kopecek, J. Hydrogel biomaterials: A smart future? *Biomaterials* **2007**, *28*, 5185-5192.

[88]   Draghi, L.; Cigada, A. Nanostructured surfaces for biomedical applications. Part I: nanotopography. *J. Appl. Biomater. Biomech.* **2007**, *5*, 61-69.

[89]   Massia, S. P.; Stark, J.; Letbetter, D. S. Surface-immobilized dextran limits cell adhesion and spreading. *Biomaterials* **2000**, *21*, 2253-2261.

[90]   Luk, Y.-Y.; Kato, M.; Mrksich, M. Self-Assembled Monolayers of Alkanethiolates Presenting Mannitol Groups Are Inert to Protein Adsorption and Cell Attachment. *Langmuir* **2000**, *16*, 9604-9608.

[91]   Ostuni, E.; Chapman, R. G.; Liang, M. N.; Meluleni, G.; Pier, G.; Ingber, D. E.; Whitesides, G. M. Self-assembled monolayers that resist the adsorption of proteins and the adhesion of bacterial and mammalian cells. *Langmuir* **2001**, *17*, 6336-6343.

[92]   Ostuni, E.; Yan, L.; Whitesides, G. M. The interaction of proteins and cells with self-assembled monolayers of alkanethiolates on gold and silver. *Colloids Surf., B* **1999**, *15*, 3-30.

[93]   Tidwell, C. D.; Ertel, S. I.; Ratner, B. D.; Tarasevich, B.; Atre, S.; Allara, D. L. Endothelial cell growth and protein adsorption on terminally functionalized, self-assembled monolayers of alkanethiolates on gold. *Langmuir* **1997**, *13*, 3404-3413.

[94]   Lee, S. D.; Hsiue, G. H.; Chang, P. C.; Kao, C. Y. Plasma-induced grafted polymerization of acrylic acid and subsequent grafting of collagen onto polymer film as biomaterials. *Biomaterials* **1996**, *17*, 1599-1608.

[95]   Irvine, D. J.; Mayes, A. M.; Griffith, L. G. Nanoscale Clustering of RGD Peptides at Surfaces Using Comb Polymers. 1. Synthesis and Characterization of Comb Thin Films. *Biomacromolecules* **2001**, *2*, 85-94.

[96]   Caruso, F.; Niikura, K.; Furlong, D. N.; Okahata, Y. Assembly of Alternating Polyelectrolyte and Protein Multilayer Films for Immunosensing. *Langmuir* **1997**, *13*, 3427-3433.

[97]   Chluba, J.; Voegel, J. C.; Decher, G.; Erbacher, P.; Schaaf, P.; Ogier, J. Peptide hormone covalently bound to polyelectrolytes and embedded into multilayer architectures conserving full biological activity. *Biomacromolecules* **2001**, *2*, 800-805.

[98]   Elbert, D. L.; Herbert, C. B.; Hubbell, J. A. Thin Polymer Layers Formed by Polyelectrolyte Multilayer Techniques on Biological Surfaces. *Langmuir* **1999**, *15*, 5355-5362.

[99]   Schneider, S.; Feilen, P.; Slotty, V.; Kampfner, D.; Preuss, S.; Berger, S.; Beyer, J.; Pommersheim, R. Multilayer capsules: a promising microencapsulation system for transplantation of pancreatic islets. *Biomaterials* **2001**, *22*, 1961-1970.

[100] Serizawa, T.; Yamaguchi, M.; Matsuyama, T.; Akashi, M. Alternating bioactivity of polymeric layer-by-layer assemblies: anti- vs procoagulation of human blood on chitosan and dextran sulfate layers. *Biomacromolecules* **2000**, *1*, 306-309.

[101] Vautier, D.; Karsten, V.; Egles, C.; Chluba, J.; Schaaf, P.; Voegel, J.-C.; Ogier, J. Polyelectrolyte multilayer films modulate cytoskeletal organization in chondrosarcoma cells. *J. Biomater. Sci., Polym. Ed.* **2002**, *13*, 713-732.

[102] Yoo, D.; Shiratori, S. S.; Rubner, M. F. Controlling Bilayer Composition and Surface Wettability of Sequentially Adsorbed Multilayers of Weak Polyelectrolytes. *Macromolecules* **1998**, *31*, 4309-4318.

[103] Malmsten, M.; Emoto, K.; Van Alstine, J. M. Effect of chain density on inhibition of protein adsorption by poly(ethylene glycol) based coatings. *J. Colloid Interface Sci.* **1998**, *202*, 507-517.

[104] Zisch, A. H.; Lutolf, M. P.; Ehrbar, M.; Raeber, G. P.; Rizzi, S. C.; Davies, N.; Schmoekel, H.; Bezuidenhout, D.; Djonov, V.; Zilla, P.; Hubbell, J. A. Cell-demanded elease of VEGF from synthetic, biointeractive cell-ingrowth matrices for vascularized tissue growth. *FASEB J.* **2003**, *17*, 2260-2262, .

[105] Stile, R. A.; Healy, K. E. Thermo-Responsive Peptide-Modified Hydrogels for Tissue Regeneration. *Biomacromolecules* **2001**, *2*, 185-194.

[106] Shin, H.; Zygourakis, K.; Farach-Carson Mary, C.; Yaszemski Michael, J.; Mikos Antonios, G. Attachment, proliferation, and migration of marrow stromal osteoblasts cultured on biomimetic hydrogels modified with an osteopontin-derived peptide. *Biomaterials* **2004**, *25*, 895-906.

[107] Raeber, G. P.; Lutolf, M. P.; Hubbell, J. A. Molecularly engineered PEG hydrogels: A novel model system for proteolytically mediated cell migration. *Biophys. J.* **2005**, *89*, 1374-1388.

[108] Fittkau, M. H.; Zilla, P.; Bezuidenhout, D.; Lutolf, M. P.; Human, P.; Hubbell, J. A.; Davies, N. The selective modulation of endothelial cell mobility on RGD peptide containing surfaces by YIGSR peptides. *Biomaterials* **2004**, *26*, 167-174.

[109] Fittkau, M. H.; Zilla, P.; Bezuidenhout, D.; Lutolf, M. P.; Human, P.; Hubbell, J. A.; Davies, N. The selective modulation of endothelial cell mobility on RGD peptide containing surfaces by YIGSR peptides. *Biomaterials* **2005**, *26*, 167-174.

[110] Luo, Y.; Shoichet, M. S. A photolabile hydrogel for guided three-dimensional cell growth and migration. *Nat. Mater.* **2004**, *3*, 249-253.

[111] Shu, X. Z.; Ghosh, K.; Liu, Y.; Palumbo, F. S.; Luo, Y.; Clark, R. A.; Prestwich, G. D. Attachment and spreading of fibroblasts on an RGD peptide-modified injectable hyaluronan hydrogel. *J. Biomed. Mater. Res., Part A* **2004**, *68A*, 365-375.

[112] Barber, T. A.; Golledge, S. L.; Castner, D. G.; Healy, K. E. Peptide-modified p(AAm-co-EG/AAc) IPNs grafted to bulk titanium modulate osteoblast behavior in vitro. *J. Biomed. Mater. Res., Part A* **2003**, *64A*, 38-47.

[113) Stile, R. A.; Healy, K. E. Poly(N-isopropylacrylamide)-Based Semi-interpenetrating Polymer Networks for Tissue Engineering Applications. 1. Effects of Linear Poly(acrylic acid) Chains on Phase Behavior. *Biomacromolecules* **2002**, *3*, 591-600.

[114] Whang, K.; Goldstick, T. K.; Healy, K. E. A biodegradable polymer scaffold for delivery of osteotropic factors. *Biomaterials* **2000**, *21*, 2545-2551.

[115] Collier, T. O.; Anderson, J. M.; Brodbeck, W. G.; Barber, T.; Healy, K. E. Inhibition of macrophage development and foreign body giant cell formation by hydrophilic interpenetrating polymer network. *J. Biomed. Mater. Res., Part A* **2004**, *69A*, 644-650.

[116] Kim, S.; Chung, E. H.; Gilbert, M.; Healy, K. E. Synthetic MMP-13 degradable ECMs based on poly(N-isopropylacrylamide-co-acrylic acid) semi-interpenetrating polymer networks. I. Degradation and cell migration. *J. Biomed. Mater. Res., Part A* **2005**, *75A*, 73-88.

[117] Kim, S.; Healy, K. E. Synthesis and Characterization of Injectable Poly(N-isopropylacrylamide-co-acrylic acid) Hydrogels with Proteolytically Degradable Cross-Links. *Biomacromolecules* **2003**, *4*, 1214-1223.

[118] Lutolf, M. P.; Hubbell, J. A. Synthetic biomaterials as instructive extracellular microenvironments for morphogenesis in tissue engineering. *Nat. Biotechnol.* **2005**, *23*, 47-55.

[119] Urech, L.; Bittermann, A. G.; Hubbell, J. A.; Hall, H. Mechanical properties, proteolytic degradability and biological modifications affect angiogenic process extension into native and modified fibrin matrices in vitro. *Biomaterials* **2004**, *26*, 1369-1379.

[120] Lutolf, M. P.; Lauer-Fields, J. L.; Schmoekel, H. G.; Metters, A. T.; Weber, F. E.; Fields, G. B.; Hubbell, J. A. Synthetic matrix metalloproteinase-sensitive hydrogels for the conduction of tissue regeneration: Engineering cell-invasion characteristics. *Proc. Natl. Acad. Sci. U. S. A.* **2003**, *100*, 5413-5418.

[121] Gan, D. J.; Lyon, L. A. Synthesis and protein adsorption resistance of PEG-modified poly(N-isopropylacrylamide) core/shell microgels. *Macromolecules* **2002**, *35*, 9634-9639.

[122] Chang, C. C.; Rosenson-Schloss, R. S.; Bhoj, T. D.; Moghe, P. V. Leukocyte chemosensory migration on vascular prosthetic biomaterial is mediated by an integrin beta 2 receptor chain. *Biomaterials* **2000**, *21*, 2305-2313.

CHAPTER 2

SYNTHESIS AND CHARACTERIZATION OF NANOGELS

This chapter describes the synthesis and characterization of hydrogel nanoparticles (nanogels), which are the material of focus in this dissertation. Since the dissertation deals with some more complex syntheses based on a more general precipitation polymerization technique, it is necessary that the basic principle behind the polymerization technique be explained along with the synthetic protocols and the characterization techniques commonly used for hydrogel-based nanostructures, which are extensively used and described throughout this dissertation.

2.1 Synthesis of pNIPAm Nanogels

The methods employed to produce nanogels are numerous, with each method having advantages and disadvantages depending on the desired properties or application. The synthetic method is of particular importance from the point of view of the bioconjugation of the synthesized material. For example, the location, density, and identity of chemoligation sites on the nanogel would dictate the function and utility of the bioconjugate. It is also desirable that the synthetic method yield stable dispersions containing nanoparticles in desired compositions, sizes, and morphologies, with narrow size dispersity, which can be further employed in making complex assemblies based on nanostructured building blocks.

Although the most commonly used methodology for synthesis of polymeric hydrogel nanoparticles involves heterogeneous polymerization techniques such as emulsion, dispersion, or suspension polymerization, in recent years there also have been few reports where living polymerization techniques like reversible addition-fragmentation chain transfer (RAFT) and the atom transfer radical polymerization (ATRP) have been used to synthesize nanogels at room temperature.[1-4]

Surfactant-free emulsion polymerization (SFEP), or precipitation polymerization, is the most common technique to synthesize thermosensitive nanogels. It was not until 1986 that the synthesis of pNIPAm nanogels using precipitation polymerization was reported, although it is supposed to be have been first utilized by Philip Chibante in 1978.[5,6] Since the work described throughout this dissertation employs precipitation polymerization to prepare nanogels, this method is discussed here in detail. The major monomer used in this technique (e.g. NIPAm, NIPMAm extensively used in the work described in this dissertation) typically forms a temperature sensitive polymer. The growing monomer chains are kept together in a network and their dissolution is avoided by using cross-linkers like *N,N'*-methylene bisacrylamide (BIS) or PEG Diacrylate in the reaction solution. To give the polymeric network added functionality in addition to temperature sensitivity, functional comonomers can be incorporoted. Figure 2.1 shows the structures of the common monomers used in the synthesis of nanogels. The polymer network being formed is usually stabilized by using either cationic or anionic surfactant below the critical micelle concentration (CMC). The solution is purged with nitrogen to remove the dissolved oxygen because it retards the polymerization. The reaction is carried out at a temperature far above the polymer's LCST (usually ~70 °C) and the

reaction is initiated by thermally decomposing free-radical initiator such as ammonium persulfate (APS) or potassium persulfate (KPS). The solution turns turbid within few minutes, indicating successful initiation. The method results in nanogel nanoparticles with very narrow size distribution.
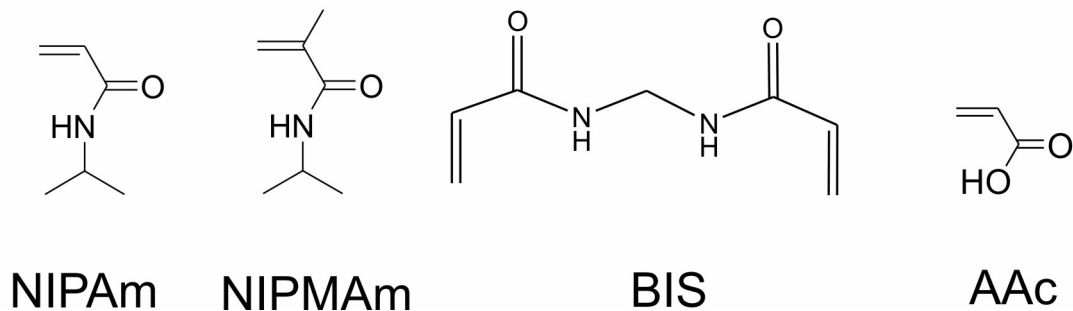
Figure 2.1. Chemical structure for the commonly used monomers in the precipitation polymerization technique used in this dissertation.
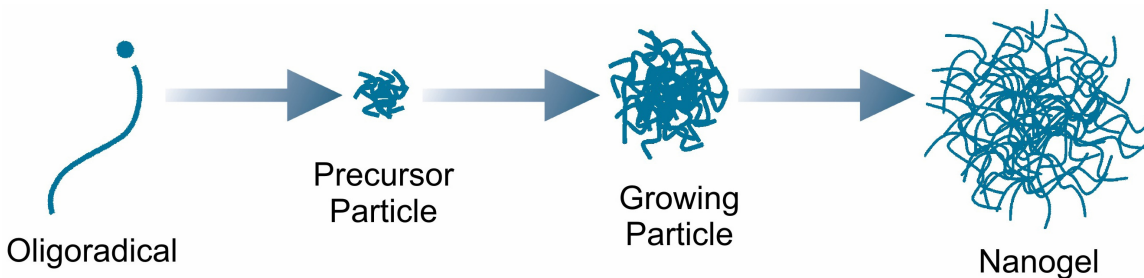
Figure 2.2. Nanogel growth process in precipitation polymerization.

Figure 2.2 illustrates the mechanism of precipitation polymerization, which is carried out at a higher temperature for two reasons: one is formation of sulfate radicals (for typical initiators), which initiate the polymerization. The second is that above the LCST of the polymer, the growing chain after reaching a critical length collapses onto

itself, which is essentially a phase separation process, hence the name precipitation polymerization. The precursor particles resulting from the precipitation can grow by addition of monomer on the precursor particle, by aggregation with the other precursor particles or by being captured by existing colloidally stable particles. Nanogels are formed by such nucleation events.[6] The charge imparted by the initiator stabilizes the nanogels.

This method is extremely versatile from the standpoint of particle size control. For example, to synthesize smaller nanogels, the precursor particles must be stabilized earlier in the reaction. Since there is not enough charge available from initiator fragments to stabilize small precursor particles, an ionic surfactant can be added to impart colloidal stability earlier in the reaction. Similarly, larger particles can be obtained by decreasing the surfactant concentration.

Although the polymerization technique offers a versatile synthetic route to multifunctional nanogels it suffers from a few drawbacks. For example, the method is useful only for synthesizing materials that are stable at high temperatures, thus limiting its utility for *in situ* incorporation of biological macromolecules. Also, since it is based on the formation of a hydrophobic precursor particle, efficient incorporation of hydrophilic monomers is usually difficult. These problems can be overcome by using inverse microemulsion polymerization, where an aqueous solution of all the monomers is added to an appropriate amount of oil and surfactant and is stirred to form thermodynamically stable microemulsions. Polymerization can be initiated by having the initiator in the aqueous or in the oil phase. This method has been used to synthesize hydrogel particles with a high wt% of ionic monomers. Neyret and Vincent used microemulsion

polymerization to prepare zwitterionic pNIPAm nanogels.[7] In this case, they used a UV-activated photoinitiator dissolved in the organic phase. McAllister *et al.* used the same technique to synthesize a highly cationically charged hydrogel.[8] Another method for the nanogel synthesis similar to the microemulsion polymerization utilizes lipids to form liposomes inside which the particle is formed.[9] Recently Kim *et al.* reported the dispersion polymerization of NIPAm in aqueous media by ATRP using poly(ethylene glycol) methyl ether (PEG) as a macro-initiator.[10] They first synthesized the PEG-*b*-*p*NIPAm block copolymer by ATRP of NIPAm in water at 25 °C. The synthesized block copolymer is homogeneous during polymerization but as the temperature is raised to 50 °C, it phase-separates to form nano-sized micelles with hydrobhobic pNIPAm chains as the core and the hydrophilic PEG chains as the corona. To form the hydrogel nanoparticles, they added a cross-linker in the monomer solution and performed ATRP using the PEG macro-initiator at 50 °C in aqueous media. Interestingly, the size of these nanoparticles could be controlled by changing the solvent for the reaction. For instance, the average sizes determined by dynamic light scattering of the hydrogel nanoparticles prepared in H_2O and H_2O/THF were reported to be 67 nm and 503 nm, respectively. This represents an attractive method to form hydrogel nanoparticles at room temperature allowing the incorporation of temperature-sensitive biomolecules.

2.2 Synthesis of Core/Shell Nanogels

An interesting architecture of these soft colloids that can be synthesized with ease is the core/shell type nanogels where the core could be a material other than a hydrogel, coated with a hydrogel shell. Such a construct was prepared by Dingenouts *et al.* with

polystyrene and small amount of NIPAm as a co-monomer using the SFEP approach.[11] The polystyrene-*co*-pNIPAm particles stabilized by the sulfate groups from the initiator were used as seeds for polymerizing a cross-linked shell of pNIPAm. The shell synthesis was carried out at 80 °C causing the pNIPAm in the core to deswell. This resulted in a hydrophobic seed onto which the pNIPAm polymerizing in solution could aggregate by a precipitation polymerization mechanism. Another interesting structure was synthesized by Xiao *et al.*, who grafted pNIPAm chains on a polystyrene core.[12]

Our group first reported the synthesis of core/shell type hydrogel particles by two-stage precipitation polymerization.[13] In this method, a polymer shell with a similar or different structure or functionality as the core is added onto preformed core particles, thereby allowing control over the radial distribution of the functional groups in the particle. This method is also termed the "seed and feed" method.

In a typical synthesis, preformed pNIPAm core particles (acting as hydrophobic seeds) are heated to ~70 °C, followed by addition and initiation of the shell monomer solution (feed). The reaction is carried out for ~4 h and then the mixture is cooled and filtered. This method gives core/shell particles, without any increase in polydispersity, as all oligomers formed in solution precipitate on pre-formed core particles. Heteronucleation can be prevented by controlling the concentration of the core, initiator, surfactant and the shell monomer. Core/shell particles prepared in this fashion can exhibit very interesting properties.[14-21] The mechanism by which this reaction takes place is somewhat similar to that for the core nanogels. Since the reaction temperature is well above the LCST of the core particles, the particles are in a collapsed state. The collapsed particles are hydrophobic and hence they tend to capture the growing oligomers, which

results in the formation of the shell. Since the shell can have different comonomers, the particles can show multiple phase transition behavior with increase in temperature.[22] Depending upon the cross-linker density of the shell, compression of the core can also be observed.[23-26] A cross-linker density gradient is also observed in the shell.[15,16,27,28] Interpenetration of the polymer networks between the core and the shell is also observed causing the core/shell interface to be very diffuse.[18,19,29]

Our group has also used this synthetic method to make hollow hydrogel capsules.[30] To accomplish this, the core is fabricated with a degradable cross-linker and the shell with a non-degradable one. The degradable cross-linker contains a vicinal diol, which can be degraded by stoichiometric addition of periodate. After core degradation, the particles are purified extensively by centrifugation. Advancement of such hollow nanocapsules as functional materials was a topic of our studies and the findings are discussed in Chapter 8.

2.3 Purification of Nanogels

The purification of the nanogels synthesized is important to remove all the unreacted monomer and short polymer chains. Typically the nanoparticles are separated from the unreacted monomers (or purified) by a centrifugation method. Since the nanogels are more dense than water the nanoparticles sediment forming a pellet, which can be easily redispersed in a solvent of choice. Sometimes if the nanogels are highly swollen (water rich), due to the more hydrophilic character of the network, which could be due to comonomers or the architecture (hollow), the nanogels do not sediment. In such cases, centrifugation at high temperature is carried out. The high temperature causes the

nanogels to deswell and become denser, hence separating out more easily. However, sometimes high temperature centrifugation can also cause aggregation and other methods of purification such as dialysis or solvent extraction need to be employed. Typically, the nanogel suspension is dialyzed for 2-3 weeks with the solvent being changed at least twice a day. This method of purification however, does not remove dissolved small polymer chains effectively. The nanogels can also be extracted from the reaction mixture if the reactants and the product other than the nanogels are insoluble in some solvent. This method of purification is used in some of the chapters in this dissertation, where post-polymerization modification of nanogels with water-insoluble molecule benzophenone was carried out.

2.4 Characterization of Nanogels

2.4.1 Dynamic Light Scattering

Characterization of pNIPAm based nanogels can be achieved with a variety of techniques,[6] including dynamic light scattering,[31-34] differential scanning calorimetry[35] and neutron scattering.[32,36,37] In this dissertation, dynamic light scattering (DLS) has been the most commonly used technique to characterize the size and the phase transition behavior of the nanogel particles. This method is therefore discussed in detail.

Dynamic light scattering is a well established technique for measuring particle size over the size range from a few nanometers to a few microns. The technique is based on the principle that small particles in a suspension move in a random pattern or in "Brownian Motion". Also, larger particles move more slowly than the smaller ones if the

temperature is the same. When a coherent source of light (such as a laser) is directed at the moving particles, the light is scattered. The intensity of the scattered light will vary as the particles move around under Brownian motion causing constructive and destructive interference of the light. For all of the DLS experiments performed in this work, a Protein Solutions DynaPro-MS/X system was used. A schematic of this setup is illustrated in Figure 2.3. The laser source uses a wavelength of 784.8 nm. This light hits the ultradilute nanogel dispersion and scattered light at 90 °C with respect to the incident light is detected by an avalanche photodiode detector. This signal is then sent to an autocorrelator board, which relays the signal to a CPU. DLS monitors fluctuations in scattered light intensity and these fluctuations are analyzed in terms of correlation functions. From the autocorrelation function, a relaxation rate can be determined, which is directly proportional to the translational diffusion coefficient. With the assumption of random Brownian motion, the hydrodynamic radius of the dispersed nanogels can be calculated using the Stokes-Einstein equation

$$R_h = k_b T / 6\pi\eta D$$

where R_h is the hydrodynamic radius, k_b is the Boltzman constant, T is the temperature, η is the viscosity and D is the diffusion coefficient.
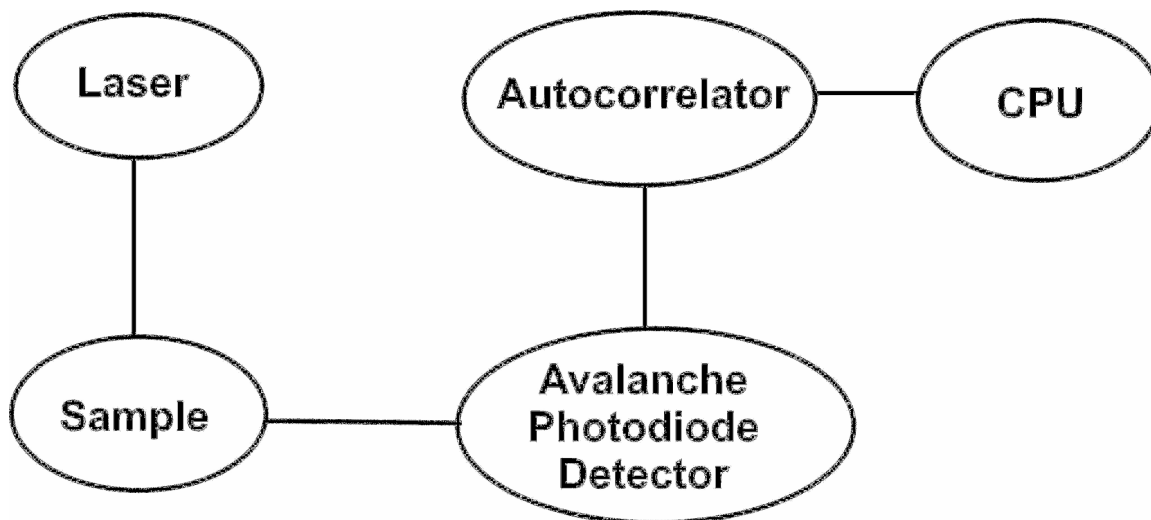
Figure 2.3. Schematic for DynaPro light scattering instrument used for measuring the particle size.

2.5 Tuning the LCST of pNIPAm Nanogels by Incorporating Comonomer

One can also incorporate comonomers in the nanogels, which can offer more functionality to the nanoparticles using the precipitation polymerization technique. Our group and others have copolymerized ionic monomers and hydrophobic monomers with pNIPAm to create nanogels with interesting properties.[13,31,35,37-40]

The hydrodynamic volume of the polymer decreases tremendously above the LCST of pNIPAm. This property makes nanogels based on this material potentially useful for many biological applications, such as in drug delivery, separation, energy transduction, and catalysis. However, many biological reactions, especially in the human body, have to be carried out around the physiological temperature of 37 °C, so the thermosensitive materials used for such applications should have a transition temperature near the human body temperature.

36

In an attempt to make nanogels useful for such applications and for other applications, which require tuning of the transition temperature, pNIPAm with other hydrophobic and hydrophilic comonomers have been synthesized and the effect of such comonomers on the transition temperature has been studied. Rearrangement of hydrogen bonds between polymer-solvent systems in combination with hydrophobic interactions of the side groups on the polymer chain strongly affects the temperature of phase separation. The general observation is that if the hydrophilicity of the comonomer is more than that of NIPAm, the LCST of the copolymer is increased. This effect can be seen in Figure 2.4 where addition of a more hydrophilic shell having copolymer like 2-hydroxyethyl methacrylate (HEMA) on the pNIPAm core nanogel decreases the LCST from 32 °C to 30 °C. Similar effects have been reported in the literature before.[41] Debord *et al.* copolymerized a hydrophobic comonomer *N-tert*-butylacrylamide (TBA) into pH/temperature responsive nanogels. These particles exhibit phase transitions at lower temperatures due to the increase in hydrophobicity of the gel, while retaining a pH tunable LCST.[40] Kawasaki *et al.* reported that the LCST of p(NIPAm-co-acrylamide) gels increased on increasing the amount of acrylamide in the copolymer.[42]
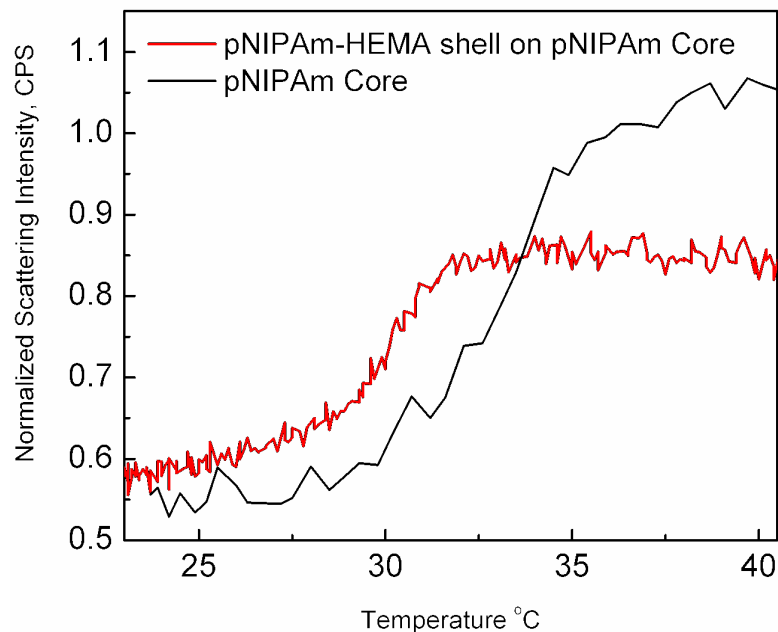
Figure 2.4. Effect of HEMA (hydrophilic comonomer) incorporation on the LCST of pNIPAm core nanogels.

Poly(NIPAm-co-NIPMAm) nanogels with varying mole % of NIPMAm have been synthesized by precipitation polymerization and the effect of increasing the NIPMAm mole % in the polymer was studied. On increasing the temperature above the LCST, an aqueous dispersion of the nanogels undergoes deswelling and the turbidity of the solution increases dramatically. Thus, the change in the turbidity of the nanogel dispersion in response to temperature can be monitored and used to obtain the LCST of the polymer network. The transmitted light intensity (turbidity) as a function of increasing temperature for the pNIPAm-co-NIPMAm nanogels is plotted in Figure 2.5. As seen from the turbidity measurement, increasing the amount of NIPMAm comonomer in the polymer increases the LCST of the copolymer network. Based on the structure of NIPMAm, one would expect that the phase transition temperature would decrease

significantly by successive addition of the hydrophobic methylene groups to the monomeric unit of the polymer. This is because it would increases the hydrophobicity of the polymer, which reduces the polymer-solvent interaction significantly.[43] However, despite the fact that pNIPMAm is more hydrophobic than pNIPAm, the demixing temperature of pNIPMAm is higher. An explanation for this behavior is possibly related to the conformation of the monomeric groups in pNIPMAm. The methyl group induces a steric hinderance such that the hydrophobic groups can not join together in the most favorable manner thus elevating the LCST to a higher temperature as compared with pNIPAm.[41]
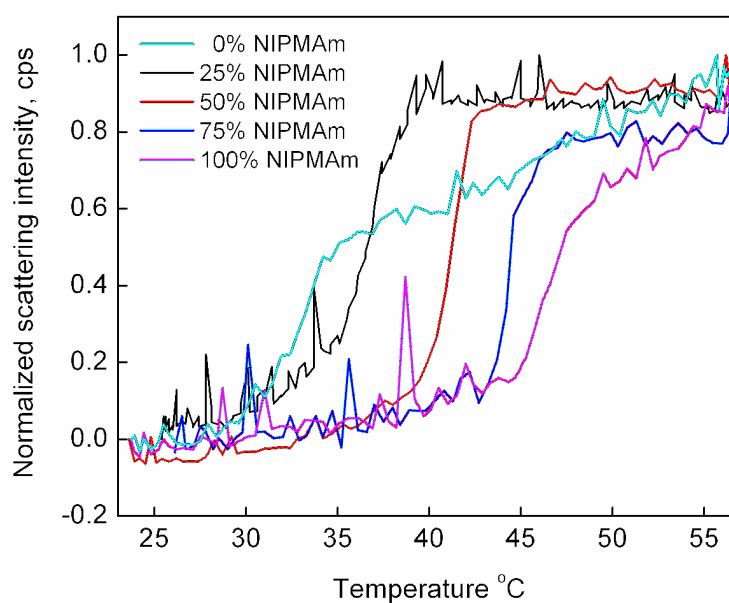
Figure 2.5. Effect of increasing NIPMAm mole % on the turbidity of pNIPAm based nanogels.

Table 2.1 reports the hydrodynamic radii (obtained from PCS) and the deswelling ratios of the nanogels synthesized with varying mole % of NIPMAm in the polymer. Comparison of the deswelling ratios can provide insight about the rigidity of the polymer network. In general as the network becomes more rigid the deswelling ratio decreases. Figure 2.6 shows a plot of the deswelling ratio with increasing mole % of NIPMAm composition in the polymer. The data does not suggest any significant decrease in the deswelling ratio on increasing the mole % of NIPMAm, indicating that the steric hinderance due to the methylene group does not significantly affect the rigidity of the polymer network.

Table 2.1. Hydrodynamic Radii Obtained by PCS for pNIPAm-co-NIPMAm Nanogels.

Sample % NIPMAm	Radius[a] (nm) 25 °C	Radius[a] (nm) 45 °C	Radius[a] (nm) 50 °C	Deswelling ratio R_{50}/R_{25}
0	101 ± 1.29	43 ± 0.97	47 ± 3.55	0.4678 ± 0.03
25	143 ± 3.04	66 ± 0.89	66 ± 1.20	0.4597 ± 0.001
50	196 ± 2.05	84 ± 0.52	82 ± 1.37	0.4189 ± 0.002
75	157 ± 3.24	100 ± 0.79	65 ± 0.58	0.4112 ± 0.005
100	158 ± 5.83	141 ± 0.11	62 ± 1.39	0.3937 ± 0.006

[a]Average of three measurements. The error is the standard deviation in the measurements.
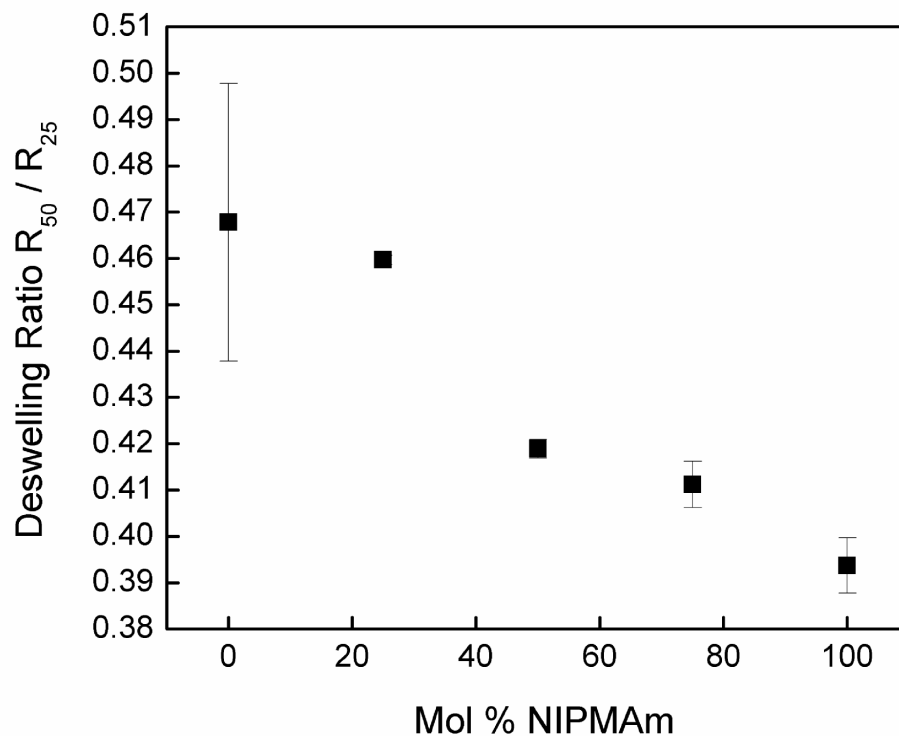
Figure 2.6. Deswelling ratio of pNIPAm-based nanogels as a function of NIPMAm comonomer molar ratio.

Thus from Figure 2.7 it can be seen that just by using NIPMAm as the copolymer and by controlling the composition of the two monomers in the copolymer, the phase transition temperature can be adjusted between 32 °C and 48 °C. So, thermosensitive nanogels with a phase transition temperature near the human temperature of 37 °C in water can be made using this strategy.
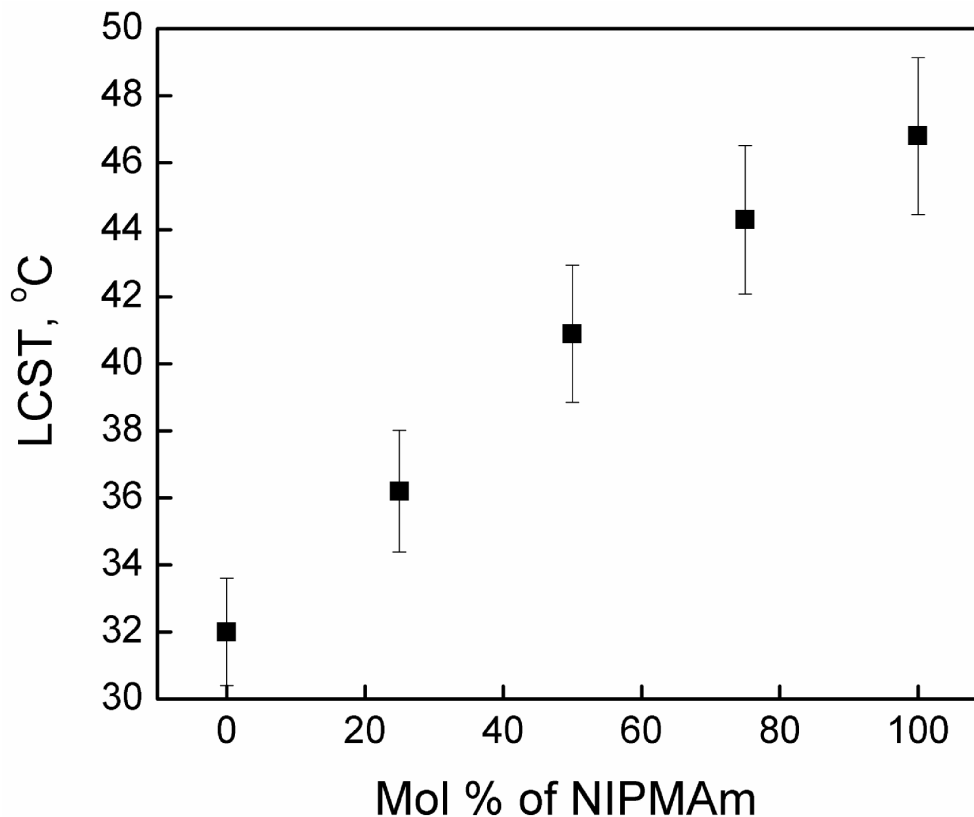
Figure 2.7. Effect of increasing NIPMAm comonomer composition on the LCST of pNIPAm-based nanogels.

Hydrogel nanoparticles have been synthesized by numerous approaches. This chapter described basic synthesis and characterization of thermoresponsive pNIPAm nanogels and gave a broad overview of how the properties of these materials can be tuned by varying the composition (e.g. comonomer). The synthetic methods described in this chapter have enabled the field to advance towards the application of hydrogel nano- and microparticles in more complex biotechnological and nanotechnological applications. However, to be able to use these materials to their full potential new synthetic strategies need to be developed so that nanogels with higher complexity and integration with biosystems can be easily obtained. The remaining chapters of this dissertation will focus

on the synthesis and characterization of various synthetically and topologically complex nanogels that have potential to be successfully incorporated into advanced nanosystems and bionanosystems. The synthetic strategies described in the following chapters are advances of the fundamental synthetic technique of precipitation polymerization introduced in this chapter.

2.6 References and Notes

[1]   Ganachaud, F.; Monteiro, M. J.; Gilbert, R. G.; Dourges, M.-A.; Thang, S. H.; Rizzardo, E. Molecular Weight Characterization of Poly(N-isopropylacrylamide) Prepared by Living Free-Radical Polymerization. *Macromolecules* **2000**, *33*, 6738-6745.

[2]   Masci, G.; Giacomelli, L.; Crescenzi, V. Atom transfer radical polymerization of N-isopropylacrylamide. *Macromolecular Rapid Communications* **2004**, *25*, 559-564.

[3]   Ray, B.; Isobe, Y.; Matsumoto, K.; Habaue, S.; Okamoto, Y.; Kamigaito, M.; Sawamoto, M. RAFT polymerization of N-isopropylacrylamide in the absence and presence of Y(OTf)3: simultaneous control of molecular weight and tacticity. *Macromolecules* **2004**, *37*, 1702-1710.

[4]   Schilli, C.; Lanzendoerfer, M. G.; Mueller, A. H. E. Benzyl and cumyl dithiocarbamates as chain transfer agents in the RAFT polymerization of N-isopropylacrylamide. In situ FT-NIR and MALDI-TOF MS investigation. *Macromolecules* **2002**, *35*, 6819-6827.

[5]   Pelton, R. H.; Chibante, P. Preparation Of Aqueous Lattices With N-Isopropylacrylamide. *Colloids Surface.* **1986**, *20*, 247-256.

[6]   Pelton, R. Temperature-sensitive aqueous microgels. *Adv. Colloid. Interface Sci.* **2000**, *85*, 1-33.

[7]   Neyret, S.; Vincent, B. The properties of polyampholyte microgel particles prepared by microemulsion polymerization. *Polymer* **1997**, *38*, 6129-6134.

[8]   McAllister, K.; Sazani, P.; Adam, M.; Cho, M. J.; Rubinstein, M.; Samulski, R. J.; DeSimone, J. M. Polymeric nanogels produced via inverse microemulsion polymerization as potential gene and antisense delivery agents. *J. Am. Chem. Soc.* **2002**, *124*, 15198-15207.

[9]   Kazakov, S.; Kaholek, M.; Kudasheva, D.; Teraoka, I.; Cowman, M. K.; Levon, K. Poly(N-isopropylacrylamide-co-1-vinylimidazole) hydrogel nanoparticles prepared and hydrophobically modified in liposome reactors: Atomic force microscopy and dynamic light scattering study. *Langmuir* **2003**, *19*, 8086-8093.

[10]   Kim, K. H.; Kim, J.; Jo, W. H. Preparation of hydrogel nanoparticles by atom transfer radical polymerization of N-isopropylacrylamide in aqueous media using PEG macro-initiator. *Polymer* **2005**, *46*, 2836-2840.

[11]   Dingenouts, N.; Seelenmeyer, S.; Deike, I.; Rosenfeldt, S.; Ballau, M.; Lindner, P.; Narayanan, T. Analysis of thermosensitive core-shell colloids by small-angle neutron scattering including contrast variation. *Phys. Chem. Chem. Phys.* **2001**, *3*, 1169-1174.

[12]   Xiao, X. C.; Chu, L. Y.; Chen, W. M.; Wang, S.; Xie, R. Preparation of submicrometer-sized monodispersed thermoresponsive core-shell hydrogel microspheres. *Langmuir* **2004**, *20*, 5247-5253.

[13]   Jones, C. D.; Lyon, L. A. Synthesis and Characterization of Multiresponsive Core-Shell Microgels. *Macromolecules* **2000**, *33*, 8301-8306.

[14]   Jones, C. D.; Lyon, L. A. Dependence of shell thickness on core compression in acrylic acid modified poly(N-isopropylacrylamide) core/shell microgels. *Langmuir* **2003**, *19*, 4544-4547.

[15]   Jones, C. D.; Lyon, L. A. Shell-Restricted Swelling and Core Compression in Poly(N-Isopropylacrylamide) Core-Shell Microgels. *Macromolecules* **2003**, *36*, 1988-1993.

[16]   Gan, D.; Lyon, L. A. Tunable Swelling Kinetics in Core-Shell Hydrogel Nanoparticles. *J. Am. Chem. Soc.* **2001**, *123*, 7511-7517.

[17]   Gan, D.; Lyon, L. A. Interfacial Nonradiative Energy Transfer in Responsive Core-Shell Hydrogel Nanoparticles. *J. Am. Chem. Soc.* **2001**, *123*, 8203-8209.

[18]   Gan, D.; Lyon, L. A. Fluorescence nonradiative energy transfer analysis of crosslinker heterogeneity in core-shell hydrogel nanoparticles. *Anal. Chim. Acta* **2003**, *496*, 53-63.

[19]   Jones, C. D.; McGrath, J. G.; Lyon, L. A. Characterization of Cyanine Dye-Labeled Poly(N-isopropylacrylamide) Core/Shell Microgels Using Fluorescence Resonance Energy Transfer. *J. Phys. Chem. B* **2004**, *108*, 12652-12657.

[20]   Berndt, I.; Richtering, W. Doubly Temperature Sensitive Core-Shell Microgels. *Macromolecules* **2003**, *36*, 8780-8785.

[21]   Berndt, I.; Pedersen, J. S.; Richtering, W. Structure of Multiresponsive "Intelligent" Core-Shell Microgels. *J. Am. Chem. Soc.* **2005**, *127*, 9372-9373.

[22]   Jones, C. D.; Lyon, L. A. Synthesis and characterization of multiresponsive core-shell microgels. *Macromolecules* **2000**, *33*, 8301-8306.

[23]   Berndt, I.; Pedersen, J. S.; Richtering, W. Temperature-sensitive core-shell microgel particles with dense shell. *Angew. Chem., Int. Ed.* **2006**, *45*, 1737-1741.

[24]   Gan, D.; Lyon, L. A. Interfacial nonradiative energy transfer in responsive core-shell hydrogel nanoparticles. *J. Am. Chem. Soc.* **2001**, *123*, 8203-8209.

[25]   Jones, C. D.; Lyon, L. A. Shell-Restricted Swelling and Core Compression in Poly(N-isopropylacrylamide) Core-Shell Microgels. *Macromolecules* **2003**, *36*, 1988-1993.

[26]   Jones, C. D.; McGrath, J. G.; Lyon, L. A. Characterization of Cyanine Dye-Labeled Poly(N-isopropylacrylamide) Core/Shell Microgels Using Fluorescence Resonance Energy Transfer. *J. Phys. Chem. B* **2004**, *108*, 12652-12657.

[27]   Gan, D. J.; Lyon, L. A. Tunable swelling kinetics in core-shell hydrogel nanoparticles. *J. Am. Chem. Soc.* **2001**, *123*, 7511-7517.

[28]   Gan, D. J.; Lyon, L. A. Fluorescence nonradiative energy transfer analysis of crosslinker heterogeneity in core-shell hydrogel nanoparticles. *Anal. Chim. Acta* **2003**, *496*, 53-63.

[29]   Gan, D. J.; Lyon, L. A. Interfacial nonradiative energy transfer in responsive core-shell hydrogel nanoparticles. *J. Am. Chem. Soc.* **2001**, *123*, 8203-8209.

[30]   Nayak, S.; Gan, D.; Serpe, M. J.; Lyon, L. A. Hollow thermoresponsive microgels. *Small* **2005**, *1*, 416-421.

[31]   Kratz, K.; Hellweg, T.; Eimer, W. Influence of charge density on the swelling of colloidal poly(N-isopropylacrylamide-co-acrylic acid) microgels. *Colloids Surf., A* **2000**, *170*, 137-149.

[32]   Crowther, H. M.; Saunders, B. R.; Mears, S. J.; Cosgrove, T.; Vincent, B.; King, S. M.; Yu, G. E. Poly(NIPAM) microgel particle de-swelling: a light scattering and small-angle neutron scattering study. *Colloids Surf. A* **1999**, *152*, 327-333.

[33]   Bouillot, P.; Vincent, B. A comparison of the swelling behaviour of copolymer and interpenetrating network microgel particles. *Colloid Polym. Sc.* **2000**, *278*, 74-79.

[34]   Crowther, H. M.; Vincent, B. Swelling behavior of poly N-isopropylacrylamide microgel particles in alcoholic solutions. *Colloid Polym. Sci.* **1998**, *276*, 46-51.

[35]   Snowden, M. J.; Chowdhry, B. Z.; Vincent, B.; Morris, G. E. Colloidal copolymer microgels of N-isopropylacrylamide and acrylic acid: pH, ionic strength and temperature effects. *J. Chem. Soc.-Faraday Trans.* **1996**, *92*, 5013-5016.

(36)   Kratz, K.; Lapp, A.; Eimer, W.; Hellweg, T. Volume transition and structure of triethyleneglycol dimethacrylate, ethylenglykol dimethacrylate, and N,N '-methylene bis-acrylamide cross-linked poly(N-isopropyl acrylamide) microgels: a small angle neutron and dynamic light scattering study. *Colloids Surf. A* **2002**, *197*, 55-67.

[37]   Kratz, K.; Hellweg, T.; Eimer, W. Effect of connectivity and charge density on the swelling and local structural and dynamic properties of colloidal PNIPAM microgels. *Ber. Bunsen-Ges.* **1998**, *102*, 1603-1608.

[38]   Zhou, S.; Chu, B. Synthesis and Volume Phase Transition of Poly(methacrylic acid-co-N-isopropylacrylamide) Microgel Particles in Water. *J. Phys. Chem. B* **1998**, *102*, 1364-1371.

[39]   Suzuki, H.; Wang, B.; Yoshida, R.; Kokufuta, E. Potentiometric Titration Behaviors of a Polymer and Gel Consisting of N-Isopropylacrylamide and Acrylic Acid. *Langmuir* **1999**, *15*, 4283-4288.

[40]   Debord, J. D.; Lyon, L. A. Synthesis and Characterization of pH Responsive Copolymer Microgels with Tunable Volume Phase Transition Temperatures. *Langmuir* **2003**, *19*, 7662-7664.

[41]   Djokpe, E.; Vogt, W. N-isopropylacrylamide and N-isopropylmethacrylamide: Cloud points of mixtures and copolymers. *Macromol. Chem. Phys.* **2001**, *202*, 750-757.

[42]   Kawasaki, H.; Sasaki, S.; Maeda, H. Effect of introduced electric charge on the volume phase transition of N-isopropylacrylamide gels. *J. Phys. Chem. B* **1997**, *101*, 4184-4187.

[43]   Seker, F.; Ellis, A. B. Correlation of chemical structure and swelling behavior in N-alkylacrylamide hydrogels. *J. Polym. Sci., Part A: Polym. Chem.* **1998**, *36*, 2095-2102.

CHAPTER 3

AU NANOPARTICLE TEMPLATED SYNTHESIS OF PNIPAM NANOGELS

In this chapter we have explored a synthetic route towards sub-50 nm poly(*N*-isopropylacrylamide) (pNIPAm) nanogels by growing a pNIPAm shell onto a metal nanoparticle seed. Nuclei compatible with precipitation polymerization of thermoresponsive polymers were formed by adsorption of NH_2-terminated pNIPAm on Au nanoparticles. The adsorbed pNIPAm layer, when heated above the LCST, collapses onto the Au nanoparticle surface. This polymer layer thus serves as a hydrophobic nucleus for growing pNIPAm oligoradicals during polymer synthesis, resulting in the formation of a pNIPAm shell. Etching of the Au core from the polymer coated particles with KCN results in hollow hydrogel nanoparticles. The rate of Au core etching as studied by the decrease in Au nanoparticle plasmon absorbance was shown to depend on polymer shell composition, shell thickness, and the thermosensitivity of the polymer. Efficient quenching of fluorophores incorporated in the polymer shell by the core Au nanoparticles was observed, however, the shell fluorescence was regained after core

dissolution. Future studies are aimed at understanding the encapsulation of small molecules and proteins within the nanocapsule structure.

3.1 Introduction

The synthesis and application of small hollow polymeric nanoparticles for drug delivery and protein/enzyme encapsulation is an expanding area of research.[1-4] For applications in this area, good control over size at the nanometer scale and low size dispersity is highly desirable. Also required is the ease of conjugation of these nanoparticles to biological macromolecules and their assembly into higher order structures. With advances in the synthesis of polymeric nanoparticles, researchers have designed various interesting architectures, one being the core/shell structure, which can provide a robust platform for incorporating multiple orthogonal functionalities into a nanoparticle.[5]

An interesting subclass of polymeric nanoparticles is responsive hydrogel nanoparticles (or nanogels), which are useful in a wide range of applications on account of their stimuli-sensitive phase transition behavior. One of the most commonly studied thermoresponsive polymers is poly(*N*-isopropylacrylamide) (pNIPAm), which undergoes a phase transition from a hydrophilic, water swollen state to a hydrophobic, globular state when heated to above its lower critical solution temperature (LCST) which is about 31 $^{\circ}$C in water. Incorporation of other co-monomers can produce a wide variety of stimuli responsivities such as pH, ionic-strength and light. Our group and many others have extensively studied the synthesis, characterization and applications of such stimuli-responsive materials.[6-8]

In the past, methods towards the production of sub-50 nm polymer particles have utilized cross-linking of block co-polymer micelles, metathesis polymerization of covalently bound monomer monolayers, surface initiated polymerization of monomers in solution and layer-bylayer adsorption of polyelectrolytes on spherical nanoparticles using metal templating method.[9-21] Metal templating is a widely used approach to synthesize hollow nanoparticles. Here, a metal template of desired size can be used to grow a polymer shell, which can be followed by metal dissolution to yield stable hollow polymeric nanoparticles. In this procedure, the size of the inner cavity is basically the diameter of the metal nanoparticles used as the template. Recently, Lee and coworkers synthesized hydrogel coated Au nanoparticles using such a metal templating approach. They used Au nanoparticles, 60-nm in diameter, as the template and grew a pNIPAm shell by surfactant-free-emulsion polymerization.[22] In another example, Fu and coworkers synthesized pNIPAm microcontainers using silica nanoparticle templates.[23] These methods, however, yielded large nanoparticles with radii in the range of 100-200 nm; this size range is typically regarded as not appropriate for many applications in targeted gene and drug delivery. Thus there still exists a need to develop an *in-situ* free-radical polymerization method for yielding colloidally stable hollow nanogels with good synthetic control over the properties and dimensions in the nanometer range.

In this report, we describe a strategy for synthesizing hollow nanogels based on the widely used sacrificial metal nanoparticle templating method. We have combined the metal templating approach with a "seed and feed" method previously used by our group to synthesize hydrogel nanoparticles.[24] The "seed and feed" method involves the initial formation of hydrophobic polymer nuclei, which act as seeds for the precipitation of the

growing polymer (feed) chains. When the polymerization conditions are maintained above the polymer's LCST, the growing polymer chains phase separate and collapse onto the hydrobhobic nuclei to form a cross-linked polymer shell around the core nanoparticle. In order to make hydrogels with sizes in the range of sub-50 nm, it was envisioned that the use of a small metal nanoparticles based hydrophobic nucleus can facilitate the formation of a polymer shell with nanometer dimensions. The synthetic route towards the formation of small hollow pNIPAm nanogels involves the *in situ* polymerization of NIPAm onto Au nanoparticles followed by the dissolution of the Au core as depicted in Scheme 3.1. This approach can be generalized to synthesize nanogels with the varied sizes and compositions needed for a variety of applications ranging from sensors to cellular biology as well as delivery vehicles.
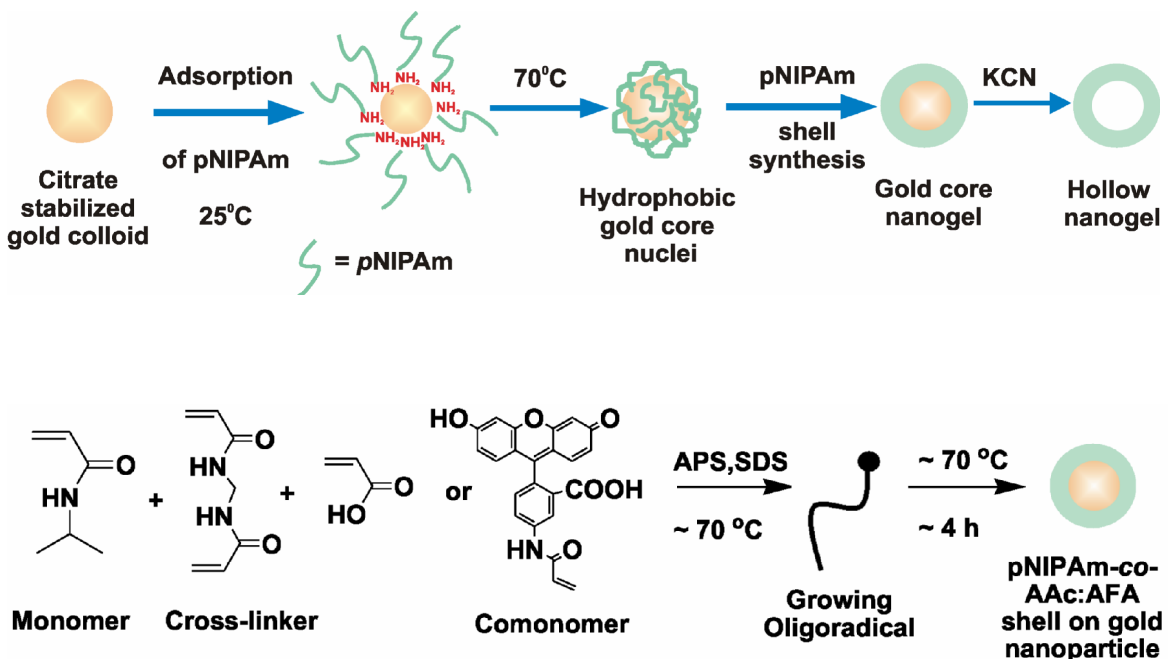
Scheme 3.1. Au nanoparticle-templated synthesis of pNIPAm nanogels via aqueous free radical precipitation polymerization.

3.2 Experimental Section

3.2.1 Materials

Most of the materials used in this Chapter can be found in Chapter 2. Those not listed in Chapter 2 but used here were also obtained from Sigma Aldrich unless otherwise specified. Amino terminated pNIPAm with M_n of 10 400 was obtained from Polymer Source Inc. Acetate buffer solution (pH 5.4, 10 mM) was prepared from acetic acid and NaCl obtained from Fischer.

3.2.2 Au Nanoparticle Synthesis

Au colloids were prepared according to a procedure developed by Natan and coworkers.[25] All glassware was purified in aqua regia (3 parts HCl, 1 part HNO$_3$) [Caution! aqua regia is corrosive in nature and should be handled with care], and rinsed with deionized water (DI water) before use. First, 500 mL of 0.01% HAuCl$_4$ was brought to boil with vigorous stirring in a round-bottom flask equipped with a condenser. To this solution, 7.5 mL of 1% sodium citrate was added and an instant color change from blue to red-violet was observed. After boiling for 10 min the solution was cooled while stirring for an additional 15 min. Note that transmission electron microscopy (TEM) images of the synthesized colloid showed particles with a mean diameter of 12-nm, while a larger size (mean hydrodynamic radius of 12-nm at 25 °C) was obtained by photon correlation spectroscopy (PCS) measurements.

3.2.3 Nanogel Synthesis

To form hydrophobic Au nuclei, the Au colloid was incubated with NH$_2$-terminated pNIPAm. To determine the amount of NH$_2$-terminated pNIPAm required to

cover the surface of the Au nanoparticles, the following assay was performed (Figure 3.1): 500 μL of 1 M NaCl solution was added to 500 μL of Au colloid solution (depicted as red solution in Figure 3.1) after the Au colloid had been incubated overnight with different volumes of 0.1 mM NH$_2$-terminated pNIPAm. The solutions were then kept on a shaker table for 10 min at room temperature. The Au nanoparticle aggregation (depicted by blue solution in figure 3.1) was monitored by UV-Vis spectroscopy by observing the position and shape of the plasmon absorbance peak (*vide infra*). For the synthesis of the Au core nuclei, Au nanoparticles were mixed on a shaker table with appropriate amount of NH$_2$-terminated pNIPAm, as determined by the aggregation assay and allowed to incubate with shaking overnight. The solution was purified by centrifugation to remove any non-adsorbed NH$_2$-terminated pNIPAm followed by resuspension in DI water. The polymer adsorbed Au nanoparticles were then heated to ~70 °C under a N$_2$ atmosphere and stirred in a glass vial pre-cleaned with aqua-regia. A filtered (using a 0.2 μm membrane filter), aqueous solution of appropriate amount of monomer NIPAm, crosslinker *N,N*-methylenebis(acrylamide) (BIS) and 65 μL of 0.1 M aqueous solution of surfactant, sodium dodecyl sulfate (SDS) was added to the reaction vial. After 1 h, the reaction was initiated by injection of 130 μL of 0.1 M ammonium persulfate (APS) solution and the reaction (total volume = 10 mL) was kept at 70 °C for 4 hours. The co-monomers acrylic acid (AAc) or 4-acrylamido-fluorescein (AFA) were added just before the reaction initiation to synthesize pNIPAm-*co*-AAc or fluorescent pNIPAm-*co*-AFA nanogels. A molar composition of 85% monomer, 5% cross-linker and 10% co-monomer was used. The total monomer concentration used in the shell synthesis was 0.25 mM, 0.5

mM, or 1.0 mM. The synthesized Au core nanogels were purified by several cycles of centrifugation/resuspension.
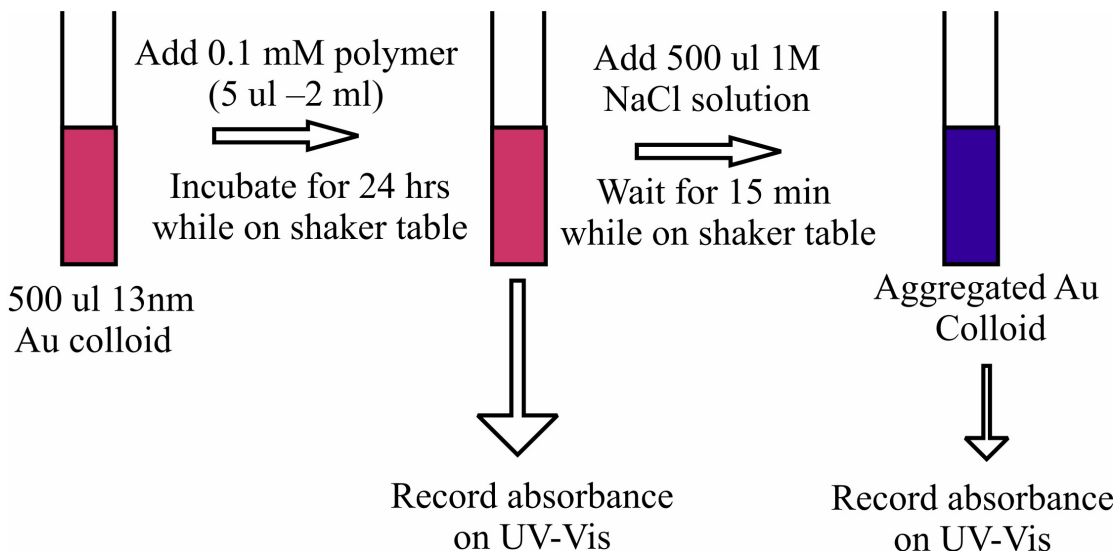
Figure 3.1. Assay procedure to determine the amount of NH_2-terminated pNIPAm required to cover the surface of the Au nanoparticles.

3.2.4 Dissolution of the Au core

Following shell synthesis, the template Au cores were dissolved by adding 0.1 M KCN solution to a clean Au core nanogel solution while stirring. The core dissolution was monitored by the disappearance of the Au plasmon absorption band using UV-Vis spectroscopy. For studying the etching rate, 1 mL of the Au core nanogel solution was etched using 0.5 mL of a 0.1 M KCN solution. Etching was also studied at a higher temperature by monitoring the etching of the nanogel solution (equilibrated for 30 min at 45 ^{o}C) after addition of the KCN solution, which was also maintained at 45 ^{o}C. The hollow nanogels were then purified by dialysis using Spectra/Por 10,000 MWCO dialysis

membrane (VWR) against DI water for ~2 weeks with the water being changed twice per day.

3.2.5 UV-vis Spectroscopy

All absorption spectra were obtained in quartz cuvettes using a Shimadzu UV 1601 spectrophotometer equipped with a recirculating water bath-based temperature controller.

3.2.6 Photon Correlation Spectroscopy

Particle sizes were determined by photon correlation spectroscopy (PCS, Protein Solution Inc.) equipped with an integrated Peltier temperature control device, which gives temperature accuracy within $\pm$ 0.1 ^{o}C. The instrument collects scattered light at 90° with a single-mode optical fiber coupled to an avalanche photodiode detector. The samples were thermally equilibrated at each temperature for 10 min before measurement. The data presented is an average of at least 15 measurements with acquisition time of 10 s. The hydrodynamic radii of the particles were calculated from the diffusion coefficients using the Stokes-Einstein equation. All the data analysis was done using Dynamic Software version 5.25.44 provided by Protein Solutions Inc.

3.2.7 Transmission Electron Microscopy

The synthesized nanoparticles were imaged on a JEOL 100CX II (100 kV) transmission electron microscope (TEM). All TEM samples were prepared by casting a drop of the nanoparticle solution (diluted 10 times) on a Formvar-coated Cu TEM grid (Ted Pella) placed on a Kimwipe. The grid was then dried overnight at ambient temperature. For the imaging of the hydrogel nanoparticles following core etching, the

AAc groups in the polymer shell were stained with an electron microscopy contrast agent. Briefly, 0.050 mL of 1 mM pNIPAm-*co*-AAc nanogels following dissolution of the gold cores and dialysis were mixed with 0.5 mL of 1 mM uranyl acetate (Polysciences) and stirred for 1 h.

3.2.8 Atomic Force Microscopy

All the images were obtained in AC mode on an Asylum Research MFP-3D atomic force microscope (AFM). Spring constants were calculated using the thermal method. Imaging and analysis was performed using the Asylum Research MFP-3D software (IgorPro, WaveMetrics, Inc., Lake Oswego, OR). An Olympus AC160 cantilever with k = 42 N/m, f_0 = 300 kHz was used for imaging. AFM samples were prepared by casting a drop of the sample on micro cover glass slips (VWR) and drying overnight. Images were also obtained on cationic glass cover slips. Briefly, glass cover slips were first treated in an Ar plasma (Harrick Scientific) for 30 min followed by immersion of the glass substrate in 1% 3-aminopropyltrimethoxysilane solution in absolute ethanol (200 proof) for ~2 hrs. They were rinsed several times with 95% ethanol followed by rinsing with DI water and drying in a stream of N_2 gas. One drop of 1 mM pNIPAm-*co*-AAc nanoparticle solution was cast onto the functionalized glass substrate. After 15 min, the substrate was immersed in DI water for 2 hrs, rinsed with DI water, and dried with N_2 gas, leaving behind nanoparticles that are strongly attached to the cationic substrate by Coulombic interactions.

3.2.9 Dithiol Aggregation Studies

To prepare samples for dithiol induced aggregation, 0.5 mL of the bare Au colloid and the clean Au core nanogels were centrifuged and redispersed in 0.5 mL ethanol. A

0.1 mL sample of 1,6-hexanedithiol dissolved in 0.4 mL ethanol was added to the solutions, which were then agitated on a shaker table. The solutions were monitored by UV-vis spectroscopy to observe the changes in the Au plasmon band at various time intervals.

3.2.10 Fluorescence Spectroscopy

All emission measurements were done using Photon Technology International fluorescence spectrophotometer, equipped with a Model 814 PMT photon-counting detector. The slits were adjusted to achieve a spectral bandwidth of 2 nm and the spectra were obtained with a 1 nm step size and a 1 s integration time. The samples were excited at a wavelength of 478 nm.

3.3 Results and Discussion

Citrate stabilized Au nanoparticles synthesized by the reduction of $HAuCl_4$ were used for the formation of polymerization seeds due to the ease of their preparation and characterization. The UV-vis spectra for the synthesized colloid showed an absorption band with a maximum around 518 nm due to the well known surface plasmon resonance of spherical Au nanoparticles.[26] Seeds compatible with the precipitation polymerization of NIPAm were formed by the adsorption of a layer of amino-terminated pNIPAm onto the Au nanoparticles.[27,28] When heated to 70 °C (above the LCST of pNIPAm) the adsorbed pNIPAm layer collapses onto the Au nanoparticle surface, thus serving as a hydrophobic nucleus for the subsequent precipitation polymerization step. In order to avoid the formation of separate hydrophobic nuclei from any excess pNIPAm in solution

(not adsorbed on Au), we determined the minimum amount of polymer required for surface coverage of the Au nanoparticles. It is well known that citrate stabilized Au nanoparticles tend to aggregate on the addition of NaCl resulting in the red-shift of the nanoparticle absorption band, whereas protein or polymer-protected Au nanoparticles resist salt-induced aggregation. The minimum amount of NH_2-terminated pNIPAm required for complete surface coverage of the Au nanoparticles was determined by monitoring the resistance of the Au colloid towards NaCl induced aggregation by following the red shift in the plasmon absorbption band. Onto these polymer-stabilized Au nanoparticles, pNIPAm shells were synthesized by free radical polymerizaton as described in the experimental section. In order to form pH-responsive nanogel particles, acrylic acid (AAc) was used as co-monomer. It should be noted that the amount of monomer used for the synthesis was also kept at very low concentrations to avoid the formation of separate (non-Au containing) nuclei in the reaction solution.

Due to the presence of Au cores it is easy to characterize the synthesized nanogels by UV-vis spectroscopy. The absorption spectra of the Au nanoparticles before and after shell synthesis are shown in Figure 3.2a. The plasmon band for the Au-core nanogels has a maximum (λ_{max}) around 526 nm. There was no evidence of aggregation of the Au colloid after the polymer shell synthesis. The plasmon absorption band reflects an isolated Au nanoparticle core encapsulated by a polymer shell rather than multiple Au particles trapped in close proximity within the polymer gel. A slight red shift in the plasmon band is observed due to an increase in the refractive index around the Au nanoparticle due to the polymer shell ($RI_{polymer} > RI_{water}$).[29]
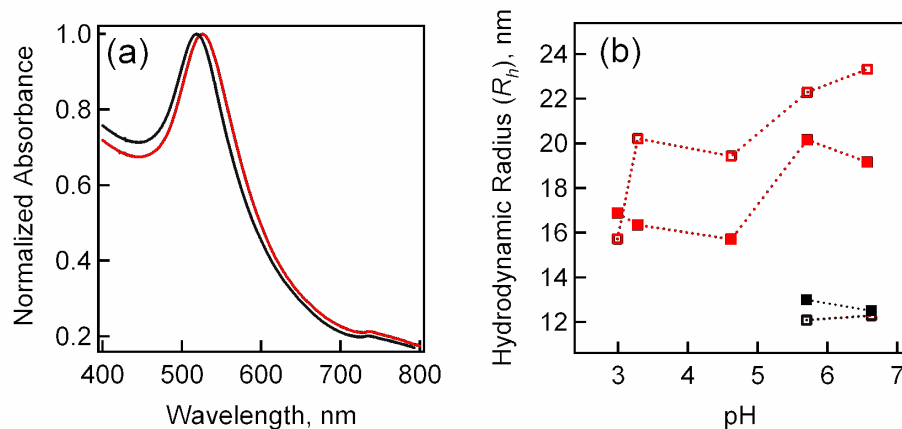
Figure 3.2. (a) Absorption spectra of the Au nanoparticles before (black) and after pNIPAm-*co*-AAc shell synthesis (red). (b) Plot of hydrodynamic radius versus pH at 25 °C (open squares) and 45 °C (filled squares) for Au nanoparticles before (black) and after pNIPAm-*co*-AAc shell synthesis (red).

Particle size (via PCS) measurements of the nanogels revealed a mean hydrodynamic radius (R_h) ranging from 20 to 80 nm depending on the monomer concentration used in synthesis. The pNIPAm-*co*-AAc coated Au nanoparticles show a decrease in size at high temperature and low pH (Figure 3.2b) as a result of the dual (pH and temperature) responsivity of the hydrogel. Note that the uncoated Au nanoparticles (black symbols) aggregated at low pH due to the presence of salt in the buffer solution. However, the nanogels showed no aggregation under any of the studied conditions, suggesting that the Au cores in these particles were well protected.

The nanogels were also stable to more effective aggregating agents such as 1,6-hexanedithiol. These results further confirm the passivating nature of the cross-linked pNIPAm shell (Figure 3.3a). The uncoated Au nanoparticles, on addition of 1,6-hexanethiol (Figure 3.3b), show a greatly red-shifted absorption spectrum with

diminished intensity, indicating extensive particle aggregation. On the other hand, the Au-core nanogel solution shows very limited aggregation (Figure 3.3a). The slight changes in peak breadth observed here may be due to some amount of non-polymer-coated Au nanoparticles remaining in the solution. Interestingly, the aggregation with hexanedithiol could therefore be used as a method for separating non-polymer-coated Au nanoparticles from the nanogels following synthesis, which is otherwise difficult to accomplish via centrifugation.
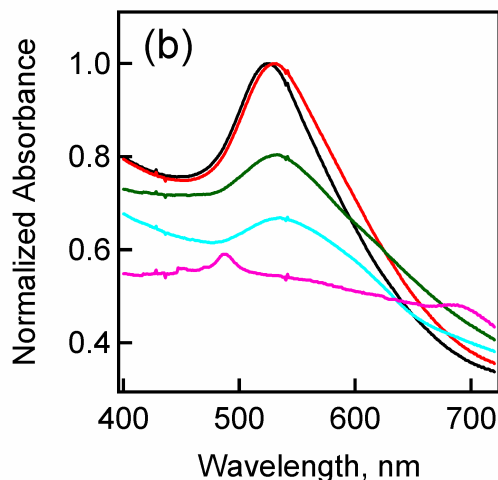
Figure 3.3. Change in absorption spectra following addition of 1,6-hexanedithiol for (a) Au core nanogels and (b) bare Au nanoparticles. Spectra were obtained over time: initial spectrum (black), t = 0 min (red), t = 5 min (green), t = 15 min (cyan), t = 30 min (magenta), and t = 1 hr (blue).

Nanogels of pNIPAm and pNIPAm-*co*-AAc with different shell thicknesses (Table 3.1) were synthesized by varying the total monomer concentration (0.25 mM, 0.5 mM and 1 mM) while keeping the cross-linker (5 mol%) and co-monomer (10 mol%

AAc) percentage, surfactant and initiator concentrations the same across all batches. Nanogels with AAc co-monomer in the polymer shell were larger in size (R_h) as compared to nanoparticles without AAc at the same total monomer concentration. This size difference could be due to the repulsive interaction between the charged carboxyl groups in the AAc shell or the greater free energy of mixing with water due to the more hydrophilic nature of the pNIPAm-*co*-AAc polymer.

Table 3.1. Hydrodynamic Radii (R_h) Determined by PCS.

Total Monomer Concentration (mM)	pNIPAm Nanogels[a] (in DI water)		pNIPAm-*co*-AAc Nanogels[a] (in pH 5.4 buffer solution)	
	Average[b] R_h at 25 $^{\circ}$C (nm)	Average[b] R_h at 45 $^{\circ}$C (nm)	Average[b] R_h at 25 $^{\circ}$C (nm)	Average[b] R_h at 45 $^{\circ}$C (nm)
0.25	15 ± 1	13 ± 1	19 ± 2	18 ± 1
0.50	23 ± 2	16 ± 0.3	27 ± 2	19 ± 0.2
1.00	30 ± 1	19 ± 0.4	39 ± 3	27 ± 1

[a] The nanogels contain a Au core with R_h of 12 ± 0.6 nm at 25 $^{\circ}$C and 13 ± 0.3 nm at 45 $^{\circ}$C.

[b] Average of three measurements.

To obtain hollow nanogels from the Au core nanogels, the Au was dissolved by the addition of a 0.1 M KCN solution. Gold etching occurs via transport of the etchant (cyanide ion) through the polymer shell to the core, where Au^0 is converted to $[Au(CN)_4]^-$ in the presence of oxygen.[30,31] The Au core etching was followed by a loss of the Au

plasmon absorbance. An example of core etching for Au core pNIPAm nanoparticles synthesized using a 0.5 mM total monomer concentration, has been shown in Figure 3.4.
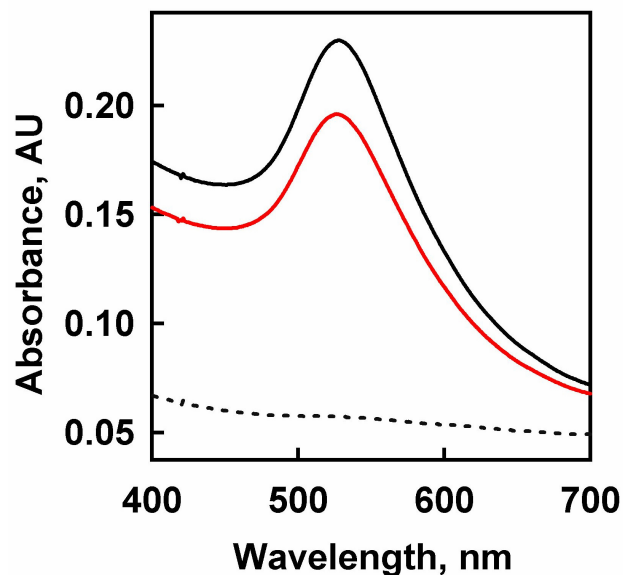
Figure 3.4. Decrease in Au plasmon absorbance after adding KCN to Au core pNIPAm nanoparticles synthesized using a 0.5 mM total monomer concentration. The spectrum shown in black was obtained before KCN addition, whereas the spectrum shown in red was taken immediately (<20 seconds) after addition. The spectrum shown as a black dashed line was obtained after one day.
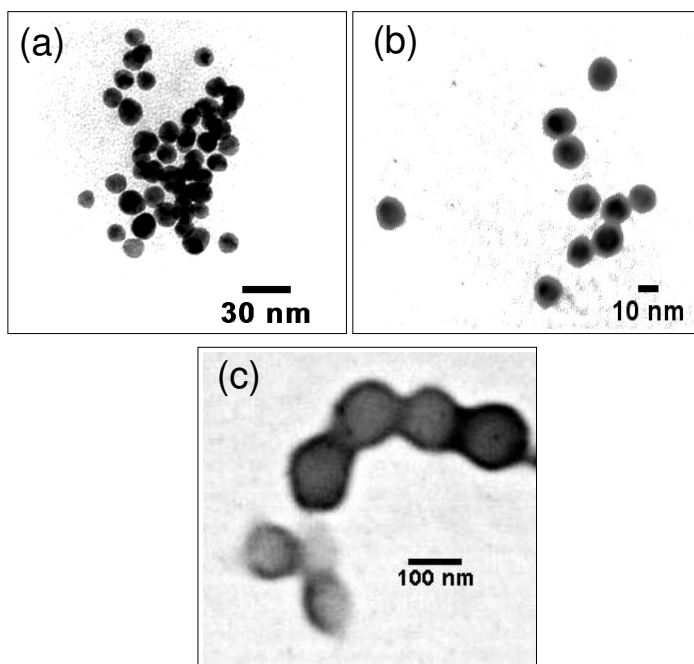
Figure 3.5. TEM image of (a) bare gold nanoparticles (b) 1 mM pNIPAm-*co*-AAc nanogels containing gold nanoparticle template cores (c) 1 mM pNIPAm-*co*-AAc nanogels after core etching and uranyl acetate staining.

In order to characterize the architecture, shape and morphology of the nanogels before and after dissolution of the templating core, TEM and AFM imaging was performed. Figure 3.5 shows representative TEM images of 1 mM pNIPAm-*co*-AAc nanogels before (Figure 3.5b) and after dissolution (Figure 3.5c) of the templating gold cores (Figure 3.5a). Nanogels following gold core dissolution were imaged by the staining of the AAc groups in the polymer shell with uranyl acetate. As seen from Figure 3.5c, the polymer shell integrity is maintained following the dissolution of the gold cores. Note that soft hydrogel nanoparticles following core dissolution tend to flatten on the

TEM grid during sample preparation and imaging conditions. Thus, size determination of the hollow nanogels cannot be reliably done based on these images.
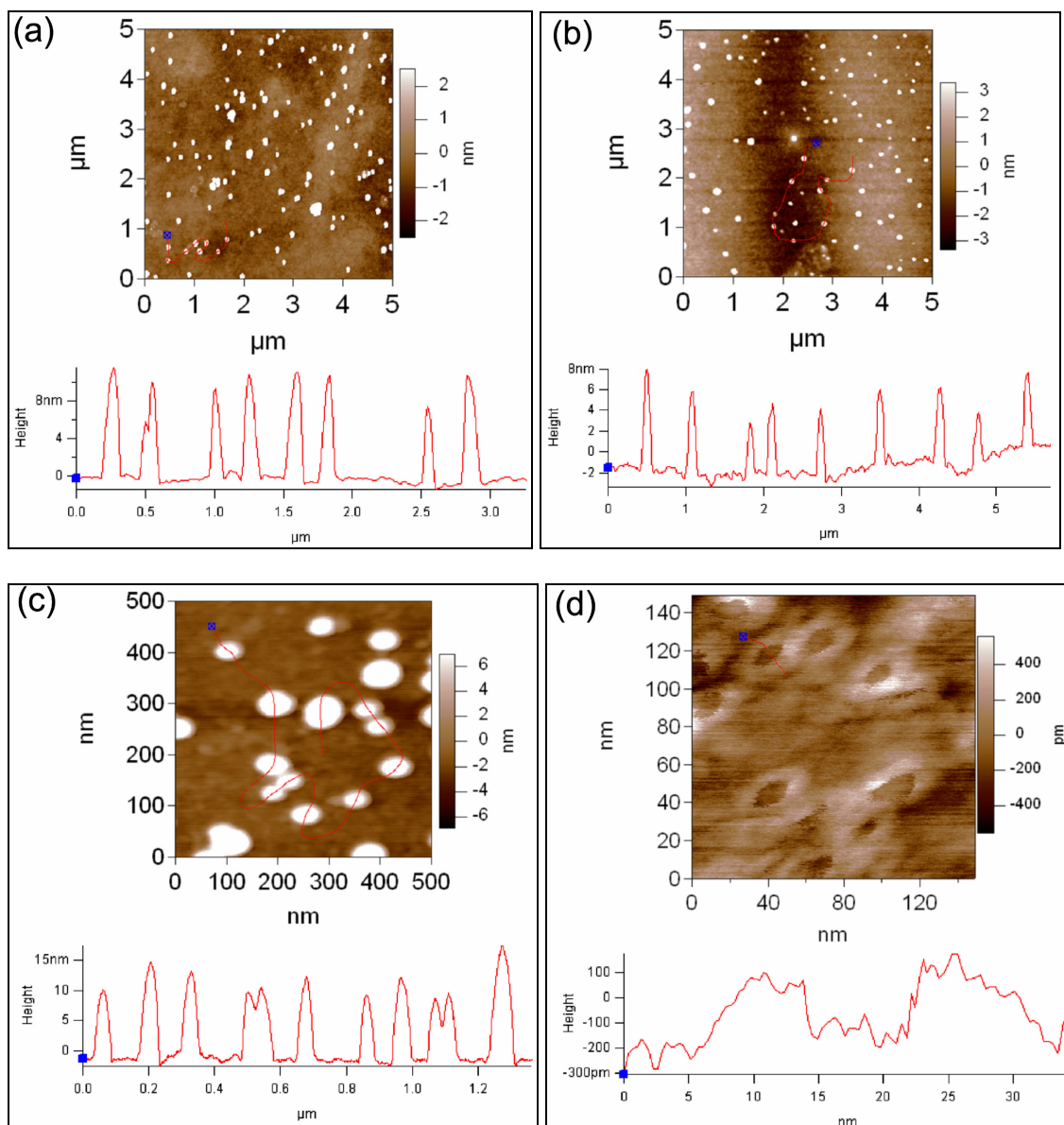
Figure 3.6. AFM images of 1 mM pNIPAm-*co*-AAc nanogels on a glass substrate (a) before and (b) after etching of the gold template cores, and on aminosilane functionalized glass substrate (c) before and (d) after etching of the gold cores.
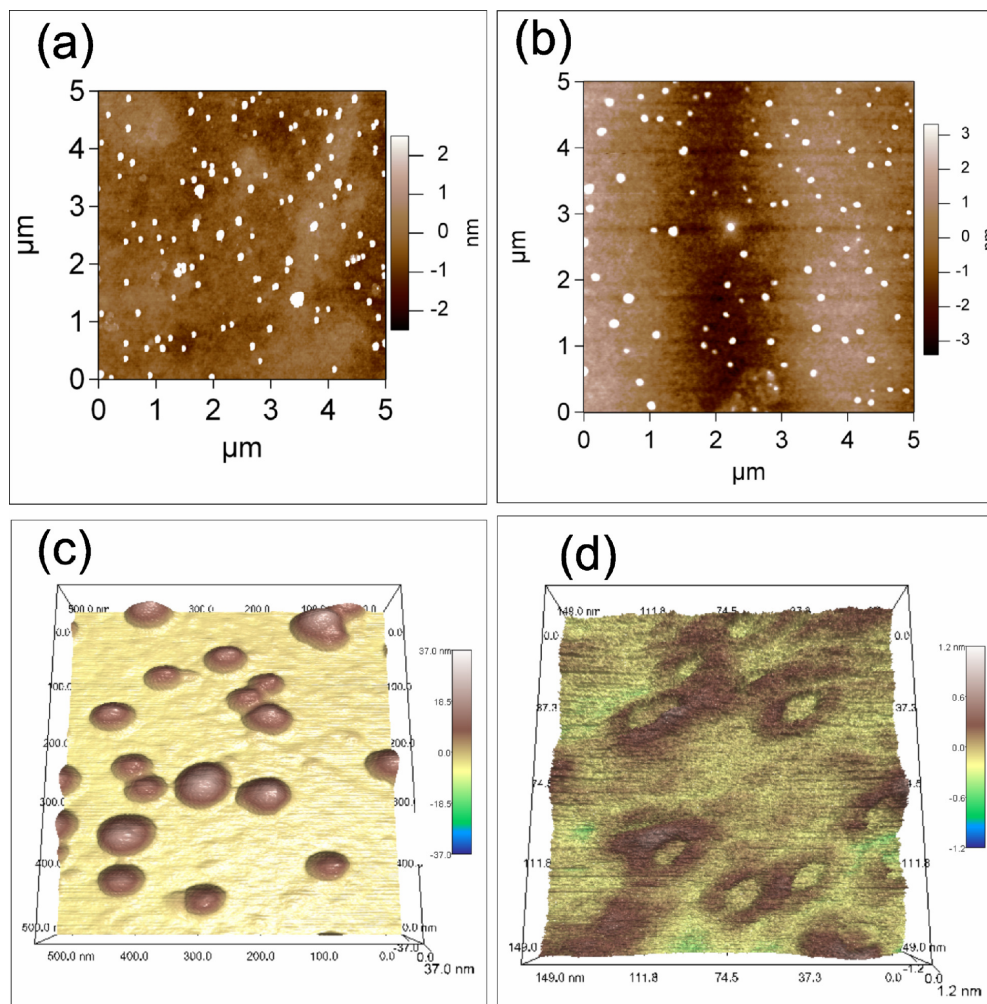
Figure 3.7. AFM images of 1mM pNIPAm-*co*-AAc nanogels on a glass substrate, (a) before and (b) after etching of the gold template cores. 3D rendering of AFM images of 1mM pNIPAm-*co*-AAc nanogels on aminosilane functionalized glass substrate, (c) before and (d) after etching of the gold cores.

Figure 3.6 and 3.7 shows AFM images of 1 mM pNIPAm-*co*-AAc nanogels. AFM images of particles deposited on a glass substrate show feature heights in the range of 10-15 nm (Figure 6a) before the dissolution of the templating cores (Figure 3.6a and 3.7a), which correlates well with the diameter of the gold core inside the nanogels. A

similar height range was observed for images obtained on a functionalized glass substrate, in which case the polymer shell has strong interactions with the substrate (Figure 3.6c and 3.6d). However, the soft nature of the nanogels following core dissolution is clearly reflected in Figures 3.7b and 3.7d. Images obtained on a simple glass substrate showed heights in the range of 6-10 nm (Figure 3.6b and 3.7b) whereas when imaged on functionalized glass substrate (Figure 3.6d and 3.7d), the nanoparticles appear to be flattened on the substrate due to strong polymer-substrate interactions. The hollow nature of the nanogels is clearly observable in Figure 3.7d. AFM imaging thus also gives a strong indication of the variation in the nanoparticle sizes due to the particle-substrate-interactions, as was observed in the TEM analyses.

The effect of polymer shell thickness and composition on the Au core etching rate was investigated. Figure 3.8a shows the etching rates of Au cores of pNIPAm and pNIPAm-*co*-AAc nanogels for different polymer shell thicknesses at 25 $^{\circ}$C. The etching rates were obtained by fitting, the plot of the observed decrease in absorbance with time as shown in Figure 3.8c and 3.8d. The slower etching rates for the polymer coated Au nanoparticles relative to uncoated ones indicates that the polymer shell indeed slows down the etching process. Furthermore, the etching rate decreased with increasing polymer thickness (R_h) for both types of nanogels. Interestingly, pNIPAm-*co*-AAc nanogels showed a faster Au etching rate as compared to pNIPAm nanogels synthesized with the same monomer concentration. The AAc carboxyl groups and the larger free volume of pNIPAm-*co*-AAc may facilitate the diffusion of cyanide ions through the polymer shell relative to pNIPAm shells. The effect of polymer deswelling on the etching rate was also studied by following the etching at 45 $^{\circ}$C, a temperature above the LCST of

66

the nanogels (Figure 3.8b). The measured etching rate for the polymer coated nanoparticles was normalized to that of the uncoated Au nanoparticles in order to account for any intrinsic temperature dependence of the etching chemistry (Figure 3.9). The temperature-induced deswelling of the polymer shell significantly increases the etching rate for 0.25 mM and 0.5 mM pNIPAm and pNIPAm-*co*-AAc nanogels, but for 1 mM nanogels the change was insignificant as evident from Figure 3.9. Apparently, for thinner coatings the major factor controlling the etching rate is the absolute thickness of the hydrogel coating, regardless of its degree of solvation (above vs. below the LCST). However, one should note the presence of other complicating factors such as the decrease in the ionic diffusion resulting from the reduced porosity of the deswollen polymer shell. This factor may become more important as the shell thickness increases. The details of ionic transport through these shells therefore deserve further investigation; we are currently performing such studies in our group.
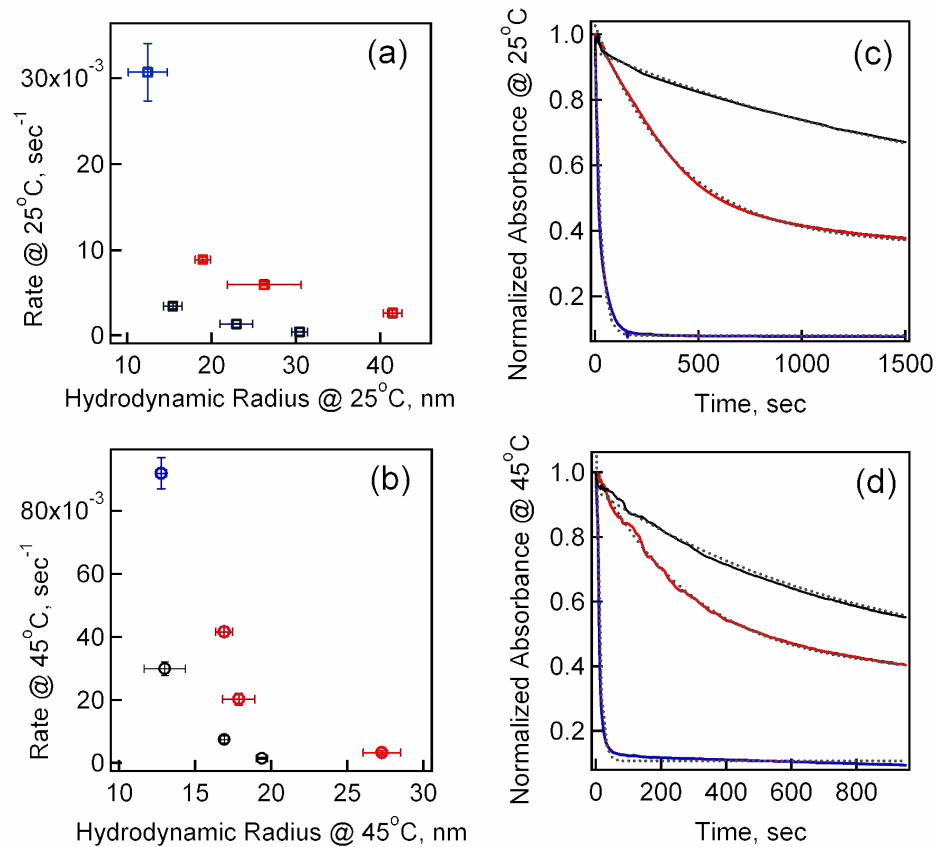
Figure 3.8. Etching rates of Au cores in water at (a) 25 ^{o}C and (b) 45 ^{o}C for bare Au (blue) and pNIPAm (black), pNIPAm-*co*-AAc (red) nanogels plotted against the hydrodynamic radius. Absorbance of Au nanoparticles at λ_{max} w.r.t time at (c) 25 ^{o}C and (d) 45 ^{o}C for bare Au (blue), 1 mM pNIPAm nanogel (black) and 1 mM pNIPAm-co-AAc nanogel. The dotted curves (gray) are the exponential fit to the data. Each data point is an average from 3 different experiments.
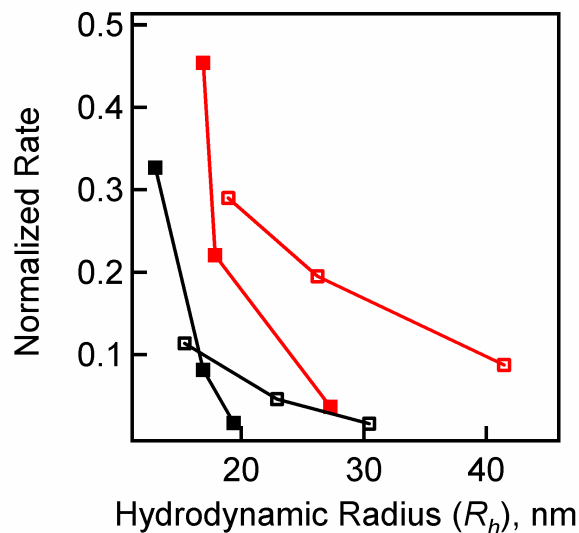
Figure 3.9. Effect of shell thickness and shell deswelling on the etching rate of Au cores from pNIPAm (black) and pNIPAm-*co*-AAc (red) nanogels. The rate of Au core etching for the nanogels were normalized w.r.t. the rate of bare Au etching at particular temperatures. Open square symbols are rates at 25 $^{\circ}$C and filled squares symbols are rates at 45 $^{\circ}$C.

In order to facilitate particle characterization we incorporated a fluorescent co-monomer, 4-acrylamido-fluorescein (AFA) into the polymer shell during polymerization. Gold nanoparticles are known to quench the emission of fluorophores in close proximity *via* efficient resonance energy transfer.[32,33] We observed that indeed the fluorescence from the shell-incorporated AFA was quenched (Figure 3.10a) thus giving additional confirmation that our synthesis yielded a Au core surrounded by a thin pNIPAm-*co*-AFA shell. A control study with the Au colloid incubated with a solution of AFA showed no loss in the fluorescence intensity. In fact, the AFA fluorescence in the nanogels was regained when the Au core was etched, resulting in fluorescent, hollow nanogel particles. Figure 3.10a shows the increase in the fluoresence of the pNIPAm-*co*-AFA nanogel

solution following cyanide etching of the Au cores. The evolution of the fluorescence intensity follows the progress of the etching process (see Figure 3.10b) in a manner similar to the observed decrease in plasmon absorbance resulting from the etching of the Au.
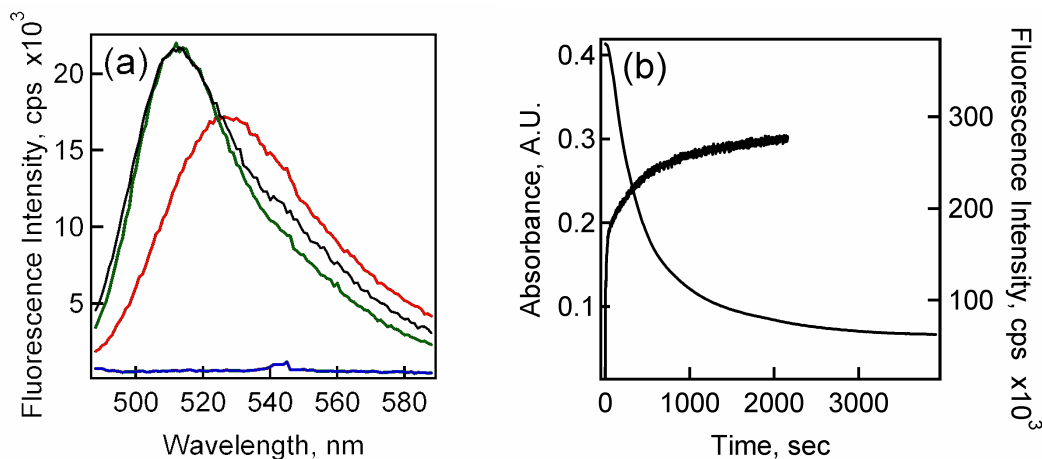
Figure 3.10. (a) Fluorescence quenching of shell fluorophores due to the close proximity of Au nanoparticles. Fluorescence spectrum of pNIPAm-*co*-AFA particles before (blue) and after (red) Au core dissolution. No fluorescence quenching was observed in a physical mixture of AFA and bare Au (green) when compared to AFA solution (black). (b) Disappearance of absorbance intensity (525 nm) of Au nanoparticle and appearance of fluorescence intensity of the shell fluorophore (525 nm) with. time follows the progress of core dissolution. λ_{exc}= 478 nm.

3. 4 Conclusions

In conclusion, we have developed a synthetic route to synthesize nanosized, hollow pNIPAm hydrogel particles via a straightforward precipitation polymerization method. The sub-50 nm dimensions make the nanogels ideal for drug and gene delivery, cellular imaging, as nanoreactors, as protective shells for enzymes, and as transfection

vectors in gene therapy. The presence of carboxyl functional groups not only gives pH responsivity to the nanoparticles but also gives a handle to tune the properties by providing convenient handles for postpolymerization modification/bioconjugation. Incorporation of the fluorescent monomer not only helps in easy characterization but also adds a useful property to the nanogel for their possible use in sensing and imaging applications. These attributes combined with the ability to tune the particle size as well as the inner cavity makes the nanogels attractive for biological applications. Future studies are aimed at understanding the encapsulation of small molecules and proteins within the hollow nanogels.

3.5 References and Notes

[1]   Meier, W. Polymer nanocapsules. *Chem. Soc. Rev.* **2000**, *29*, 295-303.

[2]   Langer, R. New methods of drug delivery. *Science* **1990**, *249*, 1527-1533.

[3]   Peppas, N. A.; Langer, R. New challenges in biomaterials. *Science* **1994**, *263*, 1715-1720.

[4]   Marinakos, S. M.; Anderson, M. F.; Ryan, J. A.; Martin, L. D.; Feldheim, D. L. Encapsulation, Permeability, and Cellular Uptake Characteristics of Hollow Nanometer-Sized Conductive Polymer Capsules. *J. Phys. Chem. B* **2001**, *105*, 8872-8876.

[5]   Nayak, S.; Lee, H.; Chmielewski, J.; Lyon, L. A. Folate-mediated cell targeting and ytotoxicity using thermoresponsive microgels. *J. Am. Chem. Soc.* **2004**, *126*, 10258-10259.

[6]   Nayak, S.; Lyon, L. A. Soft nanotechnology with soft nanoparticles. *Angew. Chem. Int. Ed. Engl.* **2005**, *44*, 7686-7708.

[7]   Pelton, R. Temperature-sensitive aqueous microgels. *Adv. Colloid. Interface Sci.*
        2000, *85*, 1-33.

[8]   Wang, C.; Flynn, N. T.; Langer, R. Controlled structure and properties of
        thermoresponsive nanoparticle-hydrogel composites. *Adv. Mater.* **2004**, *16*, 1074-
        1079.

[9]   Thurmond, K. B., II; Kowalewski, T.; Wooley, K. L. Shell Cross-Linked Knedels:
        A Synthetic Study of the Factors Affecting the Dimensions and Properties of
        Amphiphilic Core-Shell Nanospheres. *J. Am. Chem. Soc.* **1997**, *119*, 6656-6665.

[10]   MacKnight, W. J.; Ponomarenko, E. A.; Tirrell, D. A. Self-Assembled
        Polyelectrolyte-Surfactant Complexes in Nonaqueous Solvents and in the Solid
        State. *Acc. Chem. Res.* **1998**, *31*, 781-788.

[11]   Caruso, F. Hollow capsule processing through colloidal templating and self-
        assembly. *Chemistry--A European Journal* **2000**, *6*, 413-419.

[12]   Quaroni, L.; Chumanov, G. Preparation of Polymer-Coated Functionalized Silver
        Nanoparticles. *J. Am. Chem. Soc.* **1999**, *121*, 10642-10643.

[13]   Watson, K. J.; Zhu, J.; Nguyen, S. T.; Mirkin, C. A. Hybrid Nanoparticles with
        Block Copolymer Shell Structures. *J. Am. Chem. Soc.* **1999**, *121*, 462-463.

[14]   Wu, M.; O'Neill, S. A.; Brousseau, L. C.; McConnell, W. P.; Shultz, D. A.;
        Linderman, R. J.; Feldheim, D. L. Synthesis of nanometer-sized hollow polymer
        capsules from alkanethiol-coated gold particles. *Chem. Commun.* **2000**, 775-776.

[15]   Huang, H.; Remsen, E. E.; Kowalewski, T.; Wooley, K. L. Nanocages Derived
        from Shell Cross-Linked Micelle Templates. *J. Am. Chem. Soc.* **1999**, *121*, 3805-
        3806.

[16]   Gittins, D. I.; Caruso, F. Multilayered polymer nanocapsules derived from gold
        nanoparticle templates. *Adv. Mater.* **2000**, *12*, 1947-1949.

[17]   Nardin, C.; Thoeni, S.; Widmer, J.; Winterhalter, M.; Meier, W. Nanoreactors
        based on (polymerized) ABA-triblock copolymer vesicles. *Chem. Commun.* **2000**,
        1433-1434.

[18]   Schneider, G.; Decher, G. From Functional Core/Shell Nanoparticles Prepared via Layer-by-Layer Deposition to Empty Nanospheres. *Nano Lett.* **2004**, *4*, 1833-1839.

[19]   Marinakos, S. M.; Novak, J. P.; Brousseau, L. C., III; House, A. B.; Edeki, E. M.; Feldhaus, J. C.; Feldheim, D. L. Gold Particles as Templates for the Synthesis of Hollow Polymer Capsules. Control of Capsule Dimensions and Guest Encapsulation. *J. Am. Chem. Soc.* **1999**, *121*, 8518-8522.

[20]   Nuss, S.; Bottcher, H.; Wurm, H.; Hallensleben, M. L. Gold nanoparticles with covalently attached polymer chains. *Angew. Chem. Int. Ed. Engl.* **2001**, *40*, 4016-4018.

[21]   Li, D.; Jones, G. L.; Dunlap, J. R.; Hua, F.; Zhao, B. Thermosensitive Hairy Hybrid Nanoparticles Synthesized by Surface-Initiated Atom Transfer Radical Polymerization. *Langmuir* **2006**, *22*, 3344-3351.

[22]   Kim, J.-H.; Lee, T. R. Thermo- and pH-Responsive Hydrogel-Coated Gold Nanoparticles. *Chem. Mater.* **2004**, *16*, 3647-3651.

[23]   Zha, L.; Zhang, Y.; Yang, W.; Fu, S. Monodisperse temperature-sensitive microcontainers. *Adv. Mater.* **2002**, *14*, 1090-1092.

[24]   Jones, C. D.; Lyon, L. A. Synthesis and Characterization of Multiresponsive Core-Shell Microgels. *Macromolecules* **2000**, *33*, 8301-8306.

[25]   Grabar, K. C.; Freeman, R. G.; Hommer, M. B.; Natan, M. J. Preparation and Characterization of Au Colloid Monolayers. *Anal. Chem.* **1995**, *67*, 735-743.

[26]   Link, S.; El-Sayed, M. A. Size and Temperature Dependence of the Plasmon Absorption of Colloidal Gold Nanoparticles. *J. Phys. Chem. B* **1999**, *103*, 4212-4217.

[27]   Plunkett, M. A.; Wang, Z.; Rutland, M. W.; Johannsmann, D. Adsorption of pNIPAM Layers on Hydrophobic Gold Surfaces, Measured in Situ by QCM and SPR. *Langmuir* **2003**, *19*, 6837-6844.

[28]   Seker, F.; Malenfant, P. R. L.; Larsen, M.; Alizadeh, A.; Conway, K.; Kulkarni, A. M.; Goddard, G.; Garaas, R. On-demand control of optoelectronic coupling in gold nanoparticle arrays. *Adv. Mater.* **2005**, *17*, 1941-1945.

[29]   Underwood, S.; Mulvaney, P. Effect of the Solution Refractive Index on the Color of Gold Colloids. *Langmuir* **1994**, *10*, 3427-3430.

[30]   Paulini, R.; Frankamp, B. L.; Rotello, V. M. Effects of Branched Ligands on the Structure and Stability of Monolayers on Gold Nanoparticles. *Langmuir* **2002**, *18*, 2368-2373.

[31]   Templeton, A. C.; Hostetler, M. J.; Kraft, C. T.; Murray, R. W. Reactivity of Monolayer-Protected Gold Cluster Molecules: Steric Effects. *J. Am. Chem. Soc.* **1998**, *120*, 1906-1911.

[32]   Fan, C.; Wang, S.; Hong, J. W.; Bazan, G. C.; Plaxco, K. W.; Heeger, A. J. Beyond superquenching: Hyper-efficient energy transfer from conjugated polymers to gold nanoparticles. *Proc. Natl. Acad. Sci. USA* **2003**, *100*, 6297-6301.

[33]   Dulkeith, E.; Morteani, A. C.; Niedereichholz, T.; Klar, T. A.; Feldmann, J.; Levi, S. A.; van Veggel, F. C. J. M.; Reinhoudt, D. N.; Moller, M.; Gittins, D. I. Fluorescence quenching of dye molecules near gold nanoparticles: radiative and nonradiative effects. *Phys. Rev. Lett.* **2002**, *89*, 203002.

CHAPTER 4

SYNTHESIS OF MULTIFUNCTIONAL NANOGELS USING A PROTECTED MACROMONOMER APPROACH

Adapted from Singh, N.; Lyon, L. A., to be submitted for publication.

Colloidal nanoparticles possessing multiple functionalities provide the synthetic handles required to carry out varied surface chemistries, making such particles useful for a range of applications such as biotargeting and drug delivery. However the combination of different interfering functionalities on the same particle, e.g. amines and carboxylic acid groups, is often challenging. We have employed a synthetic scheme involving chemical protection and subsequent deprotection to combine different functional ligands on the same hydrogel nanoparticle (nanogel). The synthesis of amine-containing Poly(*N*-isopropylacrylamide) (pNIPAm) nanogels was carried out via free radical precipitation polymerization by incorporating a Fmoc-protected amine PEG macromonomer. The Fmoc group was then removed to obtain free amines, which were shown to be available for conjugation. We have thus achieved good control over the exposure of the amine groups, which is useful for further surface chemoligation reactions. We further explored the functionalization of pNIPAm-co-acrylic acid nanogels with the Fmoc protected amine PEG macromonomer, yielding zwitterionic nanogel particles possessing both acid and amine groups on the same particle. With careful attention to the order of the

chemoligation and deprotection steps, these potentially interfering functional groups can be forced to behave in a pseudo-orthogonal fashion, allowing for multiple different chemoligation steps that employ both the amine and carboxylic acid groups.

4.1 Introduction

Nanoparticles have emerged as versatile building blocks in the development of materials for biomedicine and drug delivery,[1,2] sensors,[3-5] nanophotonics,[6-8] catalysis[9] and separations.[10-12] One important class of nanoparticles is stimuli-responsive hydrogel nanoparticles, or nanogels. There has been a great deal of attention towards increasing the chemical diversity and the complexity of nanogels in order to design and tailor them for specific applications.[3,5-7,13-18] In particular, the specific chemical functionalization of nanogels provides an excellent way to manipulate their responsiveness to external stimuli such as pH, ionic strength or light.[16,19,20] Alternatively, one can impart the nanogel surface with chemical handles for covalent attachment of functionalities in the post-polymerization stage.[21-26] In order to design complex and versatile nanogels, it is often desired that the particle have multiple different chemical handles. However, in many cases chemoligations that can be carried out on nanoparticles are complicated and even prohibited by the presence of interfering functional groups. For example, presence of carboxyl and amine groups on the same particle surface can limit the extensively used carbodiimide-based amide bond forming chemistry for chemoligation as it could result in cross-reaction of the two functional groups.[27,28] Thus, a challenge in the design and synthesis of multifunctional nanoparticles is the selective incorporation of multiple functionalities that behave as orthogonally reactive groups. It is also desirable that such

an incorporation scheme be simple and straight forward, as in the approach we describe below.

Poly(*N*-isopropylacrylamide) (pNIPAm) nanoparticles are perhaps the most commonly studied nanogels. These nanoparticles undergo a volume phase transition from a hydrophilic (water-swollen state) to a hydrophobic (deswollen) state at a lower critical solution temperature (LCST) of about 31 °C in water.[29] The phase transition of these nanogels at a temperature relevant to biological systems makes them interesting for bio-applications.[30,31] A number of synthetic strategies have been developed for the production of monodisperse pNIPAm nanogels.[24,26,32-39] Interesting architectures such as core/shell nanoparticles of pNIPAm have been synthesized *via* two-stage precipitation polymerization, which offers the ability to spatially localize chemical functionalities to a defined position, to render thermoresponsivity to non-responsive particles, or to modify specific physical properties of the nanoparticles.[14,33,40,41] As argued above, the integration of multiple functional groups onto these thermosensitive nanoparticles is required to explore a range of applications. We therefore present here an improvement over our past methodologies for synthesizing monodisperse multi-functional nanogels by using a well-established organic synthesis strategy.

As illustrated in Scheme 4.1, combining the simple and well established precipitation polymerization technique of nanogel synthesis with traditional organic synthesis techniques for the protection and deprotection of reactive functional groups can yield a straightforward method for synthesizing multifuctional nanogels. This method provides a unique synthetic strategy for combining multiple orthogonal functionalities, which expands the types of chemistry that can be performed on these nanoparticles. In

the strategy used here, the nanogels are synthesized using a macromonomer that has a protected amine group. The protecting group can be removed at a later stage to yield the free primary amine for doing further chemistries. The incorporation of carboxyl groups along with the amine functionality is also easily obtained with this scheme. The synthesis of zwitterionic (having both positively and negatively charged functional groups) nanogels via traditional precipitation polymerization is limited due to colloidal instability during synthesis; the presence of both cationic and anionic co-monomers, plus charged surfactants (e.g. sodium dodecylsulfate) and initiators (e.g. ammonium persulfate) causes aggregation and the formation of coagulum. A one pot synthetic route based on the precipititation polymerization for synthesizing such zwitterionic nanogels also does not result in efficient incorporation of high concentration of the charged comonomers (especially amines).[42] However, with the described scheme, a one pot synthesis of zwitterionic nanogels with high degree of comonomer incorporation can be efficiently carried out. The protected amine comonomer allows the use of anionic surfactant and initiator in the synthesis. It also provides a route for synthesizing monodisperse, colloidally stable multifunctional nanogels with otherwise interfering functional groups on the same nanoparticles. These multiple functionalities can be further utilized orthogonally with good control over the access of the functional group at any stage in the post-polymerization modification steps.
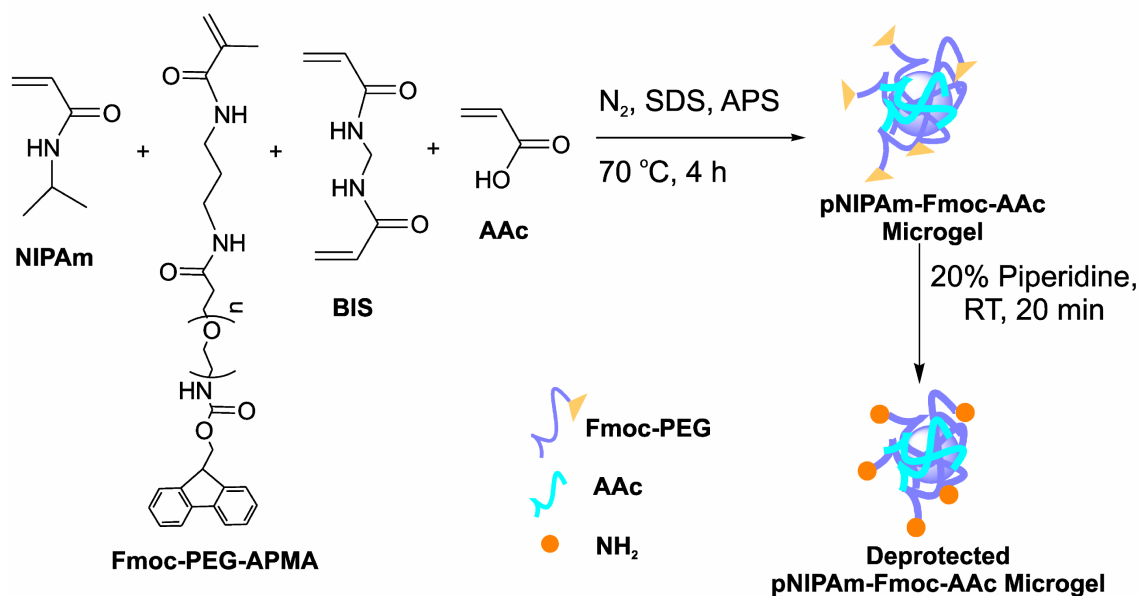
Scheme 4.1. Synthetic scheme based on precipitation polymerization for the synthesis of pNIPAm based nanogels containing multiple functional groups.

4.2 Experimental Section

4.2.1 Materials

Most of the chemicals used in this study are similar to those in Chapter 2 and 3. Additionally, a bifunctional polyethylene glycol (Fmoc-PEG-NHS, MW 5000) was obtained from Nektar Therapeutics. An amine monomer, *N*-(3-aminopropyl)methacrylamide (APMA) was obtained from PolySciences, Inc. Biotin hydrazide and 1-ethyl-3-(3-dimethylaminopropyl) carbodiimide (EDC) were purchased from Pierce. Fluorescent dyes, 5-aminofluorescein and 5-carboxytetramethylrhodamine succinimydyl ester (TAMRA-SE) were purchased from Molecular Probes.

4.2.2 Nanogel Synthesis

Synthesis of the Fmoc-Protected PEG Methacrylamide Macromonomer.

The Fmoc protected PEG-NHS (0.20 g, 0.039 mmol, 1 equiv) was reacted with APMA (0.0079 g, 0.039 mmol, 2 equiv) at room temperature for 2 hrs in pH 7.5 PBS buffer. The product was purified by dialysis for a week by changing water three times a day, using Spectra-Por 1,000 MW cut-off dialysis tubing (VWR). The removal of unreacted APMA was confirmed by ninhydrin (2 wt % ethanol solution) test on a TLC plate. The final product was characterized by ^{1}H NMR for the incorporation of double bonds from the APMA. ^{1}H NMR (D_2O): δ = 3.5 ppm from OCH_2CH_2 repeat units from PEG, δ = 7.2 to 7.8 ppm from the aromatic groups from the Fmoc, and δ = 5.25 and δ = 5.45 from the ethylene.

Synthesis of Fmoc Protected amine Containing Nanogels

The pNIPAm nanogels containing an Fmoc-protected amine macromonomer were synthesized using the precipitation polymerization method using the Fmoc-Protected PEG methacrylamide macromonomer synthesized above as a comonomer.

Synthesis of 5 mol % pNIPAm-Fmoc Core nanogels

The total monomer concentration for the core synthesis was ~70 mM. In a typical synthesis, 0.0737 g (93 mol %) of the monomer NIPAm, 0.183 g (5 mol %) of Fmoc-protected PEG methacrylamide macromonomer, 0.0022 g (2 mol %) of the cross-linker *N,N*-methylenebis(acrylamide) (BIS) and 0.0043 g surfactant, sodium dodecyl sulfate (SDS) was dissolved in 9 mL distilled, deionized (DI) water and filtered through 0.2 µm membrane filter. The filtered reaction solution was transferred to a three neck flask,

stirred and heated to ~70 °C under a N_2 atmosphere. After 1 h, the reaction was initiated by the addition of 0.0041 g (dissolved in 1 mL DI water) ammonium persulfate (APS) solution and kept at 70 °C for 4 hours. The reaction was allowed to cool at room temperature and stirred overnight followed by filtration through Whatman filter paper (No.2). The filtered nanogels were then purified by dialysis against water for ~2 weeks with the water being changed twice per day, using Spectra-Por 10,000 MW cut-off dialysis tubing (VWR). The clean nanogels were freeze dried overnight using Labconco lyophilizer. The synthesized nanogels had hydrodynamic radius (R_h) of 46 ± 3.5 nm at 25 °C and 27 ± 2.9 nm at 45 °C as measured by photon correlation spectroscopy (PCS).

Synthesis of pNIPAm Core nanogels

For synthesizing core/shell type nanogels, pNIPAm cores were first synthesized. The total monomer concentration for these cores was also kept ~70 mM. For the synthesis, 1.55 g (98 mol %) of NIPAm, 0.0432 g (2 mol %) of BIS and 0.055 g SDS, was dissolved in 199 mL distilled, deionized (DI) water and filtered through 0.2 μm membrane filter. The reaction solution was transferred to a three neck flask, stirred and heated to ~70 °C under a N_2 atmosphere. After 1 h, the reaction was initiated by the addition of 0.0378 g (dissolved in 1 mL DI water) APS solution and kept at 70 °C for 4 hours followed by stirring at room temperature overnight. The synthesized pNIPAm core nanogels were filtered through a Whatman filter paper (No.2) and used for synthesizing the shell without any further purification. The synthesized pNIPAm cores had hydrodynamic radius (R_h) of 136 ± 0.9 nm at 25 °C and 56 ± 2.8 nm at 45 °C as measured by PCS.

Synthesis of Fmoc-protected PEG shell on pNIPAm cores

81

The pNIPAm cores synthesized above were used as seeds in the addition of a pNIPAm-Fmoc shell, using a seed and feed method previously described by our group.[35] In this method a polymer shell with the same or different structure or functionality to that of the core, is added onto preformed core particles. In a typical synthesis, preformed pNIPAm core particles are heated to ~70 °C, followed by addition and initiation of the shell monomer solution. Since the reaction temperature is well above the VPTT of the core particles, the particles are in a collapsed state. The collapsed particles are hydrophobic and hence tend to capture the growing oligomers, which results in the formation of the cross-linked hydrogel shell.

Synthesis of 5 mol % pNIPAm-Fmoc Shell

The total monomer concentration for the shell synthesis was ~40 mM. The pNIPAm cores (2 mL) were stirred and heated to ~70 °C under a N_2 atmosphere in a three neck reaction flask. A filtered (0.2 μm membrane filter), 7 mL aqueous solution of 0.0421 g (93 mol %) NIPAm, 0.1044 g (5 mol %) of Fmoc-protected PEG methacrylamide, 0.0012 g (2 mol %) of BIS, and 0.0025 g of SDS was added to the reaction flask containing the heated cores. After 1 h, the reaction was initiated by injection of 0.0037 g APS dissolved in 1 mL DI water and kept at 70 °C for 4 hours. The reaction was kept stirring at room temperature overnight and filtered through Whatman filter paper (No.2) the next day. The filtered nanogels were then purified by dialysis against water for ~2 weeks with the water being changed twice per day, using Spectra-Por 10,000 MW cut-off dialysis tubing (VWR). The clean nanogels were freeze dried overnight using Labconco lyophilizer. The PCS measured R_h values for the 5 mol % pNIPAm-Fmoc shells were 153 ± 8.9 nm at 25 °C and 103 ± 0.5 nm at 45 °C.

82

Synthesis of 1 mol % pNIPAm-Fmoc Shell

A similar procedure as described above was followed for synthesizing 1 mol % Fmoc containing shells. The total monomer concentration was again ~40 mM. The pNIPAm cores (0.0156 g dispersed in 2 mL DI water) were stirred and heated to ~70 °C under a N_2 atmosphere in a three neck reaction flask. To the reaction flask containing the heated cores was added 7 mL of aqueous filtered (0.2 µm membrane) solution of 0.0439 g (97 mol %) NIPAm, 0.0208 g (1 mol %) of Fmoc-protected PEG methacrylamide macromonomer, 0.0012 g (2 mol %) of BIS, and 0.0025 g of SDS. After 1 h, the reaction was initiated by injection of 0.0037 g APS dissolved in 1 mL DI water and kept at 70 °C for 4 hours. The reaction was kept stirring at room temperature overnight and filtered through Whatman filter paper (No.2). The filtered nanogels were then purified by dialysis against water for ~2 weeks with the water being changed twice per day, using Spectra-Por 10,000 MW cut-off dialysis tubing (VWR). The clean nanogels were freeze dried overnight using Labconco lyophilizer. The 1 mol % pNIPAm-Fmoc nanogels yielded R_h values of 184 ± 2.2 nm at 25 °C and 134 ± 3.9 nm at 45 °C.

Synthesis of pNIPA-Fmoc-AAc Shell

For synthesizing both carboxyl and amine functional group containing shells, acrylic acid (AAc) was used as comonomer along with the Fmoc-protected PEG methacrylamide macromonomer. The total monomer concentration for the shell was again kept ~40 mM. The pNIPAm cores (1 mL) were stirred and heated to ~70 °C under a N_2 atmosphere in a three neck reaction flask. A filtered (filtered using 0.2 µm membrane filter), 3 ml aqueous solution of 0.0188 g (83 mol %) NIPAm, 0.0522 g (5 mol

%) of the synthesized Fmoc-protected PEG methacrylamide, 0.0008 g (2 mol %) of BIS and 0.0013 g of SDS, was added to the reaction flask containing the heated cores. To avoid self polymerization of AAc at high temperatures, it was added just before the initiation of the reaction. After 1 h, 1.5 μL (10 mol %) AAc was added followed by the initiation of the reaction by injection of 0.0019 g APS dissolved in 1 mL DI water. The reaction proceeded at 70 °C for 4 hours followed by stirring at room temperature overnight. The reaction was filtered through Whatman filter paper (No.2) and then purified by dialysis against water for ~2 weeks with the water being changed twice per day, using Spectra-Por 10,000 MW cut-off dialysis tubing (VWR). The clean nanogels were freeze dried overnight using Labconco lyophilizer.

4.2.3 Removal of the Fmoc Protecting Group

The Fmoc-protected nanogels (~15 mg) were dissolved in 1 mL 20% (v/v) piperidine in dimethylformamide (DMF) solution and stirred for 10 min at room temperature. Fresh 1 mL 20% (v/v) piperidine in DMF solution was added after 10 min and allowed to stir for 10 more minutes at room temperature. The deprotected nanogels were then purified by dialysis against water for ~2 weeks with the water being changed twice per day, using Spectra-Por 10,000 MW cut-off dialysis tubing (VWR). The successful removal of the Fmoc protecting group was confirmed by ^{1}H NMR.

4.2.4 Conjugation of 5-carboxytetramethylrhodamine succinimydyl ester to the deprotected nanogels

For conjugating the amine reactive fluorophore, 0.2 mg of deprotected nanogels were dispersed in 743.8 μL of pH 7.4 PBS buffer and 256.2 μL of 1 mg/mL solution of 5-carboxytetramethyl rhodamine succinimydyl ester (TAMRA-SE) was added. The

solution was stirred at room temperature for 2 hrs. The conjugated nanogels were then purified by dialysis against water for ~2 weeks with the water being changed twice per day, using Spectra-Por 10,000 MW cut-off dialysis tubing (VWR). The nanogels were finally freeze-dried overnight.

4.2.5 5-Aminofluorescein and TAMRA-SE conjugation to pNIPAm-Fmoc-AAc

The carboxyl groups on the pNIPAm-Fmoc-AAc were first conjugated with 5-aminofluorescein using carbodiimide coupling. For the reaction, 1.4 mg of pNIPAm-Fmoc-AAc (~0.5 μmol of AAc) nanogels were dispersed in 348 μL of 2-[*N*-morpholino]ethanesulfonic acid (MES) buffer of pH 4.7. To this well dispersed nanogel solution, 0.173 mg of 5-aminofluorescein and 0.479 mg of EDC were added and the reaction was allowed to proceed overnight at 4 °C. The nanogels were then purified via dialysis for 2 weeks against 10% aqueous ethanol, with the solvent being changed twice every day. The Fmoc groups on the fluorescein conjugated pNIPAM-Fmoc-AAc nanogels were then removed and the nanogels were purified and dried as described above. The free amines thus obtained on the fluorescein conjugated pNIPAM-Fmoc-AAc nanogels were further used for conjugating TAMRA-SE using a similar protocol as described above.

4.2.6 ^{1}H NMR Spectroscopy

All ^{1}H NMR spectra were recorded on solutions formed by re-dispersing freeze-dried nanogels in either D_2O or DMSO-d_6 at room temperature; a 300 MHz Mercury Varian Unity spectrometer was used for data collection. The water peak arising from residual water inside the nanogels was suppressed in order to more efficiently observe the proton signals. The amount of Fmoc-PEG macromonomer incorporated was determined

by calculating the ratio of the PEG peak (at 3.5 ppm, resulting from the methyl protons in the OCH_2CH_2 repeat units) to the main pNIPAm peak (at 1.1 ppm, resulting from the methyl protons of the isopropyl group) at room temperature. The major source of error in such analysis of the amount of monomer incorporated is from the error in the integration of the individual signals, and it is therefore dependent on the signal-to-noise ratio of the respective signals. Signals with a fair signal-to-noise ratio have moderate errors, whereas poorly resolved signals lead to larger errors. Thus the errors for the amount of monomer incorporated reported in the paper have been derived from the integration error of the individual signals.

4.2.7 UV-Vis Spectroscopy

All the absorption spectra were obtained in quartz cuvettes using a Shimadzu UV 1601 spectrophotometer equipped with a temperature controller.

4.2.8 Photon Correlation Spectroscopy (PCS)

Similar to procedure in Chapter 3.

4.2.9 Fluorescence Spectroscopy

Similar to procedure in Chapter 3. The samples were excited at a wavelength of 490 nm.

4.2.10 Atomic Force Microscopy (AFM)

Similar to the procedure in Chapter 3.

4. 3 Results and Discussion

We have synthesized pNIPAm based nanogels possessing multiple orthogonal functionalities using the scheme illustrated and discussed above (Scheme 4.1). Fmoc-protected PEG macromonomer was synthesized by simple conjugation of *N*-(3-aminopropyl)methacrylamide with Fmoc-PEG-NHS. Synthesis of pNIPAm nanogels with this macromonomer using precipitation polymerization gave pNIPAm nanogels with Fmoc-protected amine groups. These amine groups can be further deprotected using mild conditions yielding the free amines. Using the synthetic scheme, we have also synthesized nanogels with a multifunctional shell on a pNIPAm core. A core-shell architecture can help increase the surface localization of the functional groups on the nanoparticles, which is often required for effective bioconjugation.[23]

The synthesis produced monodisperse, spherical, colloidally stable nanogels as seen from the AFM image (Figure 4.1) and the PCS studies (Table 4.1 and Figure 4.4). The pNIPAM-Fmoc cores were about 46 nm in radius as measured by PCS before deprotection, whereas they swell to about 57 nm in radius after deprotection. This swelling is likely due to the exposure of free amine groups, which makes the polymer chains more hydrophilic. The nanogels with Fmoc shells showed a similar increase in radius after deprotection (153 nm to 176 nm at 25 °C) again suggesting the more hydrophilic nature of the deprotected nanogels.

Table 4.1. Hydrodynamic Radii (R_h) Determined by PCS.

Sample	Temperature (°C)	R_h^a Before deprotection (nm)	R_h^a After deprotection (nm)
5 mol % pNIPAm-Fmoc Core	25	46 ± 3.5	57 ± 0.9
	45	27 ± 2.9	32 ± 2.4
5 mol % pNIPAm-Fmoc[b] Shell	25	153 ± 8.9	176 ± 0.9
	45	103 ± 0.5	105 ± 2.8

[a]Average of three measurements. The errors are standard deviation obtained for the measurements. [b]contains pNIPAM core with R_h=136 ± 0.9 nm at 25 °C and R_h=56 ± 2.8 nm at 45 °C
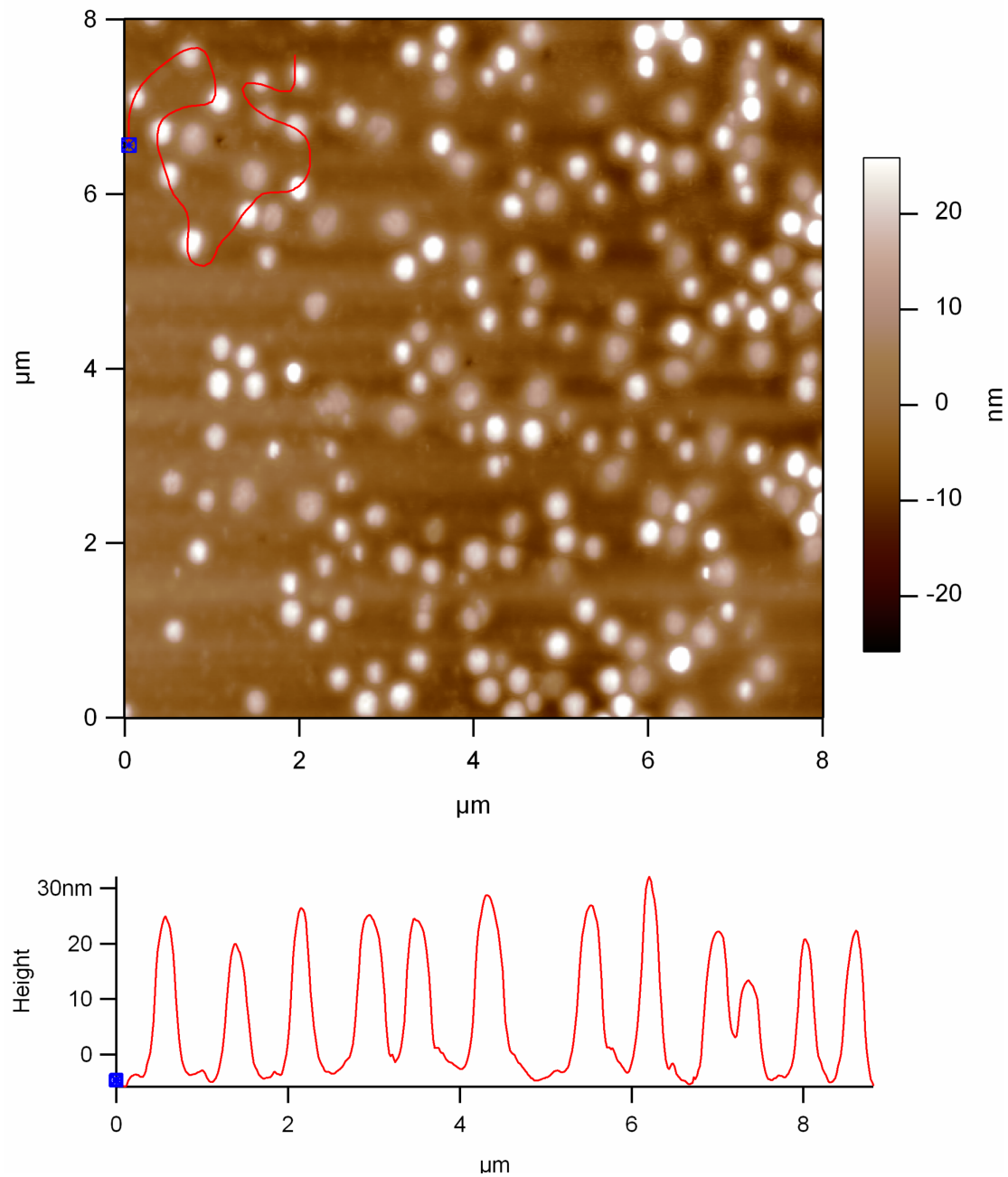
Figure 4.1. AFM image (top) and the line profile (bottom) indicating the morphology and height of protected pNIPAm-Fmoc core particles on a glass substrate.
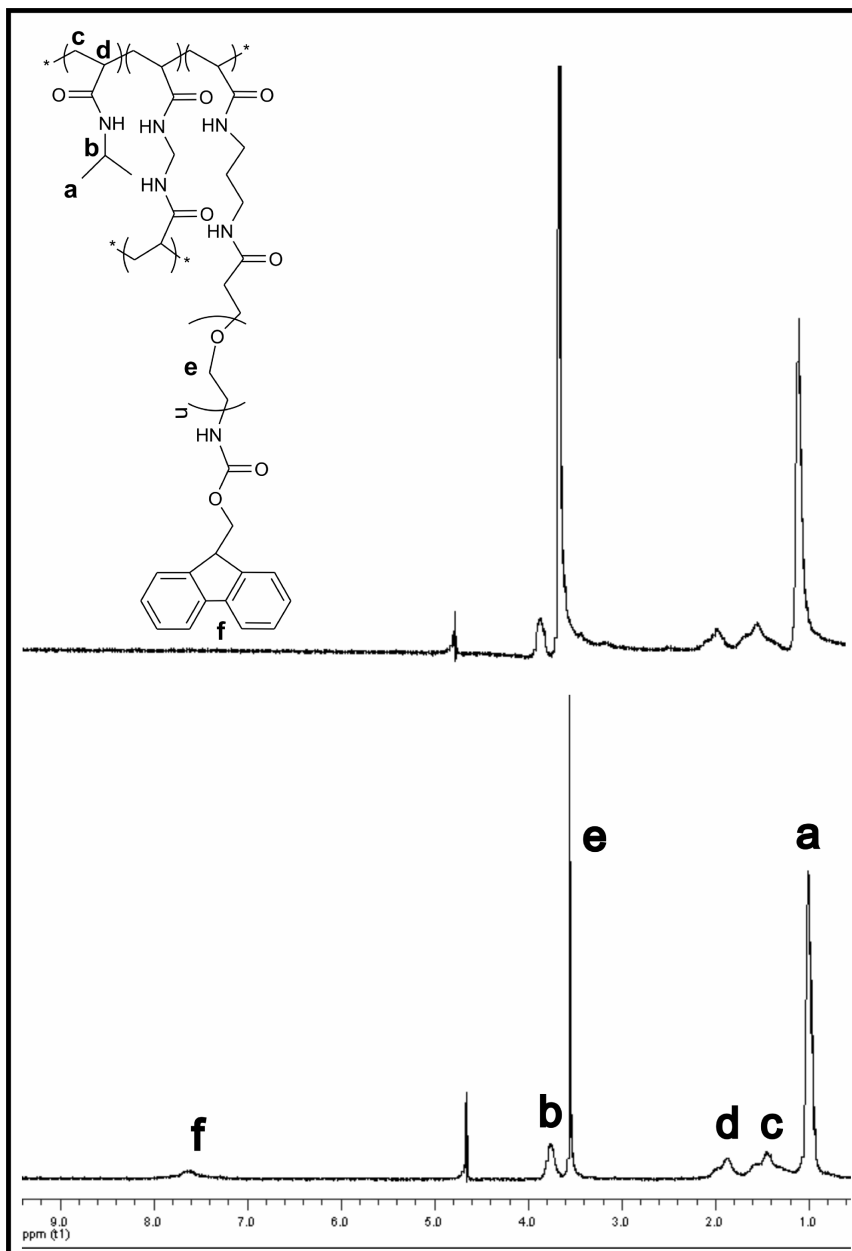
Figure 4.2. ^{1}H NMR in D_2O of the pNIPAm-Fmoc core nanogels before (top) and after (bottom) Fmoc group removal.

^{1}H NMR of the synthesized nanogels indicated incorporation of the Fmoc protected PEG macromonomer. The proton assignments for the pNIPAm polymer are in agreement with its chemical structure and are illustrated in Figure 4.2.[43,44] The peak at 1.1

ppm can be attributed to the methyl protons of the *N*-isopropyl group (peak a). The resonance for the methylene proton of the isopropyl group is observed at 3.8 ppm (peak b) while the resonances from 1.2 to 2.2 ppm (peaks c and d) are attributed to the protons on the polymer backbone. The methyl protons in the OCH_2CH_2 repeat units from PEG macromonomer show up at 3.5 ppm (peak e), and the aromatic groups from the Fmoc are seen between 7.2 to 7.8 ppm (peak f). After deprotection, the peak due to Fmoc moiety disappears confirming the removal of the protecting group.

The LCST of the synthesized pNIPAm-Fmoc nanogels (~37 °C) is elevated relative to that of the pNIPAm nanogels (32 °C). This is attributed to the fact that with the incorporation of high molecular weight PEG, the phase transition shifts considerably to a higher temperature, which is due to an increased hydrophilic balance of the particles and therefore, a reduction in the tendency for the hydrophobic collapse of pNIPAm. Increased LCST values with incorporation of hydrophilic moieties has been observed previously.[45] Virtanen *et al.* have also observed increased solubilization and increased LCST of pNIPAm by incorporation of poly(ethylene oxide) (PEO) chains.[46,47] Another interesting effect on the LCST of the nanogels is observed after the deprotection of the nanogels. As can be seen from Figure 4.3, the LCST of the nanogels in water is further elevated to ~40 °C from ~37 °C upon removal of the Fmoc group. The increased LCST after deprotection is again attributed to the increased hydrophilicity of the polymer network in the nanogels due to the exposure of free amine groups following Fmoc deprotection.
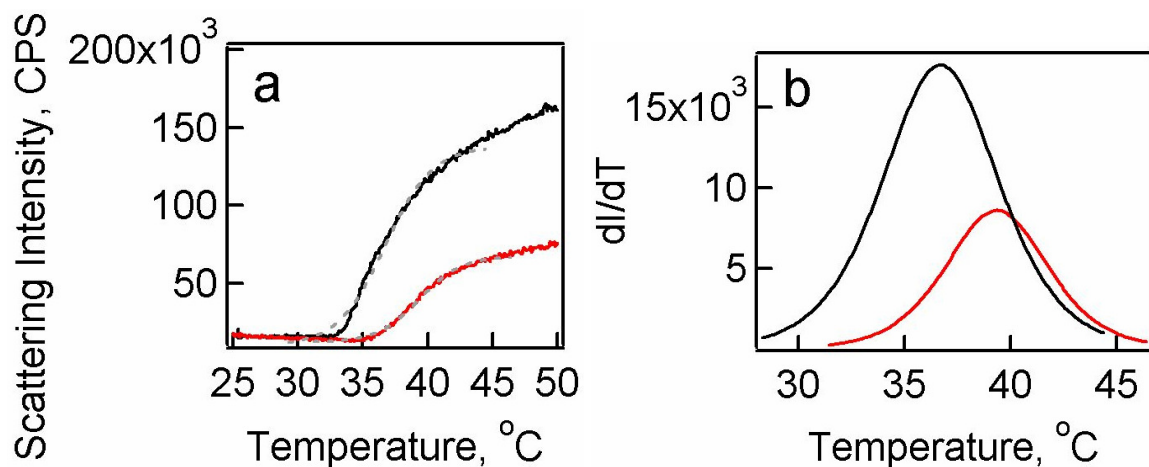
Figure 4.3. LCST changes measured by turbidity measurement (a) and also depicted as the first derivative of the fit for the turbidity curves (b) for protected pNIPAm-Fmoc core (black) and deprotected pNIPAm-Fmoc (red).

In order to produce multifunctional nanogels containing differential functionalities, we incorporated both the Fmoc-PEG methacrylamide macromonomer and AAc as comonomers. The goal was to determine whether we could both amine and carboxyl groups on the surface of same nanoparticles in high concentrations and further utilize them both for bioconjugation. This has been a challenge in the past as amine and carboxyl groups have interfering functionalization chemistries. The use of protected amine comonomer allowed the use of anionic surfactant and initiator and the synthesis proceeded without any aggregation even with high concentrations of the two comonomers (5 mol % amine and 10 mol% carboxylic acid). The nanogels obtained were highly monodisperse (~13-15 % according to PCS) and colloidally stable as can be seen from the regularization histogram (Figure 4.4) obtained for the pNIPAm-Fmoc-AAc nanogels at pH 5.0 at 25 °C. The successful incorporation of the AAc comonomer is indicated by the pH responsivity of the nanogels, as seen in the PCS studies (Table 4.2);

pNIPAm-Fmoc-AAc nanogels at 25 °C showed a decrease in radius from 167 nm at pH 5.0 to 145 nm at pH 3.0. This change in size in response to the change in pH for AAc containing pNIPAm nanogels is well established and is due to change in the interaction between the polymer chains and the solvent, as well as a decrease in the internal osmotic pressure upon protonation of the AAc moieties.[35,48] At a pH above the pKa of AAc (pKa = 4.2) there is Coulombic repulsion between the polymer chains due to the negatively charged carboxyl groups this repulsion is reduced at a pH below the pKa since the carboxyl groups are mostly protonated, causing the nanogels to deswell. Also, IR spectra of the nanogels (Figure 4.5) showed appearance of the carbonyl stretching peak at 1715 cm^{-1} due to the carboxyl groups of AAc. The incorporation and deprotection of the Fmoc-PEG macromonomer was confirmed by ^{1}H NMR.

Table 4.2. Hydrodynamic Radii (R_h) Changes with pH for pNIPAm-Fmoc-AAc Nanogels as Determined by PCS.

Temperature (°C)	$R_h{}^a$ at pH 5.0 (nm)	$R_h{}^a$ at pH 3.0 (nm)
25	167 ± 1.6	145 ± 4.1
45	102 ± 1.4	84 ± 8.2

[a]Average of three measurements. The errors are standard deviation obtained for the measurements.
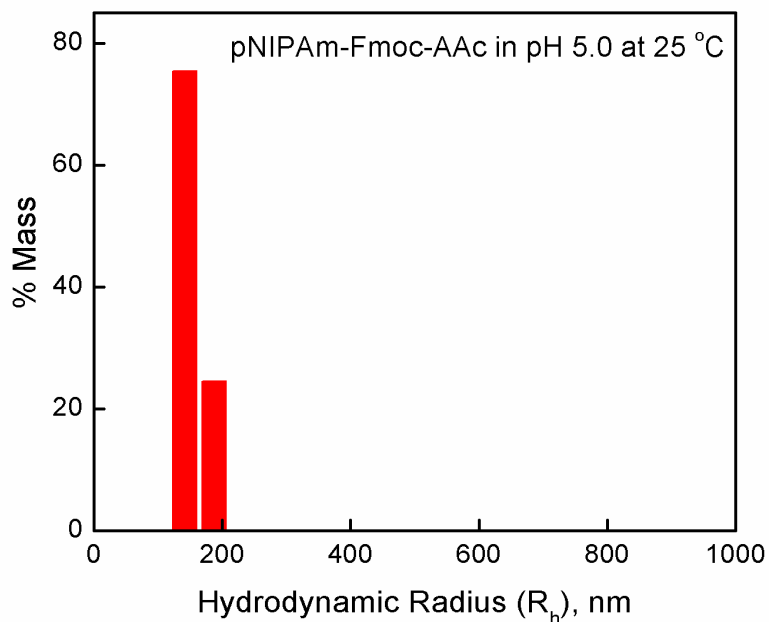
Figure 4.4. Representative regularization histogram obtained from PCS indicating the monodispersity and colloidal stability (lack of aggregation) of the multifunctional nanogels.
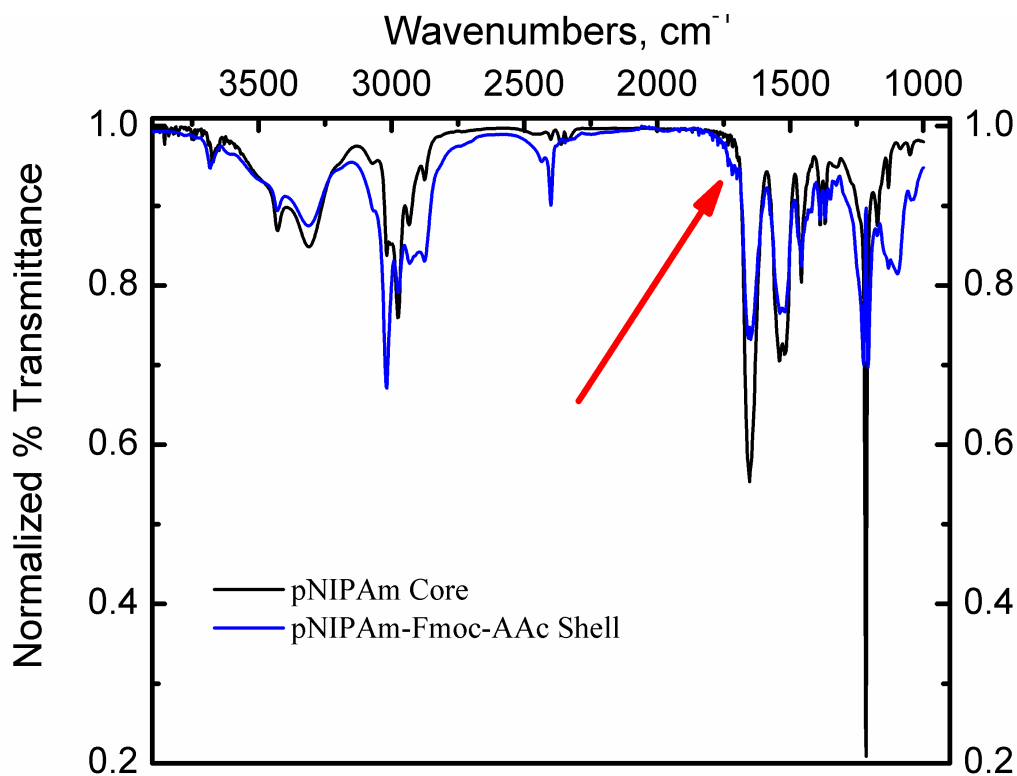
Figure 4.5. IR spectra for pNIPAm-Fmoc-AAc nanogels.

We investigated the incorporated amount of the Fmoc-PEG macromonomer in the nanogels by ^{1}H NMR following the synthesis and purification. The amount of Fmoc-PEG macromonomer incorporated was determined by the ratio of the PEG peak (at 3.5 ppm, resulting from the methyl protons in the OCH$_2$CH$_2$ repeat units) to the main pNIPAm peak (at 1.1 ppm, resulting from the methyl protons of the isopropyl group) calculated at room temperature. All of the ratio calculations are shown in Table 4.3. From the table it can be seen that incorporating the very hydrophilic PEG macromonomer in the synthesis is difficult at high mole %. This is because the synthesis is based on the hydrophobic collapse of growing pNIPAm chains and this typically makes the incorporation of hydrophilic monomer difficult in the growing polymer.[19,38] However, our results suggest

that if the growing chain is relatively hydrophilic (as obtained from incorporation of AAc), then the targeted concentration of PEG can be effectively incorporated. This phenomenon is currently under further investigation.

Table 4.3. Fmoc Protected Macromonomer Incorporation.

Sample	Mole % of Monomer added	Mole % of Monomer detected by ^{1}H NMR[49]
pNIPAm-Fmoc Core	5.0	3.9 ± 0.2
pNIPAm-Fmoc Shell	1.0	1.3 ± 0.1
pNIPAm-Fmoc Shell	5.0	3.5 ± 0.3
pNIPAm-Fmoc-AAc Shell	5.0	5.3 ± 0.2

To further explore whether the amine and carboxylic acid groups are available for chemoligation, we conjugated 5-aminofluorescein to the carboxyl groups and TAMRA-SE to the amine groups. Figures 4.6a and 4.6b show the absorption and the fluorescence spectra of the conjugated nanogels, respectively. The carboxyl group can be easily conjugated to 5-aminofluorescein using carbodiimide chemistry if the amine group is kept protected, as seen by an emission maximum at 520 nm due to the conjugated fluorescein. After the conjugation of carboxyl group the deprotection of the amines

yielded free amine groups, which were further used for conjugation with TAMRA-SE. The pNIPAm-Fmoc and pNIPAm-Fmoc-AAc nanogels both showed emission maxima at 578 nm due to conjugated TAMRA. From the spectrum it can be seen that for pNIPAm-Fmoc-AAc nanogels conjugated with both 5-aminofluorescein and TAMRA-SE two distinct absorption and emission peaks were observed for the fluorophores conjugated. There is a shift in the emission wavelength of TAMRA-SE from 578 nm to 570 nm for the pNIPAM-Fmoc-AAc nanogels conjugated with both 5-aminofluorescein and TAMRA-SE. Although the precise reason for this is not known, we tentatively attribute the spectral shift to the difference in the environment of the TAMRA fluorophores due to the presence of fluorescein molecules on the same nanoparticles. These studies clearly suggest the accessibility and ease of conjugation with molecules of interest for both the functional groups on the nanogels.
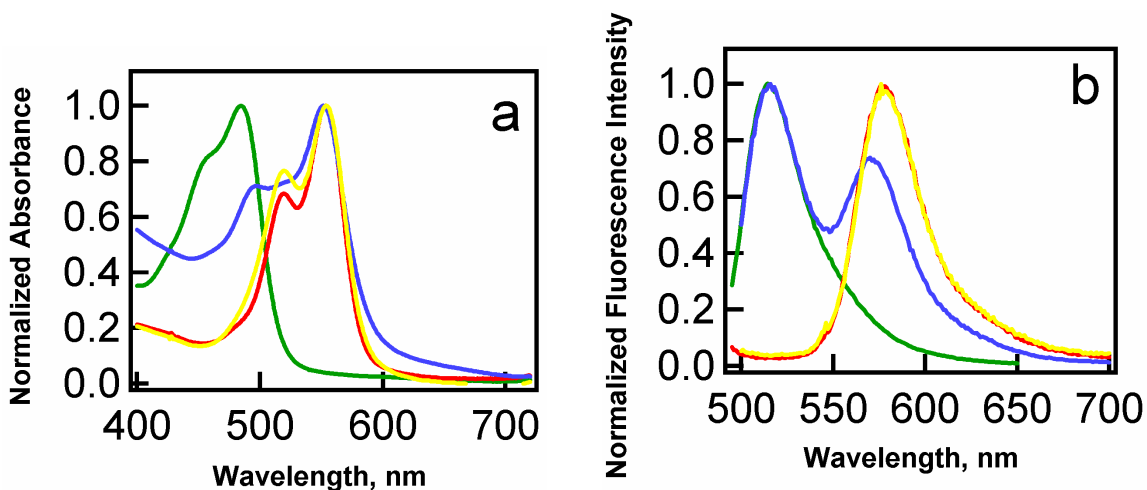
Figure 4.6. Absorption (a) and emission (b) spectra for the multifunctional nanogels conjugated with fluorescent dyes. (Green) 5-aminofluorescein conjugated to the carboxyl groups on the Fmoc-protected pNIPAm-Fmoc-AAc nanogels. (Yellow) TAMRA-SE conjugated with the free amines on the deprotected pNIPAm-Fmoc-AAc nanogels and (red) pNIPAm-Fmoc nanogels. (Blue) 5-aminofluorescein and TAMRA-SE conjugated to the carboxyl and free amine groups respectively on the deprotected pNIPAm-Fmoc-AAc nanogels.

4.4 Conclusions

We have reported a very simple synthetic procedure for incorporating traditionally interfering functional groups such as amine and carboxylic acid in hydrogel nanoparticles. Well established synthetic methodologies for protection and deprotection borrowed from organic chemistry were used in synthesizing colloidally stable nanogels equipped with these interfering groups. One advantage of using this technique is that it gives control over the access and availability of the functional groups at any stage in a post-polymerization bioconjugation strategy. The multiple functional groups present on the nanogels can be readily conjugated to multiple ligands. In summary, even though the functional groups are interfering, the protection of one of the groups allows the use of an

98

otherwise interfering chemoligation step. The two functional groups on the nanogel can thus be functionalized in a pseudo-orthogonal fashion. This scheme for nanoparticle synthesis and subsequent functionalization provides a facile route for the future attachment of biologically important molecules such as targeting ligands, reporter molecules, and therapeutic agents onto the same nanoparticle thus broadening their utility. Also, the synthetic route described provides very good control over the size, composition and architecture of the nanoparticles making it an attractive way to synthesize materials with complex topology.

4.5 References and Notes

[1]   Katz, E.; Willner, I. Nanobiotechnology: integrated nanoparticle-biomolecule hybrid systems: Synthesis, properties, and applications. *Angew. Chem., Int. Ed.* **2004**, *43*, 6042-6108.

[2]   Langer, R. New methods of drug delivery. *Science* **1990**, *249*, 1527-1533.

[3]   Holtz, J. H.; Asher, S. A. Polymerized colloidal crystal hydrogel films as intelligent chemical sensing materials. *Nature* **1997**, *389*, 829-832.

[4]   Ohko, Y.; Tatsuma, T.; Fujii, T.; Naoi, K.; Niwa, C.; Kubota, Y.; Fujishima, A. Multicolor photochromism of TiO2 films loaded with silver nanoparticles. *Nat. Mater.* **2003**, *2*, 29-31.

[5]   Kim, J.; Singh, N.; Lyon, L. A. Label-free biosensing with hydrogel microlenses. *Angew. Chem., Int. Ed.* **2006**, *45*, 1446-1449.

[6]   Debord, J. D.; Eustis, S.; Debord, S. B.; Lofye, M. T.; Lyon, L. A. Color-tunable colloidal crystals from soft hydrogel nanoparticles. *Adv. Mater.* **2002**, *14*, 658-662.

[7]   Lyon, L. A.; Debord, J. D.; Debord, S. B.; Jones, C. D.; McGrath, J. G.; Serpe, M. J. Microgel Colloidal Crystals. *J. Phys. Chem. B* **2004**, *108*, 19099-19108.

[8]   Niemeyer, C. M. Functional hybrid devices of proteins and inorganic nanoparticles. *Angew. Chem., Int. Ed.* **2003**, *42*, 5796-5800.

[9]   Bergbreiter, D. E.; Case, B. L.; Liu, Y.-S.; Caraway, J. W. Poly(N-isopropylacrylamide) Soluble Polymer Supports in Catalysis and Synthesis. *Macromolecules* **1998**, *31*, 6053-6062.

[10]   Anastase-Ravion, S.; Ding, Z.; Pelle, A.; Hoffman, A. S.; Letourneur, D. New antibody purification procedure using a thermally responsive poly(N-isopropylacrylamide)-dextran derivative conjugate. *J. Chromatogr., B: Biomed. Sci. Appl.* **2001**, *761*, 247-254.

[11]   Brugger, B.; Richtering, W. Magnetic, thermosensitive microgels as stimuli-responsive emulsifiers allowing for remote control of separability and stability of oil in water-emulsions. *Adv. Mater.* **2007**, *19*, 2973-2978.

[12]   Umeno, D.; Kawasaki, M.; Maeda, M. Water-soluble conjugate of double-stranded DNA and Poly(N-isopropylacrylamide) for one-pot affinity precipitation separation of DNA-binding proteins. *Bioconjug. Chem.* **1998**, *9*, 719-724.

[13]   Das, M.; Zhang, H.; Kumacheva, E. Microgels, old materials with new applications. *Annu. Rev. Mater. Res.* **2006**, *36*, 117-142.

[14]   Pelton, R. Temperature-sensitive aqueous microgels. *Adv. Colloid Interface Sci.* **2000**, *85*, 1-33.

[15]   Daly, E.; Saunders, B. R. Temperature-dependent electrophoretic mobility and hydrodynamic radius measurements of poly(N-isopropylacrylamide) microgel particles: structural insights. *Phys. Chem. Chem. Phys.* **2000**, *2*, 3187-3193.

[16]   Nayak, S.; Lyon, L. A. Soft nanotechnology with soft nanoparticles. *Angew. Chem., Int. Ed.* **2005**, *44*, 7686-7708.

[17]   Dingenouts, N.; Seelenmeyer, S.; Deike, I.; Rosenfeldt, S.; Ballauff, M.; Lindner, P.; Narayanan, T. Analysis of thermosensitive core-shell colloids by small-angle

neutron scattering including contrast variation. *Phys. Chem. Chem. Phys.* **2001**, *3*, 1169-1174.

[18]   Duracher, D.; Sauzedde, F.; Elaissari, A.; Pichot, C.; Nabzar, L. Cationic amino-containing N-isopropylacrylamide-styrene copolymer particles. Part 2. Surface and colloidal characteristics. *Colloid Polym. Sci.* **1998**, *276*, 920-929.

[19]   Debord, J. D.; Lyon, L. A. Synthesis and Characterization of pH-Responsive Copolymer Microgels with Tunable Volume Phase Transition Temperatures. *Langmuir* **2003**, *19*, 7662-7664.

[20]   Lyon, L. A.; Nayak, S.; Kim, J. Photothermal control of microgel phase transitions. *Spectrum* **2004**, *17*, 18-23.

[21]   Kawaguchi, H.; Fujimoto, K.; Nakazawa, Y.; Sakagawa, M.; Ariyoshi, Y.; Shidara, M.; Okazaki, H.; Ebisawa, Y. Modification and functionalization of hydrogel microspheres. *Colloids Surf., A* **1996**, *109*, 147-154.

[22]   Wong, J. E.; Richtering, W. Surface modification of thermoresponsive microgels via layer-by-layer assembly of polyelectrolyte multilayers. *Prog. Colloid Polym. Sci.* **2006**, *133*, 45-51.

[23]   Nayak, S.; Lee, H.; Chmielewski, J.; Lyon, L. A. Folate-mediated cell targeting and cytotoxicity using thermoresponsive microgels. *J. Am. Chem. Soc.* **2004**, *126*, 10258-10259.

[24]   Nayak, S.; Lyon, L. A. Ligand-functionalized core/shell microgels with permselective shells. *Angew. Chem., Int. Ed.* **2004**, *43*, 6706-6709.

[25]   Pichot, C.; Duracher, D.; Elaissari, A.; Mallet, F. Immobilization of modified HIV-1-capsid p24 protein onto thermosensitive cationic core/shell particles. *Polym. Prepr.* **2000**, *41*, 1026-1027.

[26]   Zhou, G.; Elaissari, A.; Delair, T.; Pichot, C. Synthesis and characterization of surface-cyano-functionalized poly(N-isopropylacrylamide) latexes. *Colloid Polym. Sci.* **1998**, *276*, 1131-1139.

[27]   Grabarek, Z.; Gergely, J. Zero-Length Crosslinking Procedure with the Use of Active Esters. *Anal. Biochem.* **1990**, *185*, 131-135.

[28]   Hermanson, G. T. *Bioconjugate Techniques*; Academic Press: San Diego, **1996**.

[29]   Heskins, M.; Guillet, J. E. Solution properties of poly(N-isopropylacrylamide). *J. Macromol. Sci. Chem.* **1968**, *A2*, 1441-1455.

[30]   Hoffman, A. S.; Stayton, P. S.; El-Sayed, M. E. H.; Murthy, N.; Bulmus, V.; Lackey, C.; Cheung, C. Design of "smart" nano-scale delivery systems for biomolecular therapeutics. *J. Biomed. Nanotechnol.* **2007**, *3*, 213-217.

[31]   Kopecek, J. Hydrogel biomaterials: A smart future? *Biomaterials* **2007**, *28*, 5185-5192.

[32]   Wang, C.; Flynn, N. T.; Langer, R. Controlled structure and properties of thermoresponsive nanoparticle-hydrogel composites. *Adv. Mater.* **2004**, *16*, 1074-1079.

[33]   Berndt, I.; Pedersen, J. S.; Richtering, W. Temperature-sensitive core-shell microgel particles with dense shell. *Angew. Chem., Int. Ed.* **2006**, *45*, 1737-1741.

[34]   Gan, D.; Lyon, L. A. Amphiphilic, peptide-modified core/shell microgels. *Prog. Colloid Polym. Sci.* **2006**, *133*, 1-8.

[35]   Jones, C. D.; Lyon, L. A. Synthesis and Characterization of Multiresponsive Core-Shell Microgels. *Macromolecules* **2000**, *33*, 8301-8306.

[36]   Nayak, S.; Gan, D.; Serpe, M. J.; Lyon, L. A. Hollow thermoresponsive microgels. *Small* **2005**, *1*, 416-421.

[37]   Singh, N.; Lyon, L. A. Au Nanoparticle Templated Synthesis of pNIPAm Nanogels. *Chem. Mater.* **2007**, *19*, 719-726.

[38]   Gan, D.; Lyon, L. A. Synthesis and Protein Adsorption Resistance of PEG-Modified Poly(N-isopropylacrylamide) Core/Shell Microgels. *Macromolecules* **2002**, *35*, 9634-9639.

[39]   Meister, A.; Bastrop, M.; Koschoreck, S.; Garamus, V. M.; Sinemus, T.; Hempel, G.; Drescher, S.; Dobner, B.; Richtering, W.; Huber, K.; Blume, A. Structure-

[28]   Hermanson, G. T. *Bioconjugate Techniques*; Academic Press: San Diego, **1996**.

[29]   Heskins, M.; Guillet, J. E. Solution properties of poly(N-isopropylacrylamide). *J. Macromol. Sci. Chem.* **1968**, *A2*, 1441-1455.

[30]   Hoffman, A. S.; Stayton, P. S.; El-Sayed, M. E. H.; Murthy, N.; Bulmus, V.; Lackey, C.; Cheung, C. Design of "smart" nano-scale delivery systems for biomolecular therapeutics. *J. Biomed. Nanotechnol.* **2007**, *3*, 213-217.

[31]   Kopecek, J. Hydrogel biomaterials: A smart future? *Biomaterials* **2007**, *28*, 5185-5192.

[32]   Wang, C.; Flynn, N. T.; Langer, R. Controlled structure and properties of thermoresponsive nanoparticle-hydrogel composites. *Adv. Mater.* **2004**, *16*, 1074-1079.

[33]   Berndt, I.; Pedersen, J. S.; Richtering, W. Temperature-sensitive core-shell microgel particles with dense shell. *Angew. Chem., Int. Ed.* **2006**, *45*, 1737-1741.

[34]   Gan, D.; Lyon, L. A. Amphiphilic, peptide-modified core/shell microgels. *Prog. Colloid Polym. Sci.* **2006**, *133*, 1-8.

[35]   Jones, C. D.; Lyon, L. A. Synthesis and Characterization of Multiresponsive Core-Shell Microgels. *Macromolecules* **2000**, *33*, 8301-8306.

[36]   Nayak, S.; Gan, D.; Serpe, M. J.; Lyon, L. A. Hollow thermoresponsive microgels. *Small* **2005**, *1*, 416-421.

[37]   Singh, N.; Lyon, L. A. Au Nanoparticle Templated Synthesis of pNIPAm Nanogels. *Chem. Mater.* **2007**, *19*, 719-726.

[38]   Gan, D.; Lyon, L. A. Synthesis and Protein Adsorption Resistance of PEG-Modified Poly(N-isopropylacrylamide) Core/Shell Microgels. *Macromolecules* **2002**, *35*, 9634-9639.

[39]   Meister, A.; Bastrop, M.; Koschoreck, S.; Garamus, V. M.; Sinemus, T.; Hempel, G.; Drescher, S.; Dobner, B.; Richtering, W.; Huber, K.; Blume, A. Structure-

Property Relationship in Stimulus-Responsive Bolaamphiphile Hydrogels. *Langmuir* **2007**, *23*, 7715-7723.

[40]   Berndt, I.; Pedersen, J. S.; Richtering, W. Structure of Multiresponsive "Intelligent" Core-Shell Microgels. *J. Am. Chem. Soc.* **2005**, *127*, 9372-9373.

[41]   Senff, H.; Richtering, W.; Norhausen, C.; Weiss, A.; Ballauff, M. Rheology of a Temperature Sensitive Core-Shell Latex. *Langmuir* **1999**, *15*, 102-106.

[42]   Santos, A. M.; Elaissari, A.; Martinho, J. M. G.; Pichot, C. Synthesis of cationic poly(methyl methacrylate)-poly(N-isopropyl acrylamide) core-shell latexes via two-stage emulsion copolymerization. *Polymer* **2005**, *46*, 1181-1188.

[43]   Larsson, A.; Kuckling, D.; Schonhoff, M. 1H NMR of thermoreversible polymers in solution and at interfaces: the influence of charged groups on the phase transition. *Colloids Surf., A* **2001**, *190*, 185-192.

[44]   Tokuhiro, T.; Amiya, T.; Mamada, A.; Tanaka, T. NMR study of poly(N-isopropylacrylamide) gels near phase transition. *Macromolecules* **1991**, *24*, 2936-2943.

[45]   Shibayama, M.; Mizutani, S.-y.; Nomura, S. Thermal Properties of Copolymer Gels Containing N-Isopropylacrylamide. *Macromolecules* **1996**, *29*, 2019-2024.

[46]   Virtanen, J.; Baron, C.; Tenhu, H. Grafting of Poly(N-isopropylacrylamide) with Poly(ethylene oxide) under Various Reaction Conditions. *Macromolecules* **2000**, *33*, 336-341.

[47]   Virtanen, J.; Tenhu, H. Thermal Properties of Poly(N-isopropylacrylamide)-g-poly(ethylene oxide) in Aqueous Solutions: Influence of the Number and Distribution of the Grafts. *Macromolecules* **2000**, *33*, 5970-5975.

[48]   Snowden, M. J.; Chowdhry, B. Z.; Vincent, B.; Morris, G. E. Colloidal copolymer microgels of N-isopropylacrylamide and acrylic acid: pH, ionic strength and temperature effects. *J. Chem. Soc., Faraday Trans.* **1996**, *92*, 5013-5016.

[49]   *In some cases, the value obtained is slightly higher than expected possibly due to slight overestimation of the integrated peak area.*

CHAPTER 5

BENZOPHENONE CHEMISTRY AS A VERSATILE CHEMICAL CROSSLINKING APPROACH

The central focus of this chapter is the functionalization of hydrogel nanoparticles with benzophenone (BP) chromophore and to utilize BP's ability to react with alkyl C-H bonds under UV irradiation to crosslink C-H groups of nearby polymer chains. Such a strategy can be used to photo-cross-link two BP modified particles (inter-cross-linking) for making stable crosslinked thin films, for photo-tethering of biomolecules, or for post-polymerization cross-linking of the polymer chains within a particle (intra-cross-linking) giving more densely cross-linked particles for a variety of applications.

5.1 Introduction

Benzophenone (BP) photochemistry has attracted the attention of biochemists for over two decades.[1] The expanding use of BP photoprobes can be attributed to BP's ability to be manipulated in ambient light and its activation at a wavelength around 350-360 nm causing less damage to biomolecules. Photo-activated BP reacts with C-H bonds making it a very attractive photoaffinity label for efficient covalent modifications of

macromolecules.[1,2] We have explored various applications of benzophenone modified nanogels. We discuss in this chapter how a general photo-affinity labeling approach can be used to address a number of issues in the fields of nanotechnology and drug delivery.

5.1.1 Benzophenone for Cross-linking of Colloidal Crystals

Monodisperse colloidal systems have been used as models for the study of phase transitions and as templates for the fabrication of photonic crystals.[3-9] Also, such assemblies are attractive for various bio-applications.[10-12] It was found recently that poly-N-isopropylacrylamide (pNIPAm) nanoparticles can self-assemble into colloidal crystalline arrays in water.[13-18] Thermally sensitive pNIPAm nanoparticles in colloidal glasses can be converted into ordered crystals by particle-based volume transition and can be used to make photonic crystals as demonstrated by our group.[19-21] However, uses of pNIPAm colloidal dispersions that exploit their crystalline structure are limited because the structure can be easily destroyed by any external disturbance, such as small vibrations. To solve this problem, Asher *et al*. developed a method for embedding polystyrene colloidal crystalline array inside a hydrogel.[18,22] Hu *et al*. demonstrated that the crystalline structure of pNIPAM nanoparticles can be stabilized by bonding the particles into a network.[23-25] The latter approach has the shortcoming that the particle-linking reaction has to be carried out in a harsh environment (pH 12). Furthermore, the mechanical strength of the bonded particle assembly was found to be low due to its low polymer concentration. Thus, still one of the challenges in fields, in which optical properties of the hydrogel colloidal assemblies are of interest, is to make hydrogel assemblies that retain their crystalline structure against external forces. As a potential solution, we have employed BP for phototethering neighboring nanogels (Scheme 1a) in

a colloidal assembly to create a stable free standing crystalline film. pNIPAm-AAc nanogels were modified with ABP and were crystallized by injecting appropriate weight % in a cell (two glass cover slips with a silicone gasket in between). Further, photo-irradiation of the crystals with a long-wave UV lamp was shown to lead to inter-cross-linking of the particles forming diffractive films, which retained their crystallinity.

5.1.2 Intra-crosslinking of the Nanogels

One can take advantage of the porosity of the nanogel network (swollen state) to encapsulate biomolecules or small molecules; however, a shortcoming of the network porosity is the higher possibility of diffusion of the molecules out of the nanogels. To overcome this shortcoming the polymer network can be cross-linked post-encapsulation. In order to ensure that the biomolecules are not affected at the cross-linking stage, photo-crosslinking becomes advantageous as compared to harsher synthetic techniques. Here we describe such a strategy based on intra-crosslinking of ABP modified pNIPAM-AAc nanogels.
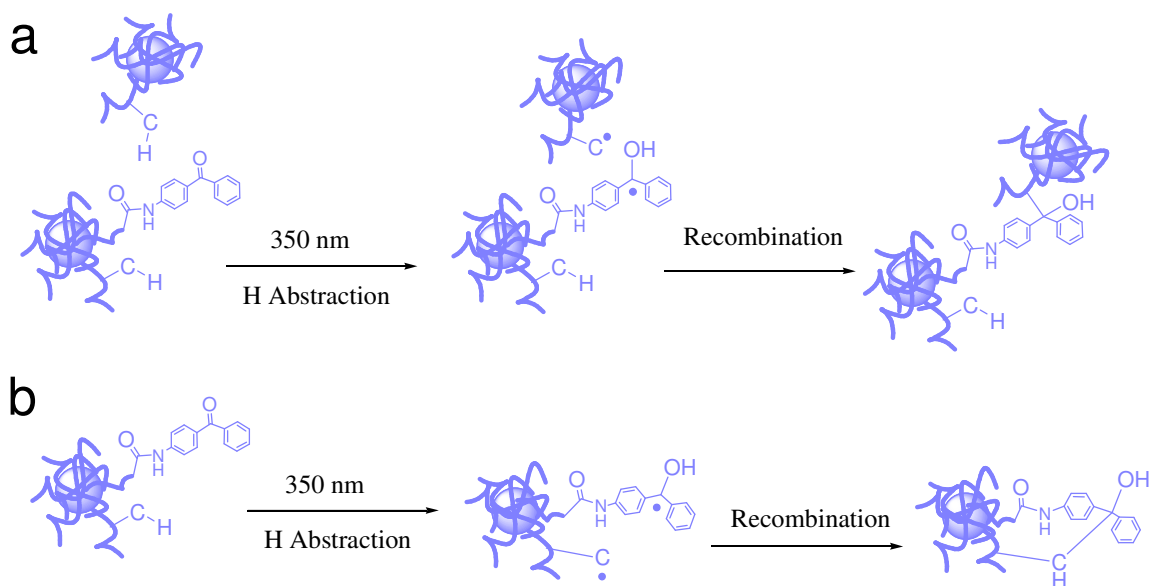
Scheme 5.1. Benzophenone-modified nanogels can be used to cross-link polymer chains (a) of two neighboring nanogels (inter-crosslinking) in a concentrated suspension (colloidal assembly) or (b) within the nanogel network (intra-crosslinking) in a dilute suspension.

5.1.3 Photo-tethering of Antibodies

Our group has recently developed responsive hydrogel microlenses in which specific protein binding events can be monitored as changes in the microlens focal length by using brightfield optical microscopy.[26] The goal for this project was to modify the existing system and develop a new microlens-based biosensing construct that is reversible. To achieve these goals, hydrogel microparticles (>1 micron in diameter) composed of poly(*N*-isopropylacrylamide-*co*-acrylic acid) (pNIPAm-*co*-AAc) were synthesized via aqueous free-radical precipitation polymerization. To render the nanogels antibody-reactive, a portion of the AAc groups were used to couple an antigen (biotin, as H$_2$N-Biotin) and aminobenzophenone (ABP) via carbodiimide coupling, respectively. Further functionalization by ABP allowed for photo-tethering of anti-biotin after it is

bound to the microlens by native antibody:antigen association. This scheme forms the basis of the biosensor's scaffolding/immobilization architecture, and allows for reversible sensing and broad tunability of the analyte concentration to which the microlens is sensitive.

Bioresponsive microlenses were prepared by exposure to a buffered solution of polyclonal anti-biotin, which binds to the microlenses via antibody:antigen interactions. Photoligation of the surface-tethered ABP to the antigen-bound antibody is accomplished via UV irradiation. Thus, the microlens surface is decorated with multiple antibody:antigen-based linkages, which can then be disrupted by introduction of free antigen to the surrounding medium. Since the antibody is covalently tethered to the microlens surface, washing with antigen-free media results in re-assembly of the tethered antibody:antigen pairs, thereby providing for a reversible biosensing microlens.

5.2 Experimental Section

5.2.1 Materials

Most of the reagents used in this chapter were described in Chapter 2 and 3. Additionally, 4-aminobenzophenone was obtained from Sigma and used as received. Glass cover slips, used as substrates were 24 x 50 mm Fisher Finest brand cover glass obtained from Fisher Scientific. 3-Aminopropyltrimethoxysilane (APTMS) was used for the functionalization of the glass substrates. Absolute (200 proof) and 95% ethanol were used for various purposes in this investigation. 1-ethyl-3-(3-dimethylaminopropyl) carbodiimide (EDC) and biotin hydrazide were purchased from Pierce. Dimethyl

sulfoxide (DMSO) was obtained from J.T. Baker. Polyclonal anti-biotin (raised in goat) were purchased from Sigma-Aldrich. For printing the pattern, 3M transparency film and a Hewlett Packard LaserJet 4000N printer was used.

5.2.2 Nanogel Synthesis

Synthesis of pNIPAm-AAc Core nanogels

Nanogels of pNIPAm crosslinked with BIS were prepared by the free-radical precipitation polymerization of NIPAm as described in Chapter 2. For incorporating carboxyl functional groups, which can be further used for modification, AAc was polymerized as a comonomer during the synthesis. This resulted in the parent pNIPAm-*co*-AAc nanogels. The total monomer concentration of 300 mM, having molar composition of 89.4% NIPAm, 0.5% BIS (crosslinker), 10% AAc, 0.1% 4-acrylamido-fluorescein was used in the nanogel synthesis. In brief, in a three-neck round-bottom flask, 100 mL of filtered aqueous solution of NIPAm and BIS was added and the mixture was heated to ~70 °C under a N_2 atmosphere while stirring with a magnetic stir bar. After 1 hr, AAc and 4-acrylamido-fluorescein were added to the flask and polymerization was immediately initiated by injecting 1 mL of a hot (~ 70 °C) APS solution (6.13 mM). The reaction was continued at 70 °C for 4 hours under a N_2 environment. Particle purification was performed by dialysis against water for ~2 weeks with the water being changed twice per day, using 10000 MW cut-off dialysis tubing (VWR).

Synthesis of pNIPAm-AAc Shells on pNIPAm Core nanogels

The pNIPAm cores (70 mM total monomer concentration) cross-linked with 2 mol% BIS were prepared by the method described in Chapter 2. A 40 mM pNIPAm-AAc

shell was added on the cores using similar protocol for shell synthesis as decribed in Chapter 2.

5.2.3 Functionalization with ABP

Functionalization for Inter and Intra cross-linking studies:

The pNIPAm-AAc shell nanogels were modified by ABP using DCC as the coupling reagent. The nanogels (0.0093 g) dispersed in 8 mL DMSO was reacted with ABP (0.0081 g in 1 mL DMSO, 1 equivalent to the carboxyl groups) in the presence of DCC (0.0088 g in 1 mL DMSO, 1 equivalent to the carboxyl groups). The reaction was carried out overnight at room temperature while stirring in dark. Adding 1 mL de-ionized water (5 times) to the reaction solution and filtration of the precipitated solid resulted in removal of insoluble side products from the nanogel solution. The filtrate was subjected to several centrifugation cycles (centrifugation and resuspension) to remove any soluble reactant or side products. Finally the solvent was replaced by desired buffer solution by several more centrifugation cycles.

Functionalization for antibody photo-tethering:

After the nanogel synthesis, the carboxyl groups on the anionic nanogel were used to functionalize them with biotin and 4-aminobenzophenone (ABP) using carbodiimides such as 1-ethyl-3-(3-dimethylaminopropyl) carbodiimide (EDC) and dicyclohexylcarbodiimide (DCC) respectively. The functionalization was done by consuming ~50% of the carboxyl groups on the particles by biotin and other ~50% by ABP. Some portion of AAc groups are expected to remain available for binding to the cationic glass substrate because the reaction efficiency of the carbodiimide coupling is

<100 %. Biotinylation of 10-fold 2-[*N*-morpholino]ehtanesulfonic acid (MES) (pH 4.7) diluted anionic nanogel (1 mL) was done by adding biotin hydrazide (3.8 mg dissolved in 0.5 mL of dimethyl sulfoxide (DMSO), 50 % of the total amount of acrylic acid in the nanogel solution) to the dilute nanogel solution. To activate the coupling reaction EDC (15 mg) was added to the nanogel and biotin solution. The reaction was carried out while stirring overnight at 4 °C. Unreacted biotin hydrazide was removed by several cycles of centrifugation followed by resuspension in phosphate buffered saline (PBS) (pH 7.5). The biotinylated acrylic acid nanogel particles were then modified by ABP using DCC as the coupling reagent. Biotinylated acrylic acid nanogel particle solution (1 mL in PBS (pH 7.5) was centrifuged and redispersed in DMSO several times to replace the solvent from buffer medium to DMSO and finally redispersed in 700 μL of DMSO. Further, 150 μL of 0.01 M ABP in DMSO was added to the nanogel solution followed by the addition of 150 μL of 0.01 M DCC in DMSO, making the total volume of reaction solution to 1 mL. The reaction was carried out overnight at room temperature while stirring in dark. Adding 0.5 mL de-ionized water to the reaction solution and filtration of the precipitated solid resulted in removal of insoluble side products from the nanogel solution. The filtrate was subjected to several centrifugation cycles (centrifugation and resuspension) to remove any soluble reactant or side products. Finally the solvent was replaced by PBS buffer (pH 7.5) by several more centrifugation cycles.

5.2.4 Colloidal Crystal and Film Formation due to Inter-crosslinking

Colloidal crystals were prepared using the ABP modified pNIPAm-AAc, particles via thermal annealing. To prepare concentrated dispersion, the nanogels were centrifuged

for ~15-30 min at 20,800 × *g* rcf at 25 °C. The supernatant was removed and the pellet was vortexed to form the concentrated suspension to be used for crystal formation.

A sample cell compartment was prepared by sandwiching a silicon chamber gasket (19 mm × 6 mm, 0.5 mm deep, Molecular Probes) between two glass cover slips (Fisher, 22 × 30 mm). The gasket was soaked and rinsed in ethanol to prior to use. To make the gasket sticky a piece of Scotch tape was applied to each side of the gasket to transfer the tape adhesive onto the gasket. Two cover slips were placed on the both the sides of the sticky gasket and pressed together firmly.

The suspensions of concentrated nanogels were heated to ~50 °C in a heating block (Temp-Blok, Lab-Line), making the suspension fluid. The suspension was then vortexed to make it homogeneous. While the nanogel sample suspension was hot it was introduced to the sample cell by syringe injection through the gasket. The samples were placed on the heating block and covered with a aluminium foil covered plastic casing lined with glass wool to keep the samples insulated and under dark. After heating for about 15 min, the heating block was turned off, this provided a cooling rate slow enough to achieve crystalline self-assembly.

Once the crystalline assembly was obtained the crystals were UV irradiated using a 100W longwave UV lamp for 30 min on each side while cooling the sample on an ice bath. After irradiation the top cover slip was carefully removed from the gasket and the films were dried. The gasket was then removed and the film was then peeled off and soaked in water.

5.2.5 Intra-crosslinking of Nanogels

Very dilute solutions of the ABP modified particles were prepared in DI water, 10 mM pH 3.5 and 10 mM pH 5.43 buffer solution. The solutions were irradiated with long-range UV lamp for 30 min and the particle size was analyzed by DLS and MALLS.

5.2.6 Bioresponsive Hydrogel Microlens Substrate Preparation

Firstly, glass cover slips were treated in an Ar plasma (Harrick Scientific) for 30 min to remove any organic residuals from the glass surface. Plasma treatment was followed by immersion of the glass substrates in an ethanolic (absolute ethanol) 1% APTMS solution for ~2 hrs, after which they were removed from the solution and rinsed several times with 95% ethanol. These silane functionalized glass substrates were stored in 95% ethanol for no longer than 5 days prior to use. Prior to assembly the substrates were rinsed with DI water and dried by a stream of N_2 gas. The silane functionalized glass substrate was then exposed to an aqueous 10% (v/v dilution of initial concentration following synthesis) biotin-ABP functionalized nanogel solution buffered by 10 mM PBS buffer pH 7.5. After 30 min, the substrate was rinsed with DI water, and dried with N_2 gas to leave behind nanogels that are strongly attached due to Coulombic interactions to the substrate. A microlens array/silicone gasket/coverslip sandwich assembly was prepared and into the void space, buffered solution of polyclonal anti-biotin was introduced. The substrate was rinsed and the medium was replaced with PBS buffer pH 7.5 after 3 hrs of incubation. As a control, a microlens array of the parent pNIPAm-*co*-AAc was also prepared in a similar fashion. The antigen-bound antibody was photoligated using the nanogel-tethered ABP via UV irradiation using a 100W longwave

UV lamp for 30 min while cooling the coverslip on an ice bath. The microlenses prepared were studied for reversibility by optical microscopy.

5.2.7 Characterization Techniques

The nanogels or the assembly before and after photo-crosslinking was characterized using UV-Vis spectroscopy, PCS and multi-angle laser light scattering (MALLS) to determine the photo-crosslinking process, particle hydrodynamic radius (R_h) and the radius of gyration (R_g), respectively. Detailed descriptions of some of these procedures can be found in Chapter 3. Additional methods used for characterization are described below.

5.2.8 Static Light Scattering

Multi-angle laser light scattering (MALLS, Wyatt Technology, Inc.) was employed to determine the radius of gyration (R_g) of the hydrated particles before and after intra-crosslinking. Asymmetric field flow fractionation (AFFF, Eclipse, Wyatt Technology, Inc.) was utilized to achieve particle separation based on hydrodynamic volume using a solvent cross-flow.[27,28] The AFFF method that was employed first concentrated the sample at one end of the AFFF channel using the focusing mode, followed by sample elution using a cross-flow rate of 0.25 mL/min that decreased consistently over a period of 36 min, followed by an additional elution time of 20 min with no cross-flow. Particle elution continued to the MALLS detector, which was equipped with a Peltier device to maintain a flow-cell temperature of 25 °C. Scattered light from a GaAs laser operating at 684 nm was collected at 16 fixed angle detectors and ASTRA 5.1.5.0 software was used to determine R_g values using the Debye fit method. Samples were diluted as necessary to achieve appropriate light scattering signals

following the AFFF separation. Uncertainty in calculated R_g values was determined from the standard deviations of each slice of data in the Debye plot, using the ASTRA software.

5.3 Results and Discussion

The pNIPAm-AAc nanogels synthesized were successfully modified with ABP as indicated by the absorption spectra (Figure 5.1) of the nanogels before and after ABP conjugation. The appearance of the absorbance peak around 300 nm indicates the presence of the benzophenone moiety on the nanogels. This peak disappears after the ABP is consumed in the photo-crosslinking by UV irradiation.
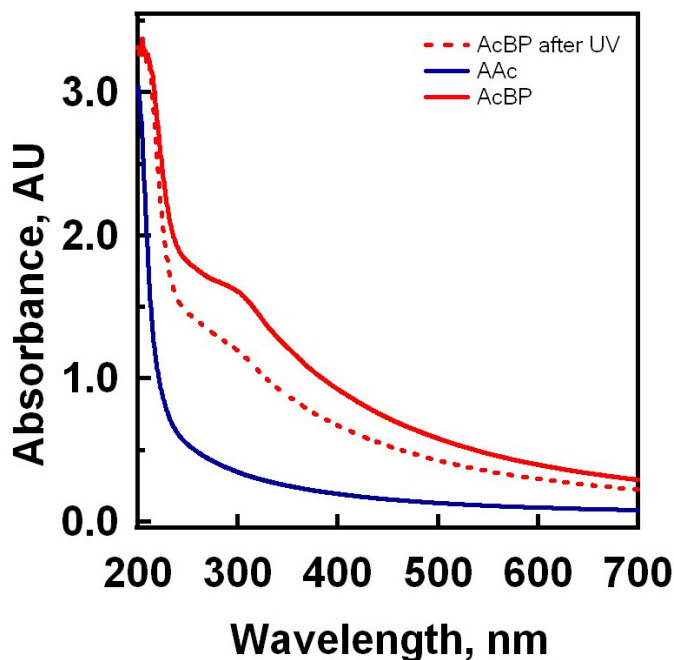
Figure 5.1. Absorption spectra for pNIPAm-AAc nanogels before ABP modification (blue), after ABP modification (red solid) and after UV irradiation of ABP-modified nanogels (red dashed).

5.3.1 Inter-crosslinking of colloidal assembly forming stable films

The cross-linking of the colloidal crystal assembly of pNIPAm-AAc nanogels resulted in a very stable free-standing film as indicated by Figure 5.2. The film when dry did not show any diffraction colors, which may be due non-visible diffraction because of the small particle size of the nanogels when dry. However when the films are soaked in water brilliant diffraction colors are observed as seen in Figure 5.2 due to the increase in the size of nanogels after film swelling. The increase in the wavelength of the diffraction colors (as observed by eye) are qualitatively consistent with the increase in the dry particle size, as per Bragg's Law.

Dried Free Standing, Benzophenone Crosslinked Crystalline Film

Benzophenone Crosslinked Crystalline Films soaked in Water
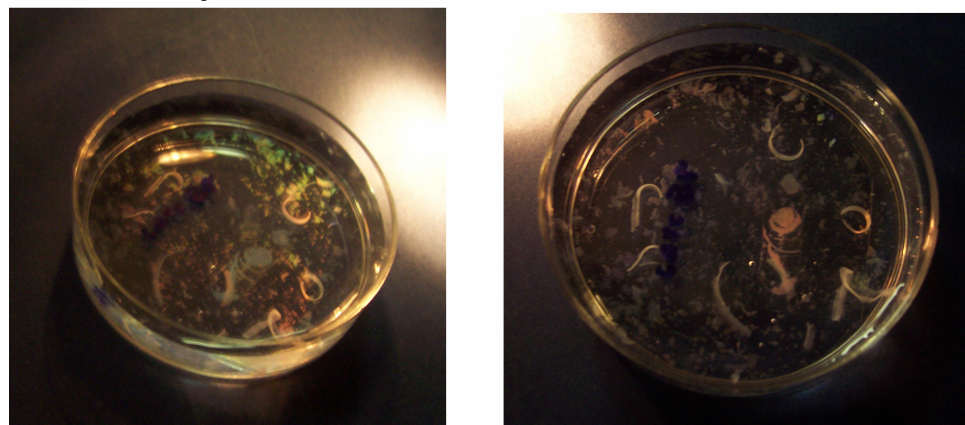
Figure 5.2. Digital camera images of photo-crosslinked crystalline films of ABP modified pNIPAm-AAc core nanogels in the presence of a flash-light.

5.3.2 Intra-crosslinking

To study the effect on the nanogels due to intra-crosslinking, a very dilute solution of the ABP-modified pNIPAm-AAc core and pNIPAm-AAc shell nanogels were prepared in DI water, 10 mM, pH 3.5 and 10 mM pH 5.43 buffer solutions. The consumption of benzophenone for the photo-crosslinking is confirmed by the change in

the absorption spectrum of the dilute solution before and after irradiation, as discussed above (Figure 5.3). The effect of intra-crosslinking was studied by PCS from which the changes in the R_h for the pNIPAm-AAc core nanogels have been tabulated in Table 5.1. It is interesting to note the changes in the size of the nanogels before and after ABP modification and also after UV irradiation (Table 5.1). The pNIPAm-AAc core nanogels in DI water became smaller by 56 nm following ABP modification. This decrease in size is probably due to reduced number of free carboxyl groups hence reduced Coulombic repulsion in the polymer network. After UV irradiation, the size is further reduced by 30 nm, which is probably due to the intra-crosslinking of the polymer chains. A more drastic effect of this intra-crosslinking is seen in the size of the nanogels at high temperature (above LCST). The nanogels after ABP modification become much smaller (R_h = 146 nm) compared to the native nanogel (R_h = 271 nm) at a higher temperature of 40 ^{o}C. Again this is because there is less repulsion in the chains after ABP modification as most of the carboxyl groups are consumed in the conjugation with ABP. The nanogels after UV-cross-linking are less deswollen (R_h = 209 nm) suggesting that the network becomes more rigid as the polymer chains are cross-linked.

The size changes in core-shell nanogels with an ABP-modified shell also suggest similar effects (shown in Table 5.2), as well as a pH dependence. When the pH of the solution (around pH = 3.5) was maintained below the pKa of AAc (pKa = 4.2) the change in size after ABP modification was less (Table 5.2a) as the carboxyl groups were already protonated. Also, since the nanogels are already slightly deswollen at pH 3.5, the change in size at high temperature is not much. In comparison, at pH = 5.4, the change in size was much larger (Table 5.2b).
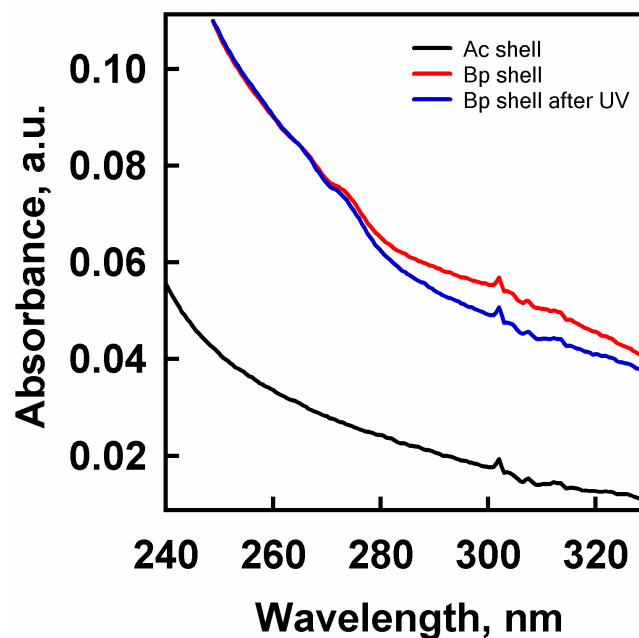
Figure 5.3. Absorption spectra of the sample solution used for intra-crosslinking in ABP modified pNIPAm-AAc nanogels before and after UV irradiation.

Table 5.1. Effect of Intra-Photocrosslinking on Hydrodynamic Radius of ABP Modified pNIPAm-AAc Nanogels UV Irradiated At Room Temperature.

Temp °C	pNIPAm-AAc in DI water		ABP modified	ABP modified after UV
	Solution pH	5.03	6.12	5.24
25	R_h (nm)	426	371	341
	% Polyd	7	14	10
40	R_h (nm)	271	146	209
	% Polyd	6	23	9

Table 5.2a. Effect of Intra-Photocrosslinking on Hydrodynamic Radius of ABP Modified Shell of pNIPAm-AAc Nanogels in 10 mM, pH 3.5 buffer solution UV Irradiated at Room Temperature.

Temp °C	pNIPAm-AAc shell in pH 3.5 buffer		BP modified shell	BP modified shell after UV
25	R_h (nm)	143	136	118
	% Polyd	6	9	14
40	R_h (nm)	74	74	75
	% Polyd	17	14	14

Table 5.2b. Effect of Intra-Photocrosslinking on Hydrodynamic Radius of ABP Modified Shell of pNIPAm-AAc Nanogels in 10 mM, pH 5.43 MES buffer solution UV Irradiated at Room Temperature.

Temp °C	pNIPAm-AAc shell in pH 5.43 buffer		BP modified shell	BP modified shell after UV
25	R_h (nm)	162	160	159
	% Polyd	14	14	14
40	R_h (nm)	92	106	111
	% Polyd	17	12	9

To observe the maximum effect of the intra-crosslinking, the UV irradiation was also performed at a higher temperature (40 °C). At this temperature (above LCST), the nanogel is in a deswollen state and the polymer chains are in close proximity of each other, thus allowing enhanced network cross-linking. The samples were then analyzed before and after irradiation by PCS and MALLS to obtain the hydrodynamic radius (R_h) and the radius of gyration (R_g) respectively. The hydrodynamic radii values obtained by PCS for the sample irradiated at 40 °C in 10 mM pH 3.5 formate buffer and in pH 5.5 MES buffer are plotted against temperature in Figure 5.4 and Figure 5.5 respectively. In both buffers, it is seen that the nanogels become smaller in size after irradiation suggesting increase in cross-linking density and therefore a tighter network. Also, the nanogels become rigid after cross-linking (as also observed earlier in this chapter) based on the degree of size change (i.e. deswelling) from 25 °C to 40 °C. The R_g values and the R_g/R_h ratios of the nanogels before and after UV irradiation are compared in Table 5.2.

Table 5.3. Comparison of the Radius of Gyration to the Hydrodynamic Radius for ABP Modified pNIPAm-AAc Shell Nanogels in pH 5.5 MES buffer. UV-crosslinking was Performed at 40 °C.

Temperature	Before UV Irradiation			After UV Irradiation		
	DLS	MALLS		DLS	MALLS	
	R_h (nm)	R_g (nm)	R_g/R_h	R_h (nm)	R_g (nm)	R_g/R_h
25 °C	120	118	0.976	100	113	1.13
40 °C	80	106	1.33	85	112	1.31
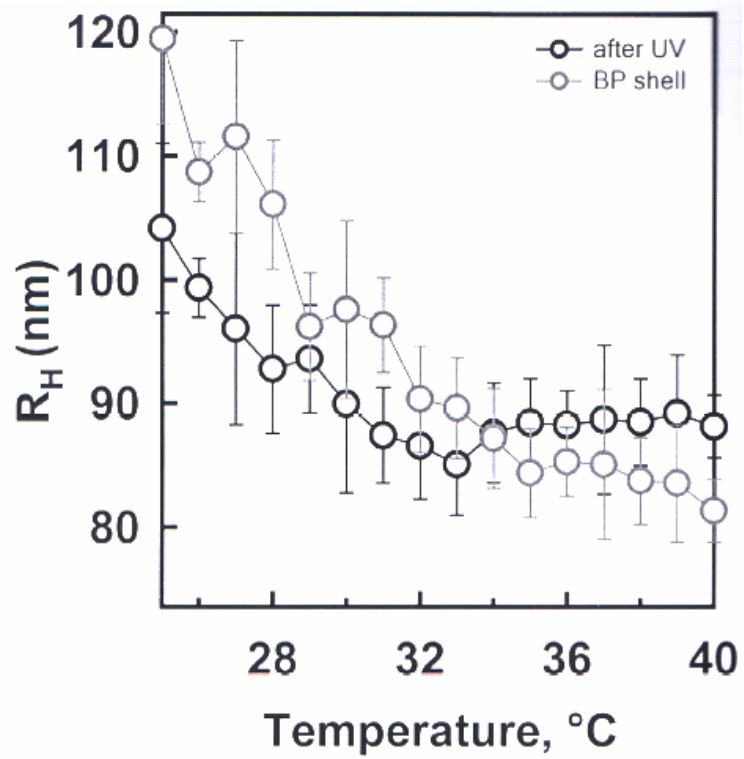
Figure 5.4. Changes in the hydrodynamic radius with temperature as observed by PCS for the ABP-modified pNIPAm-AAc shell. The sample was irradiated at 40 °C in 10 mM pH 3.5 formate buffer.
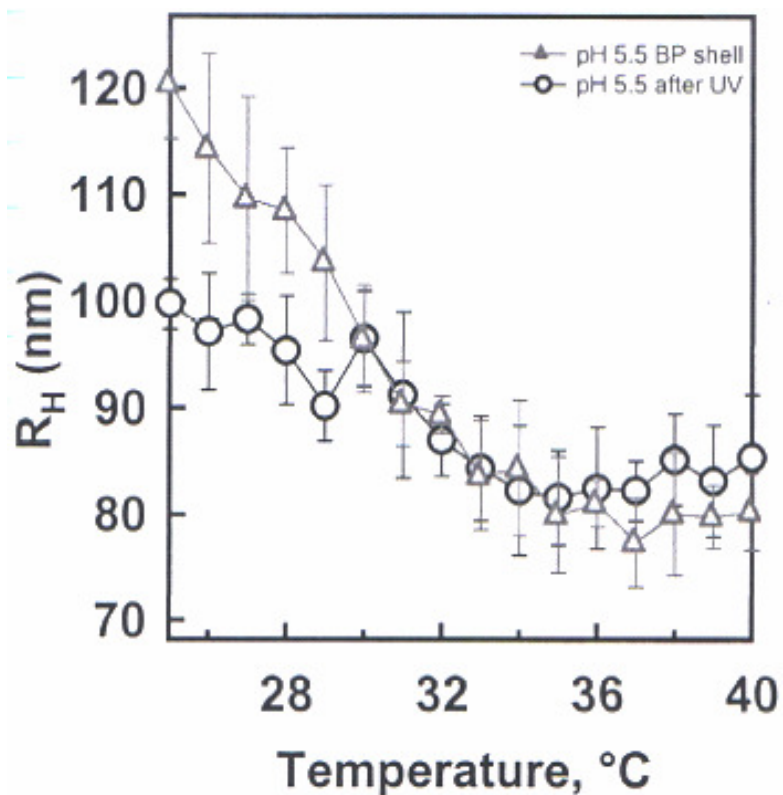
Figure 5.5. Hydrodynamic radius changes as observed by PCS for the ABP modified pNIPAm-AAc shell. The sample was irradiated at 40 °C in 10 mM pH 5.5 MES buffer.

The comparison of the R_g/R_h provides an insight into the polymer mass distribution in the nanogel network.[29] The R_g/R_h ratio for spheres with uniform polymer mass distribution is about 0.778.[30] The pNIPAm nanogel (in the swollen state) has a structure similar to the uniform sphere and hence the R_g/R_h value is close to 0.77 as shown by various other groups.[31,32] When the nanogels are swollen, the network density is low at the particle surface. This is because the cross-linker has a higher incorporation near the corona where the polymer network is denser.[33] The dangling chains at the surface increase the hydrodynamic radius but have a smaller effect on the radius of gyration, and hence the R_g/R_h is expected to be slightly smaller in the swollen state as

compared to the value for hard spheres.[30] However, at high temperature, the particle is in collapsed state and the R_g/R_h increases suggesting the compact nature of the polymer network.

The pNIPAm-AAc shell nanogels before UV irradiation has an R_g/R_h value of 0.976 whereas at high temperature it increases to 1.33 suggesting a more compact structure. Interestingly after UV irradiation, the R_g/R_h value increases to 1.13 for the nanogels even when in the swollen state. This increased ratio clearly suggest that the dangling chains, which were present at the surface before UV irradiation are cross-linked increasing the polymer mass density, giving the nanogels a more rigid network as also seen in the PCS studies (Table 5.3).

Hence, from these results, it is evident that the benzophenone can effectively cross-link the polymer network intra-molecularly thus providing a method for post-polymerization tuning of the porosity of the nanogel network.

5.3.3 Microlens Reversibility

The microlens prepared using the biotin and ABP modified pNIPAm-AAc nanogels were bioresponsive and the lens bioresponsivity was highly reversible, as shown in Figure 5.6. In this example, the biotin-ABP-functionalized hydrogel microlenses were incubated with a 6.7 μM solution (equivalent to 670 pmol) of polyclonal anti-biotin, followed by UV irradiation to covalently tether the antigen-associated antibodies to the microlens. The changes in the microlens-projected image were then monitored during exposure to 10 mM PBS (panels a, c, and e) and 1 mM biocytin (panels b, d, and f) solutions. Biocytin is a water-soluble analogue of biotin. The microlens is initially observed be in the "on" state in PBS buffer, which was characterized as the formation of

a double square image in image projection mode and the dark circle at the particle periphery in DIC image. When the microlenses are exposed to a solution of free biocytin, the microlenses are observed to switch to the "off" state, as characterized by a single square image (projection mode) and the disappearance of the black circle (DIC mode). This change in microlens focal length arises from disruption of the bound antibody:antigen pairs by competitive displacement with free antigens from solution. When the microlens is returned to an antigen-free buffer, the tethered antibody:antigen pairs re-assemble as the free antigens dissociate from the microlens. This response can then be cycled by repeated exposures to either antigen-containing or antigen-free buffer. These results indicate that the antibodies are indeed coupled to the microlens, as we would not expect reversibility if the first displacement interaction led to dissolution of antibody from the microlens surface.
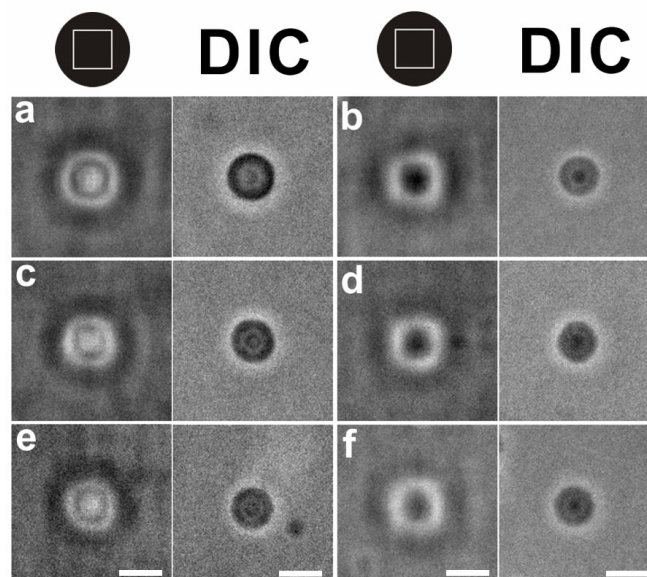
Figure 5.6. Reversibility of the bioresponsive microlenses. In each panel, the left image is the projection of the square pattern and the right image is the DIC image of the microlens. (a) Initial "on" state; (b) the lens turned "off" with 1 mM biocytin; (c, e) the lens reverts to the "on" state upon washing with PBS; (d, f) the same conditions as (b), which turns the lens "off". The scale bars are 2 μm.

5. 4 Conclusions

Benzophenone modified-pNIPAm-AAc nanogels were used to covalently cross-link a colloidal crystal array to form a free standing crystalline thin film. The free-standing crystalline nanogel film can serve as an effective Bragg-reflection based optical sensor for detecting reveal environmental changes. The photo-crosslinking strategy was also used to increase the cross-link density of the nanogel network by intra-crosslinking. The cross-linked film and the intra-crosslinked nanogels can be useful for various biomedical applications, such as loading biomolecules for controlled drug delivery. Thirdly, benzophenone photocrosslinking was employed for covalent tethering of biomolecules on a bioresponsive microlens construct, thus providing it reversibility,

making them more efficient and dynamic. The different examples discussed in this chapter illustrate the versatility of the photo-affinity labeling strategy, which can result in multitude of applications based on simple nanoparticle constructs.

5.5 References and Notes

[1]   Dorman, G.; Prestwich, G. D. Benzophenone Photophores in Biochemistry. *Biochemistry* **1994**, *33*, 5661-5673.

[2]   Murata, H.; Chang, B. J.; Prucker, O.; Dahm, M.; Ruhe, J. Polymeric coatings for biomedical devices. *Surf. Sci.* **2004**, *570*, 111-118.

[3]   Xia, Y. N.; Gates, B.; Yin, Y. D.; Lu, Y. Monodispersed colloidal spheres: Old materials with new applications. *Adv. Mater.* **2000**, *12*, 693-713.

[4]   Cheng, Z. D.; Russell, W. B.; Chaikin, P. M. Controlled growth of hard-sphere colloidal crystals. *Nature* **1999**, *401*, 893-895.

[5]   Jethmalani, J. M.; Sunkara, H. B.; Ford, W. T.; Willoughby, S. L.; Ackerson, B. J. Optical diffraction from silica-poly(methyl methacrylate) composite films. *Langmuir* **1997**, *13*, 2633-2639.

[6]   Jiang, P.; Bertone, J. F.; Colvin, V. L. A lost-wax approach to monodisperse colloids and their crystals. *Science* **2001**, *291*, 453-457.

[7]   van Blaaderen, A.; Ruel, R.; Wiltzius, P. Template-directed colloidal crystallization. *Nature* **1997**, *385*, 321-324.

[8]   Lellig, C.; Hartl, W.; Wagner, J.; Hempelmann, R. Immobilized highly charged colloidal crystals: A new route to three-dimensional mesoscale structured materials. *Angew. Chem. Int. Ed.* **2002**, *41*, 102-104.

[9]   Lu, Y.; Yin, Y. D.; Xia, Y. N. Three-dimensional photonic crystals with non-spherical colloids as building blocks. *Adv. Mater.* **2001**, *13*, 415-420.

[10]   Huang, G.; Gao, J.; Hu, Z. B.; John, J. V. S.; Ponder, B. C.; Moro, D. Controlled drug release from hydrogel nanoparticle networks. *J. Controlled Release* **2004**, *94*, 303-311.

[11]   Xia, X. H.; Hu, Z. B.; Marquez, M. Physically bonded nanoparticle networks: a novel drug delivery system. *J. Controlled Release* **2005**, *103*, 21-30.

[12]   Tsuji, S.; Kawaguchi, H. Colored thin films prepared from hydrogel microspheres. *Langmuir* **2005**, *21*, 8439-8442.

[13]   Gao, J.; Hu, Z. B. Optical properties of N-isopropylacrylamide microgel spheres in water. *Langmuir* **2002**, *18*, 1360-1367.

[14]   Hellweg, T.; Dewhurst, C. D.; Bruckner, E.; Kratz, K.; Eimer, W. Colloidal crystals made of poly(N-isopropylacrylamide) microgel particles. *Colloid. Polym. Sci.* **2000**, *278*, 972-978.

[15]   Wu, J. Z.; Huang, G.; Hu, Z. B. Interparticle potential and the phase behavior of temperature-sensitive microgel dispersions. *Macromolecules* **2003**, *36*, 440-448.

[16]   Wu, J. Z.; Zhou, B.; Hu, Z. B. Phase behavior of thermally responsive microgel colloids. *Phys. Rev. Lett.* **2003**, *90*.

[17]   Senff, H.; Richtering, W.; Norhausen, C.; Weiss, A.; Ballauff, M. Rheology of a temperature sensitive core-shell latex. *Langmuir* **1999**, *15*, 102-106.

[18]   Weissman, J. M.; Sunkara, H. B.; Tse, A. S.; Asher, S. A. Thermally switchable periodicities and diffraction from mesoscopically ordered materials. *Science* **1996**, *274*, 959-960.

[19]   Debord, J. D.; Eustis, S.; Debord, S. B.; Lofye, M. T.; Lyon, L. A. Color-tunable colloidal crystals from soft hydrogel nanoparticles. *Adv. Mater.* **2002**, *14*, 658-662.

[20]   Debord, J. D.; Lyon, L. A. Thermoresponsive photonic crystals. *J. Phys. Chem. B* **2000**, *104*, 6327-6331.

[21]   Debord, S. B.; Lyon, L. A. Influence of particle volume fraction on packing in responsive hydrogel colloidal crystals. *J. Phys. Chem. B* **2003**, *107*, 2927-2932.

[22]   Holtz, J. H.; Asher, S. A. Polymerized colloidal crystal hydrogel films as intelligent chemical sensing materials. *Nature* **1997**, *389*, 829-832.

[23]   Hu, Z. B.; Lu, X. H.; Gao, J.; Wang, C. J. Polymer gel nanoparticle networks. *Adv. Mater.* **2000**, *12*, 1173-1176.

[24]   Hu, Z. B.; Xia, X. H. Hydrogel nanoparticle dispersions with inverse thermoreversible gelation. *Adv. Mater.* **2004**, *16*, 305.

[25]   Hu, Z. B.; Huang, G. A new route to crystalline hydrogels, guided by a phase diagram. *Angew. Chem. Int. Ed.* **2003**, *42*, 4799-4802.

[26]   Kim, J.; Nayak, S.; Lyon, L. A. Bioresponsive hydrogel microlenses. *J. Amer. Chem. Soc.* **2005**, *127*, 9588-9592.

[27]   Andersson, M.; Wittgren, B.; Wahlund, K. G. Ultrahigh molar mass component detected in ethylhydroxyethyl cellulose by asymmetrical flow field-flow fractionation coupled to multiangle light scattering. *Anal. Chem.* **2001**, *73*, 4852-4861.

[28]   Wyatt, P. J.; Villapando, D. N. High-precision measurement of submicrometer particle size distributions. *Langmuir* **1997**, *13*, 3913-3914.

[29]   Wyatt, P. J. Light-Scattering and the Absolute Characterization of Macromolecules. *Anal. Chim. Acta* **1993**, *272*, 1-40.

[30]   Schmidt, M.; Nerger, D.; Burchard, W. Quasi-Elastic Light-Scattering from Branched Polymers .1. Polyvinylacetate and Polyvinylacetate-Microgels Prepared by Emulsion Polymerization. *Polymer* **1979**, *20*, 582-588.

[31]   Arleth, L.; Xia, X. H.; Hjelm, R. P.; Wu, J. Z.; Hu, Z. B. Volume transition and internal structures of small poly(N-isopropylacrylamide) microgels. *J. Polym. Sci., Part B: Polym. Phys.* **2005**, *43*, 849-860.

[32]   Wu, C. A comparison between the 'coil-to-globule' transition of linear chains and the "volume phase transition" of spherical microgels. *Polymer* **1998**, *39*, 4609-4619.

[33]   Wu, X.; Pelton, R. H.; Hamielec, A. E.; Woods, D. R.; McPhee, W. The Kinetics of Poly(N-Isopropylacrylamide) Microgel Latex Formation. *Colloid. Polym. Sci.* **1994**, *272*, 467-477.

CHAPTER 6

COVALENT TETHERING OF FUNCTIONAL NANOGEL FILMS ONTO POLY(ETHYLENE TEREPHTHALATE) SURFACES

Poly(*N*-isopropylacrylamide) (pNIPAm) nanogel films electrostatically attached on glass substrates have previously shown to be resistant towards protein adsorption and cell adhesion, provided oligomeric poly(ethylene glycol) diacrylates were incorporated into the nanogels as cross-linkers. In this Chapter a method for the surface functionalization of poly(ethylene terephthalate) (PET), an inert, flexible biomaterial, with pNIPAm nanogel films is described. This construct is geared towards the development of generalizable coatings to create cell adhesion-resistant biomaterials for *in vivo* applications. In order to provide the biomaterials with the desired stability in biological environments, the nanogel films were covalently attached to the PET surface using a photo-tethering scheme based on benzophenone. Atomic force microscopy of nanogel-modified PET substrates clearly shows the importance of the photo-tethering scheme for obtaining stable nanogel monolayers. The PET substrates coated with the nanogel monolayers exhibited reduced macrophage adhesion and spreading *in vitro*, further supporting the functionality and stability of the nanogel monolayer films deposited via our strategy. The surface chemistry described here can be used as a general

method for the modification of inert polymer substrates with stable monolayers of cell-adhesion resistant nanogels.

6.1 Introduction

Recently there has been an increasing interest in developing biotolerant polymeric surfaces that have the ability to support or immobilize biological functionalities tailored for specific biotechnological and medical applications.[1-4] As an important example, it is common to immobilize extracellular-matrix proteins (e.g., collagen, fibronectin) or cell signaling molecules on polymeric surfaces to yield functional biomaterials that have the ability to modulate cell adhesion, proliferation, and differentiation, thus mimicking a natural cellular environment.[3,5-8]

Another interesting class of polymeric materials with desirable properties for biotechnology is the hydrogel microparticle or nanogel. The synthesis, characterization and applications of stimuli-responsive nanogels have been extensively studied over the past few years. [9-13] Recently, Nolan *et al*. investigated the performance of poly(*N*-isopropylacrylamide) (pNIPAm) nanogels cross-linked with short poly(ethylene glycol) (PEG) chains, as protein adsorption-resistant films.[14] The PEG cross-linked pNIPAm nanogels having poly(acrylic acid) as co-monomer, were assembled electrostatically by spin-coating onto a cationic glass substrate. The results indicated that glass surfaces coated with nanogels showed reduced protein adsorption and cell adhesion *in vitro*, i.e. non-fouling behavior. However, the potential of these nanogel films as non-fouling base coatings for future biomedical implants cannot be probed and realized until they are assembled on a more flexible and biocompatible substrate than glass. This motivated our

current goal to design a flexible substrate-based nanogel film with potential non-fouling and anti-inflammatory behavior for *in vivo* studies. Equally important, we also aim to enhance the stability of the adherent nanogel films in comparison with the Coulombically assembled film in biological environments by improvements in the surface chemistry.

For *in vivo* studies of biomaterials, common desirable attributes for a model biomaterial (in this case, a polymer) include good mechanical strength, flexibility, chemical and physical stability in the biological environment, and a surface chemistry/composition that allows for facile biofunctionalization. In view of these properties, poly(ethylene terephthalate) (PET) was chosen as a model biomaterial onto which we could deposit non-fouling nanogel coatings in order to enhance its properties. PET has been extensively studied in biomaterial applications such as for sutures, vascular grafts, sewing cuffs for heart valves, and components for percutaneous access devices.[15-18] However, the PET surface is inert and hence not suitable for direct biofunctionalization. Major efforts have therefore been undertaken to introduce various functionalities onto the PET surface, such as amine, carboxyl, and hydroxyl moieties, which can be further employed for the covalent immobilization of biomacromolecules.[6,19,20] It is especially desirable that the methods used for the chemical modification are confined to the polymer surface, without affecting the bulk/mechanical properties of the substrate. A suitable technique in this regard has been the chemical activation of the inert polymer surface by plasma treatment, which has already been employed to render PET surfaces hydrophilic and hence more biocompatible.[21] It is also well known that the exposure of polymeric surfaces to a plasma along with oxygen

treatment generates surface-active hydroperoxide species that can be used for the chemical grafting of desired chemical and biological functional groups.[6,19,22-26]

Our method of functionalizing the PET with polymeric nanogel films (Scheme 6.1) is derived from previous methods based on plasma-induced graft polymerization of poly-acrylic acid (pAAc). Plasma- and ozone-induced graft polymerizations of various monomers on PET films, fibers, and fabrics have been demonstrated.[6,25,26] However, in order to make the method more general, and to give the adherent nanogel film more stability in biological environments, we introduced onto the PET surface a photo-affinity label, viz., aminobenzophenone. Upon excitation with UV irradiation, molecules of the benzophenone family have the ability to abstract an aliphatic hydrogen atom from any nearby polymer chain forming a covalent carbon-carbon bond.[4,27,28] Due to the presence of a nanogel in the close vicinity of the benzophenone, it can abstract hydrogen atom from the nanogel and hence covalently attach the particles to the PET surface (Scheme 6.2). Essentially, the benzophenone here serves as a glue between the base PET substrate and the nanogel film.
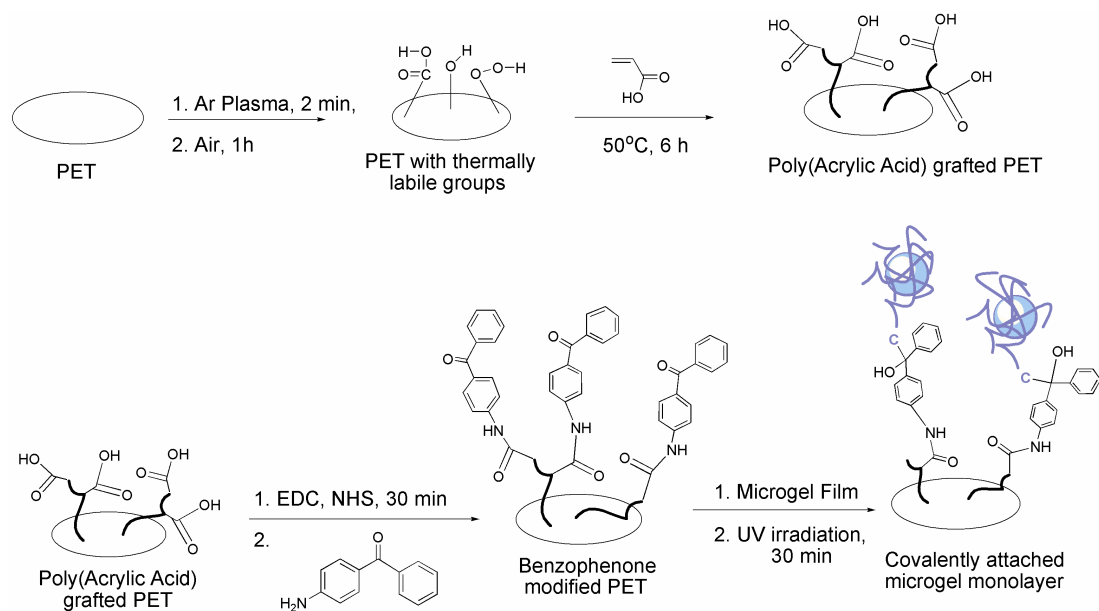
Scheme 6.1. Strategy for covalent tethering of nanogels onto a poly(ethylene terephthalate) surface.
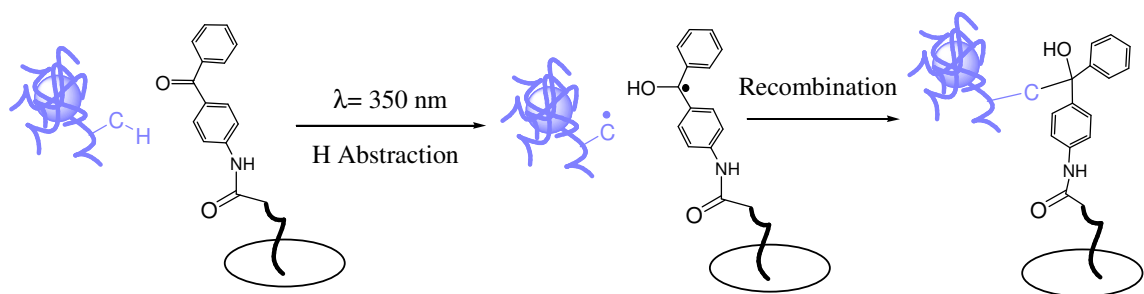
Scheme 6.2. Mechanism of covalent tethering of the nanogel onto the poly(ethylene terephthalate) surface via benzophenone chemistry.

6.2 Experimental Section

6.2.1 Materials

Most materials used in this Chapter can be found in previous Chapters. Poly(ethylene terephthalate) (PET) sheets were obtained from AIN Plastics; Marietta, GA. All other chemicals were used as received. Formate buffer solution (pH 3.47, 10 mM) was prepared from formic acid and NaCl obtained from Fisher Scientific. Poly(ethylene glycol) diacrylate (PEG) (PEG MW 575, Polysciences, Inc.) was used as received. Phosphate buffered saline (PBS) solution (pH 7.4, 10 mM) was prepared from NaCl (Fisher), Na_2HPO_4 (EM Science) and KH_2PO_4.

6.2.2 Nanogel Synthesis

Poly(*N*-isopropylacrylamide) (pNIPAm) nanogel particles (100 mM total monomer concentration) were synthesized with 2 mol % poly (ethylene glycol) (PEG) diacrylate (MW 575) by a free radical precipitation polymerization method. For incorporating functional groups that can be later modified, the nanogel particles were synthesized with 10 mol % acrylic acid as a co-monomer. Briefly, 0.4979 g of NIPAm monomer, 0.7011 g of cross-linker PEG-diacrylate, and 0.0025 g of surfactant sodium dodecyl sulfate (SDS) were dissolved in 49 mL distilled, deionized (DI) water, and filtered through a 0.2 μm filter. The solution was transferred to and stirred in a three-neck, round-bottom flask, and heated to 70 °C while purging with N_2 gas. After reaching 70 °C and purging for 1 h, 34.3 μL of acrylic acid was added, followed by the addition of 0.0114 g (dissolved in 1 mL DI water) of ammonium persulfate (APS) to initiate the reaction. The reaction was kept at 70 °C for 4 h. The synthesized nanogels were then

filtered and purified by five cycles of centrifugation at 15,422 g for 45 min. The supernatant was removed, and the particles were redispersed in DI water. The particles were then lyophilized overnight before being used for deposition onto the PET films.

6.2.3 PET Film Functionalization

PET sheets were cut into 8 mm diameter disks using biopsy punches and briefly rinsed in 70% ethanol to remove contaminants introduced during the manufacturing process. Graft polymerization of acrylic acid (AAc) on 8 mm PET films was done in two steps. PET films were first placed in an 18 W RF Ar plasma (Harrick Scientific) connected to a vacuum pump (5×10^{-4} mbar) for 2 min. Immediately after the Ar treatment, air was introduced into the plasma chamber and maintained at atmospheric pressure for 1 h to generate peroxide and other oxygen-containing functional groups on the PET surface. The films were immediately transferred to a round bottom flask containing an N_2 purged 25% (v/v) aqueous solution of acrylic acid. The grafting reaction was carried out for 6 h at 50 °C, after which the films were washed in water overnight. The degree of polymer grafting and hence the density of carboxyl groups on the PET surface can be controlled by varying the AAc concentration and reaction time.[22] The pAAc modified PET was further modified with 4-aminobenzophenone (ABP) using carbodiimide coupling.[29] The coupling of 4-aminobenzophenone is done traditionally as a one-step reaction using *N,N'*-dicyclohexylcarbodiimide (DCC) in organic media (DMSO). However, we used an aqueous carbodiimide coupling strategy based on activation of carboxyl groups with *N*-hydroxysuccinimide (NHS) and 1-ethyl-3-(3-dimethylaminopropyl) carbodiimide (EDC) and further reaction with the ABP. This is to avoid the formation of urea precipitate (the by-product in the DCC reaction), which is

difficult to remove completely from the surface being modified. Cell adhesion studies (Figure 6.1) suggests that the NHS activation strategy results in a better non-fouling surface as compared to the surface modified in one step using DCC. The pAAc modified PET films were first activated by incubation in 2 mM EDC and 5 mM NHS in 10 mM 2-[*N*-morpholino]ethanesulfonic acid (MES) buffer solution (pH 6.0) for 30 min at room temperature. The films were then and placed in 20 mM 2-mercaptoethanol solution in DI water to quench the EDC. The activated films were then reacted with ABP in DMSO for 2 h at room temperature. The ABP modified films were washed in DMSO and immersed in 10 mM hydroxylamine solution to quench the reaction. Finally, the films were washed in DI water.
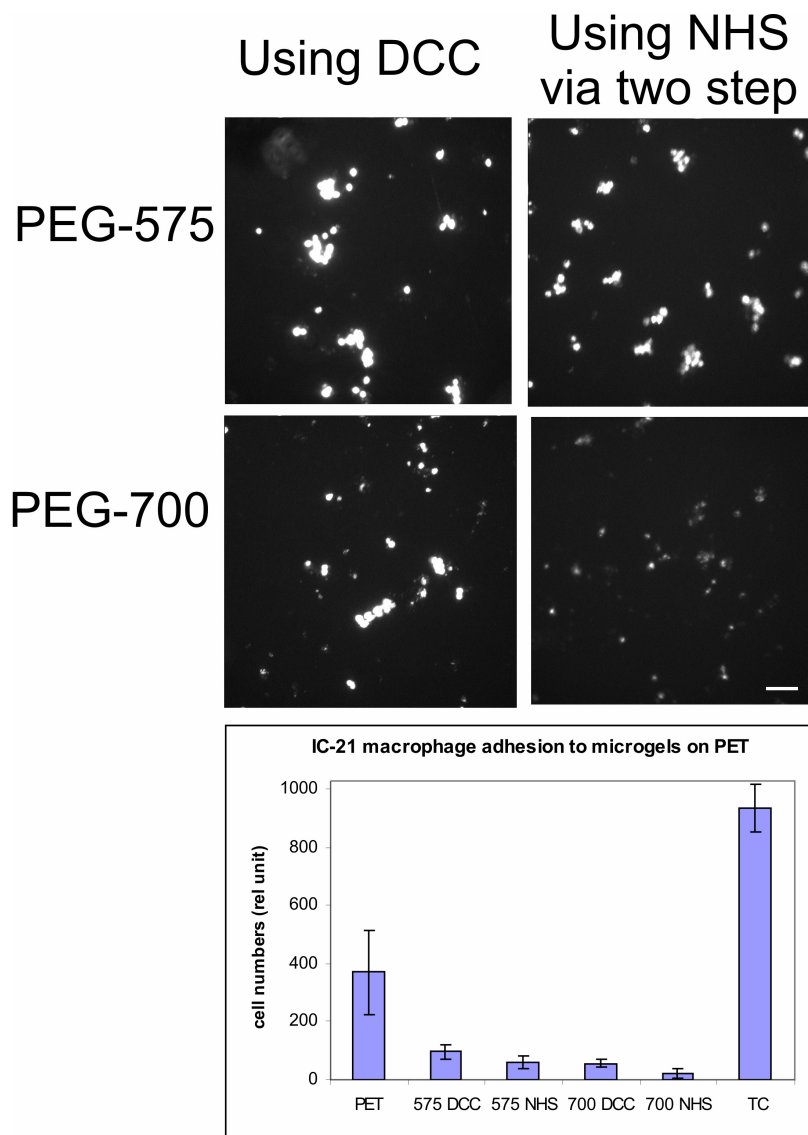
Figure 6.1. Macrophage adhesion studies on PETs covalently functionalized by nanogels using DCC and NHS+EDC. Adherent cells were stained with calcein-AM, which stains live cells. Scale bar = 100 μm.

6.2.3 Carboxyl Group Determination

The amount of pAAc grafting on the PET film surface was characterized by a colorimetric method based on Toluidine Blue O staining (Figure 6.2).[19] Briefly, the grafted film was placed for 6 h at 30 °C in a 0.5 mM Toluidine Blue O solution prepared

at pH 10. The film was then removed and thoroughly washed with NaOH (pH 10) to remove any dye nonspecifically adhered to the surface. The bound dye molecules were then desorbed from the film in a 50% acetic acid solution. The final dye content was determined from the optical density (OD) of the solution at 633 nm using a Shimadzu 1601 UV-visible spectrophotometer.
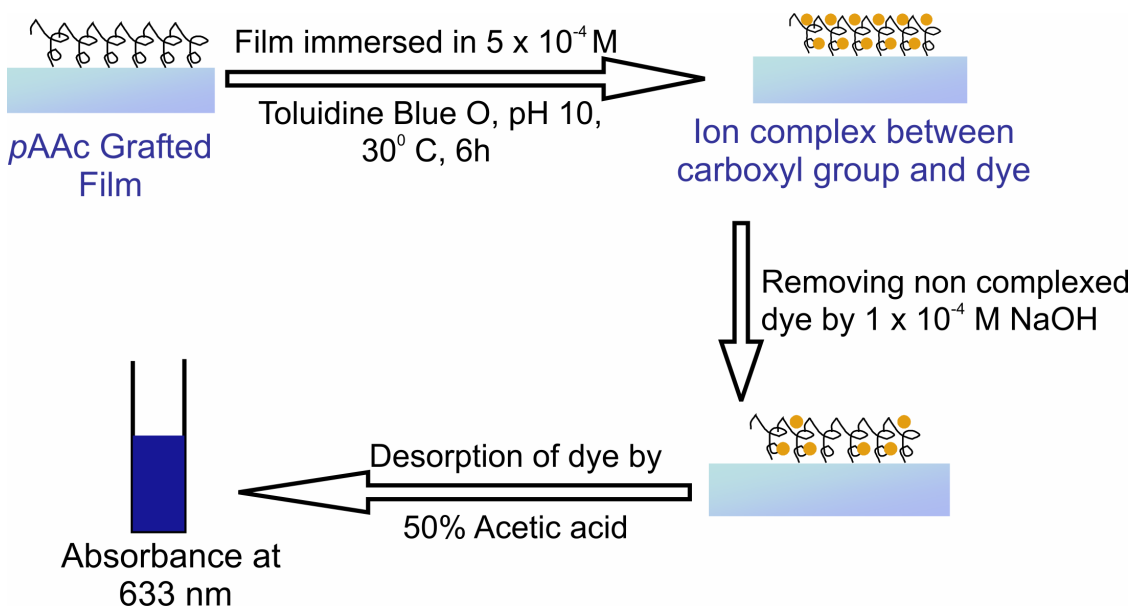
Figure 6.2. Toluidine assay for the determination of carboxyl groups on p(AAc) grafted PET.

6.2.4 Particle Deposition

A spin-coating process was used to deposit a layer of nanogel particles onto the functionalized PET films. The PET film was placed onto a glass slide, and the slide was placed onto the spin coater (Specialty Coating Systems) chuck and held in place by vacuum. The rotor speed was maintained at 500 rpm. Dried nanogels were dispersed in

a 10 mM formate buffer (pH 3.47) solution and one drop of the nanogel solution was deposited onto the PET film while spinning. After keeping the film on the spin coater for 100 s, a second drop of the nanogel solution was deposited. The PET film was left on the spin coater for additional 100 s and the film was allowed to dry. Finally, another drop of nanogel solution was deposited on the PET by the same process and the film was dried after 100 s of spinning. This process was done on both sides of the PET films under dark conditions. Each side of the PET, with the dried nanogel film, was irradiated by a 100 W longwave UV lamp (Blak-Ray) for 30 min to covalently attach the nanogels onto the PET surface. The nanogel-modified PET film was soaked in 10 mM phosphate buffer solution (pH 7.5) for 6 h and then washed with DI water.

6.2.5 Atomic Force Microscopy

Similar to the procedure in Chapters 3 and 4.

6.2.6 In vitro cell adhesion

The IC-21 murine macrophage cell line (ATCC; Manassas, VA) was used to determine the bioresistant properties of the nanogel coated PET *in vitro*. Cells were seeded at a density of 67,000 cells/cm^2 on unmodified PET and nanogel-coated PET disks in 24-well tissue culture-treated polystyrene plates in culture media containing 10% fetal bovine serum. After 48 h, adherent cells were fluorescently stained with calcein-AM (Molecular Probes, Eugene, OR) and imaged using a Nikon TE-300 microscope to determine relative cell numbers and cell spreading on each surface.

6. 3 Results and Discussion

In order to deposit uniform films of nanogels, the PET films had to be rendered amenable to robust particle attachment. The approach described above (Scheme 6.1) involves surface activation in an Ar plasma followed by the introduction of air to introduce thermally-labile groups. These thermally-labile groups thermally decompose to form radicals, thus initiating the polymerization of AAc to form pAAc-grafts on the PET surface.[22-24] The carboxyl groups of the pAAc on the PET surface are subsequently used in the functionalization of the surface with photo-affinity label (ABP) using carbodiimide coupling chemistry. We characterized the surface grafting density of pAAc by the Toluidine blue O dye binding assay. Figure 6.3 shows UV-visible absorbance spectra of Toluidine blue O dye arising from various surface treatments. Based on previous methods, by assuming a 1:1 ratio between the dye and the carboxylic acid groups, the OD at 633 nm gives a measure of the degree of grafting.[19,23] Thus, successful pAAc grafting of the PET surface is evidenced by an increase in the OD from ~0.01 for the bare PET substrate to about 2.02 for the modified surface. The color staining of the dyed films was very uniform across the samples, suggesting relatively uniform coating of the PET (data not shown). For the pAAc grafted PET, we estimate about 1.4×10^{-7} moles of carboxyl groups and following the reaction with ABP, only about 1.1×10^{-8} moles of carboxyl groups are left on the surface. Hence, this suggests that the benzophenone modification of the PET results in a loss of ~92% of the carboxyl groups due to their conversion into amide groups.
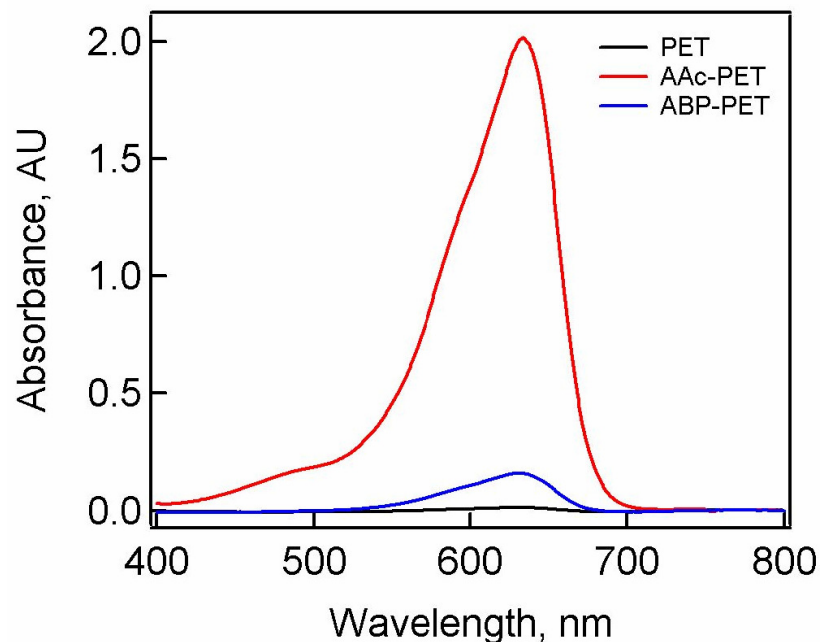
Figure 6.3. Absorption spectra for desorbed Toluidine Blue O dye from bare PET (black), poly(acrylic acid) grafted PET before (red) and after modification with 4-aminobenzophenone (blue).

Our method of surface functionalization of the PET with photo-affinity labels results in a very efficient surface modification with the nanogels. Figure 6.4 shows 3D renderings of AFM images obtained from a representative film. It can be seen from the 50×50 μm scan (Fig 6.4b) that there are no uncoated areas in the interrogated region. The nanogels also form a dense conformal monolayer as indicated by the 10 ×10 μm scan (Fig 6.4c). The unevenness in the nanogel-coated PET is due to the uneven base surface of the PET as seen in Figure 6.4a.
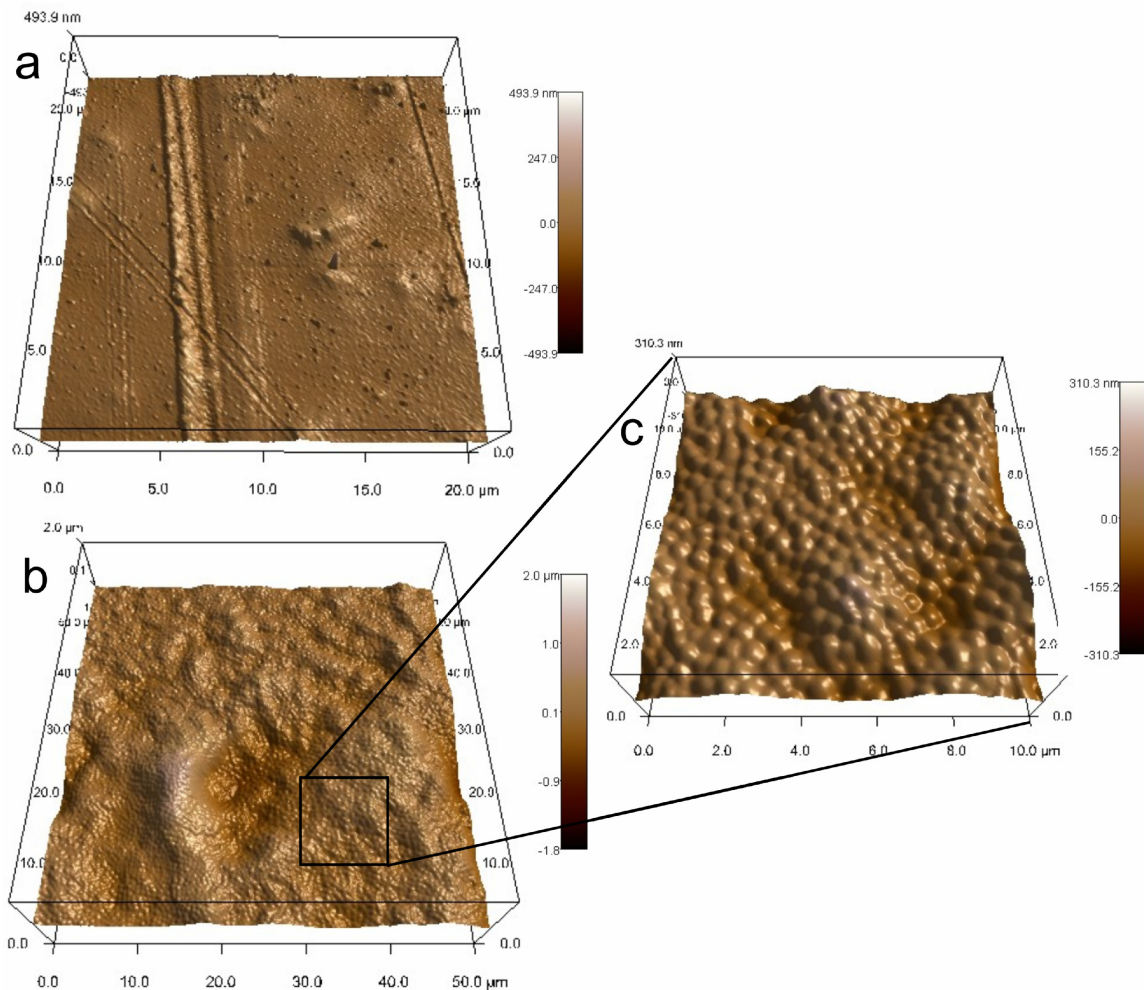
Figure 6.4. 3D rendering of AFM images for (a) bare PET, (b) and (c) nanogel-modified PET.

The benzophenone modification and photo-crosslinking are critically important steps for obtaining a stable monolayer, as suggested by Figure 6.5. Figure 6.5a shows an AFM image of a nanogel film that was spin-coated onto pAAc-grafted PET *without* benzophenone modification, followed by extensive washing. It is clear that the coverage is sparse with only a few nanogel particles retained on the surface. Since covalent linkages are not possible in the absence of the photo-affinity group, the particles cannot

remain adhered to the film during the washing step. This poor coverage is probably also due, in part, to the anionic charge on both the nanogels (due to the AAc co-monomers) and the film (due to the pAAc grafts). In the case of benzophenone-modified surface (Fig 6.5b), slightly more nanogels are retained on the PET surface, presumably due to less Coulombic repulsion between the nanogels and the modified PET. In this case, the photo-irradiation step is omitted and again, no covalent attachment is possible. However, the best results are found for the pAAc-grafted PET surfaces modified by benzophenone and further photo-irradiated (Fig 6.4b). The photo-cross-linking is thus shown to provide a nanogel film with excellent adhesion to the substrate and hence a presumed stability for use in biological environments.
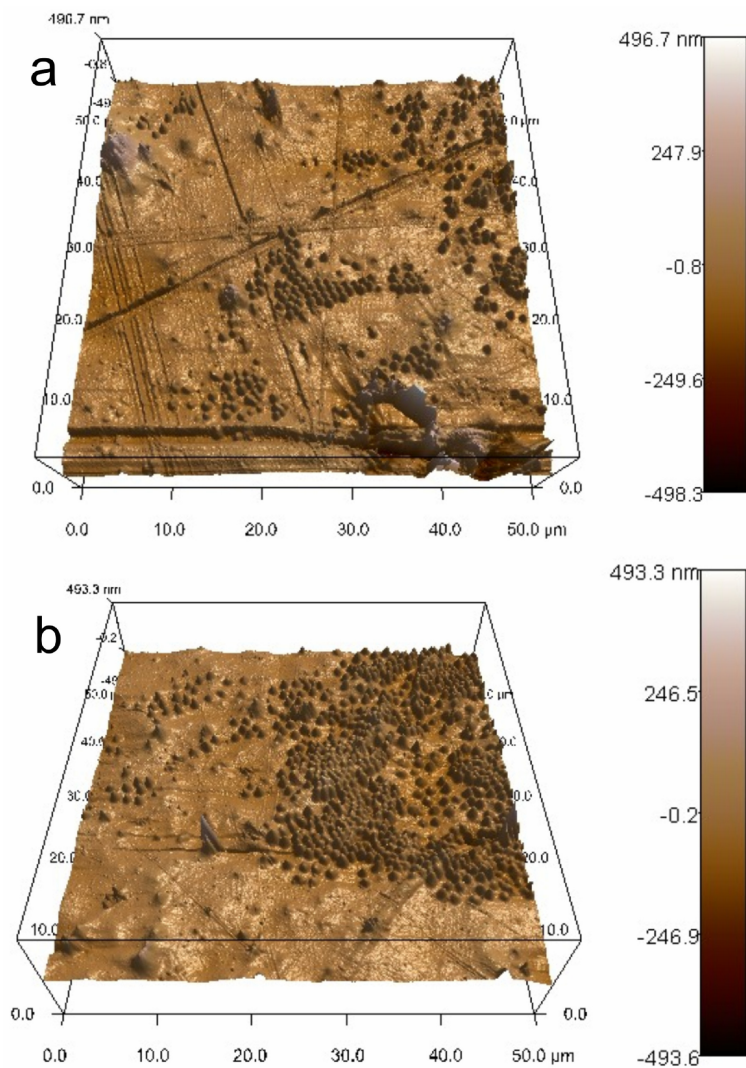
Figure 6.5. 3D rendering of AFM image of nanogels spin coated onto pAAc-grafted PET (a) without benzophenone modification and (b) with benzophenone modification but without UV irradiation.

It is known that one of the key steps in the inflammatory host response to biomaterials is non-specific protein adsorption, which then mediates cell adhesion and spreading.[30] Recent efforts in the field of biomaterials and medical implants have focused on developing non-fouling surface treatments to prevent this non-specific protein

adsorption and cell adhesion.[4,31-33] Our group has previously shown the efficacy of PEG-containing pNIPAm nanogels as protein and cell adhesion-resistant materials.[9,14] In addition to their non-fouling behavior, the facile and well-controlled synthesis of highly monodispersed nanogels in a range of sizes, ease of their biofunctionalization using various orthogonal chemical functionalities, and possibility of co-assembling varied nanogels onto a single substrate to generate complex bio-interfaces makes them interesting candidates for biomedical implant coatings for modulation of inflammatory response. We take advantage of these attributes to study and produce model biomaterials incorporating nanogels that can be tested for their functionality.

Based on the AFM confirmation of a stable uniform monolayer of nanogels on the PET surface, we tested the cell adhesion resistance of these surfaces *in vitro*. IC-21 macrophages were plated on substrates in culture media containing 10% serum. This provides a rigorous test for bioresistance as cell adhesive proteins present in serum rapidly adsorb onto synthetic surfaces and mediate cell adhesion and spreading. In contrast to bare PET films, which supported high levels of cell adhesion and spreading, nanogel-functionalized PET films exhibited no macrophage adhesion over the 48 h test period (Figure 6.6), indicating a stable cell adhesion-resistant coating. We attribute the lack of cell adhesion to nanogel-functionalized surface to the protein-resistant nature of the PEG cross-linked nanogels. The ability of nanogel-coated surfaces to resist cell adhesion and spreading was distributed throughout the entire sample, indicating uniform distribution of bioresistance. The success of this surface functionalization strategy thus allows the study of the non-fouling behavior of the PEG cross-linked pNIPAm nanogels *in vivo* and also gives us opportunities to develop more complex biomaterials

incorporating multifunctional nanogel monolayers, which will be discussed further in Chapter 7.
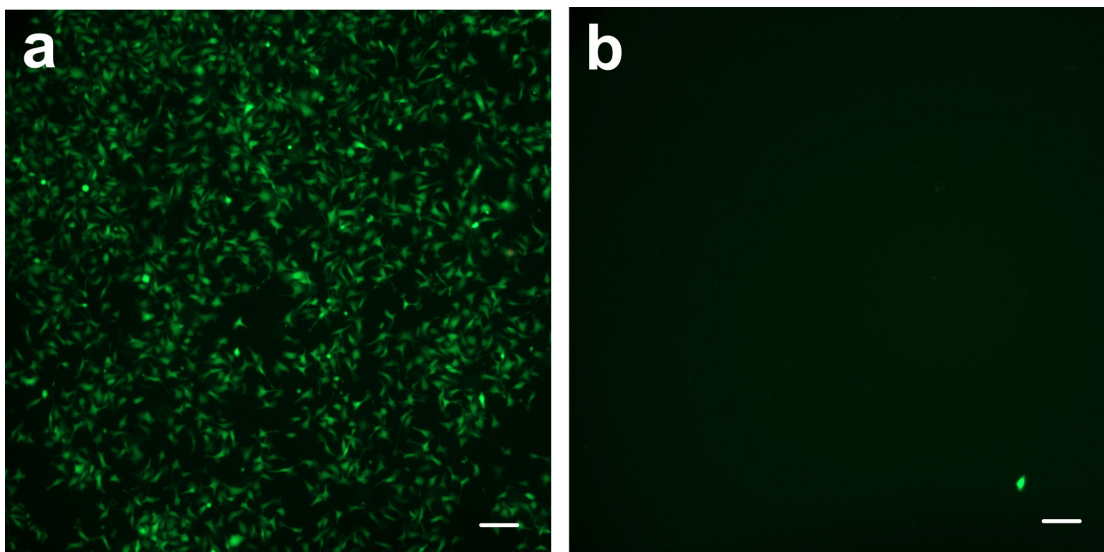
Figure 6.6. Macrophage adhesion on (a) bare PET and (b) PET covalently functionalized by nanogels. Adherent cells were stained with calcein-AM, which stains live cells (green). Scale bar = 100 μm.

6. 4 Conclusions

In conclusion, we report a simple, scalable, and reproducible method of functionalizing PET with a conformal, dense film of hydrogel microparticles. The nanogel layer is stable due to the covalent attachment of the nanogels to the PET surface via a photo-affinity technique. This method can be easily extended for modifying the inert PET surface with any organic species, providing bioactive surfaces possessing excellent stability. Note that the spin coating deposition method is used here mainly for speed, convenience, and potential scalability. However, it cannot be used to coat

substrates with complex geometries and in such cases other deposition techniques must be employed. We are currently evaluating methods for dip-coating of nanogels onto complex substrates. *In vivo* experiments to study the stability and properties of these nanogel coatings were carried out and are described in Chapter 7.

6.5 References and Notes

[1]   Langer, R.; Vacanti, J. P. Tissue engineering. *Science (New York, N.Y.)* **1993**, *260*, 920-926.

[2]   Lavik, E.; Langer, R. Tissue engineering: current state and perspectives. *Applied Microbiology and Biotechnology* **2004**, *65*, 1-8.

[3]   Lu, Z. R.; Kopeckova, P.; Wu, Z.; Kopecek, J. Functionalized semitelechelic poly[N-(2-hydroxypropyl)methacrylamide] for protein modification. *Bioconjug. Chem.* **1998**, *9*, 793-804.

[4]   Murata, H.; Chang, B. J.; Prucker, O.; Dahm, M.; Ruehe, J. Polymeric coatings for biomedical devices. *Surface Science* **2004**, *570*, 111-118.

[5]   Kim, P.; Kim, D. H.; Kim, B.; Choi, S. K.; Lee, S. H.; Khademhosseini, A.; Langer, R.; Suh, K. Y. Fabrication of nanostructures of polyethylene glycol for applications to protein adsorption and cell adhesion. *Nanotechnology* **2005**, *16*, 2420-2426.

[6]   Kulik, E. A.; Kato, K.; Ivanchenko, M. I.; Ikada, Y. Trypsin immobilization on to polymer surface through grafted layer and its reaction with inhibitors. *Biomaterials* **1993**, *14*, 763-769.

[7]   Lavik, E. B.; Klassen, H.; Warfvinge, K.; Langer, R.; Young, M. J. Fabrication of degradable polymer scaffolds to direct the integration and differentiation of retinal progenitors. *Biomaterials* **2005**, *26*, 3187-3196.

[8]   Ito, Y.; Zheng, J.; Imanishi, Y. Enhancement of cell growth on a porous membrane co-immobilized with cell-growth and cell adhesion factors. *Biomaterials* **1997**, *18*, 197-202.

[9]   Gan, D.; Lyon, L. A. Synthesis and Protein Adsorption Resistance of PEG-Modified Poly(N-isopropylacrylamide) Core/Shell Microgels. *Macromolecules* **2002**, *35*, 9634-9639.

[10]   Jones, C. D.; Lyon, L. A. Synthesis and Characterization of Multiresponsive Core-Shell Microgels. *Macromolecules* **2000**, *33*, 8301-8306.

[11]   Nayak, S.; Lyon, L. A. Soft nanotechnology with soft nanoparticles. *Angew. Chem. Int. Ed.* **2005**, *44*, 7686-7708.

[12]   Pelton, R. Temperature-sensitive aqueous microgels. *Adv. Colloid. Interface Sci.* **2000**, *85*, 1-33.

[13]   Saunders, B. R.; Vincent, B. Microgel particles as model colloids: theory, properties and applications. *Adv. Colloid Interface Sci.* **1999**, *80*, 1-25.

[14]   Nolan, C. M.; Reyes, C. D.; Debord, J. D.; Garcia, A. J.; Lyon, L. A. Phase transition behavior, protein adsorption, and cell adhesion resistance of poly(ethylene glycol) crosslinked microgel particles. *Biomacromolecules* **2005**, *6*, 2032-2039.

[15]   Homsy, C. A.; McDonald, K. E.; Akers, W. W.; Short, C.; Freeman, B. S. Surgical suture-canine tissue interaction for six common suture types. *J. Biomed. Mater. Res.* **1968**, *2*, 215-230.

[16]   Soares, B. M.; Guidoin, R. G.; Marois, Y.; Martin, L.; King, M. W.; Laroche, G.; Zhang, Z.; Charara, J.; Girard, J.-F. In vivo characterization of a fluoropassivated gelatin-impregnated polyester mesh for hernia repair. *J. Biomed. Mater. Res.* **1996**, *32*, 293-305.

[17]   Vinard, E.; Eloy, R.; Descotes, J.; Brudon, J. R.; Guidicelli, H.; Magne, J. L.; Patra, P.; Berruet, R.; Huc, A.; Chauchard, J. Stability of performances of vascular prostheses; retrospective study of 22 cases of human implanted prostheses. *J. Biomed. Mater. Res.* **1988**, *22*, 633-648.

[18]   von Recum, A. F. Applications and failure modes of percutaneous devices: a review. *J. Biomed. Mater. Res.* **1984**, *18*, 323-336.

[19]   Sano, S.; Kato, K.; Ikada, Y. Introduction of functional groups onto the surface of polyethylene for protein immobilization. *Biomaterials* **1993**, *14*, 817-822.

[20]   Tabata, Y.; Lonikar, S. V.; Horii, F.; Ikada, Y. Immobilization of collagen onto polymer surfaces having hydroxyl groups. *Biomaterials* **1986**, *7*, 234-238.

[21]   Piglowski, J.; Gancarz, I.; Staniszewska-Kus, J.; Paluch, D.; Szymonowicz, M.; Konieczny, A. Influence of plasma modification on biological properties of poly(ethylene terephthalate). *Biomaterials* **1994**, *15*, 909-916.

[22]   Gupta, B.; Hilborn, J. G.; Bisson, I.; Frey, P. Plasma-induced graft polymerization of acrylic acid onto poly(ethylene terephthalate) films. *J. App. Polym. Sci.* **2001**, *81*, 2993-3001.

[23]   Gupta, B.; Plummer, C.; Bisson, I.; Frey, P.; Hilborn, J. Plasma-induced graft polymerization of acrylic acid onto poly(ethylene terephthalate) films: characterization and human smooth muscle cell growth on grafted films. *Biomaterials* **2002**, *23*, 863-871.

[24]   Lee, S.-D.; Hsiue, G.-H.; Chang, P. C.-T.; Kao, C.-Y. Plasma-induced grafted polymerization of acrylic acid and subsequent grafting of collagen onto polymer film as biomaterials. *Biomaterials* **1996**, *17*, 1599-1608.

[25]   Suzuki, M.; Kishida, A.; Iwata, H.; Ikada, Y. Graft copolymerization of acrylamide onto a polyethylene surface pretreated with glow discharge. *Macromolecules* **1986**, *19*, 1804-1808.

[26]   Uyama, Y.; Kato, K.; Ikada, Y. Surface modification of polymers by grafting. *Adv. Polym. Sci.* **1998**, *137*, 1-39.

[27]   Prucker, O.; Naumann, C. A.; Ruehe, J.; Knoll, W.; Frank, C. W. Photochemical Attachment of Polymer Films to Solid Surfaces via Monolayers of Benzophenone Derivatives. *J. Am. Chem.Soc.* **1999**, *121*, 8766-8770.

[28]   Dorman, G.; Prestwich, G. D. Benzophenone photophores in biochemistry. *Biochemistry* **1994**, *33*, 5661-5673.

[29]   Hermanson, G. T. *Bioconjugate Techniques* Academic Press San Diego 1996.

[30]   Anderson, J. M. Biological responses to materials. *Ann. Rev. Mater. Res.* **2001**, *31*, 81-110.

[31]   Dalsin, J. L.; Hu, B.-H.; Lee, B. P.; Messersmith, P. B. Mussel Adhesive Protein Mimetic Polymers for the Preparation of Nonfouling Surfaces. *J. Am. Chem.Soc.* **2003**, *125*, 4253-4258.

[32]   Lopez, G. P.; Ratner, B. D.; Tidwell, C. D.; Haycox, C. L.; Rapoza, R. J.; Horbett, T. A. Glow discharge plasma deposition of tetraethylene glycol dimethyl ether for fouling-resistant biomaterial surfaces. *J. Biomed. Mater. Res.* **1992**, *26*, 415-439.

[33]   Tziampazis, E.; Kohn, J.; Moghe, P. V. PEG-variant biomaterials as selectively adhesive protein templates: model surfaces for controlled cell adhesion and migration. *Biomaterials* **2000**, *21*, 511-520.

CHAPTER 7

NANOGEL COATINGS FOR CONTROLLING INFLAMMATION

The longevity of medical implants suffers because bacteria, cells and proteins in the body gradually accumulate (also known as fouling) on devices, compromising their performance and threatening patients with infections.[1-9] One method by which the performance and life of the implants can be increased is by rendering the implants non-fouling. There has been an increasing interest in the development of surfaces with the ability to inhibit non-specific inflammatory responses. This chapter describes *in vitro* and *in vivo* studies of the potential non-fouling behavior of PETs covalently modified with nanogel films using the method developed in Chapter 6. Nanogels (both pNIPAm and pNIPMAm) with PEG diacrylate as cross-linker were synthesized. In order to screen for the most functional and non-fouling nanogels, pNIPAm based nanoparticles with different monomer composition (different functional comonomers) were studied *in vitro*. The cell and animal studies described in this chapter were performed by Amanda W. Bridges from A. J. Garcia's lab (Mechanical Engineering) at Georgia Tech. In this chapter, we discuss the collaborative efforts from our labs towards the design of bioactive interfaces based on hydrogel nanoparticles with reduced macrophage adhesion, cytokine release, and hence reduced inflammatory response.

8.1 Introduction

As discussed in Chapter 1 and 6, the performance of synthetic biomaterial implants is severely limited due to non-specific inflammatory host responses resulting from the adsorption of proteins and other biomolecules, eventually leading to the foreign body reaction, fibrous encapsulation, and rejection.[10,11] Immediately following implantation, proteins and other biomolecules present in blood and physiological fluids rapidly adsorb onto the surface of synthetic biomaterials,[12,13] resulting in integrin receptor-mediated leukocyte recruitment, adhesion, and activation.[14-16] In recent times, there has been an increasing interest in the development of surfaces with ability to prevent the non-specific inflammatory response to increase the performance of implants *in vivo*.[17-23] While there are examples where materials have reduced protein adsorption and cell adhesion *in vitro*, when studied *in vivo* they fail to reduce the fibrous encapsulation and adverse inflammatory responses.[19,21,22,24] The design of bioactive interfaces based on hydrogel nanoparticles with reduced macrophage adhesion, cytokine release, and hence reduced inflammatory response, is discussed in this chapter.

We were encouraged by the preliminary *in vitro* studies described in Chapter 6 on the PEG-575 diacrylate (henceforth know as PEG-575) cross-linked pNIPAm-AAc nanogels and the fact that the flexible PETs could be easily implanted and studied *in vivo*. Therefore, we further carried out the animal studies on these films, as described in the current chapter. It was intriguing that the pNIPAm based nanogels were non-fouling at a temperature above their LCST because it has been shown in literature that at 37 °C, pNIPAm becomes hydrophobic, promoting protein adsorption and, subsequently, cell adhesion.[25] Since the cell studies are done at 37 °C and the nanogels are hydrophobic at

that temperature, one would expect that the hydrophobic polymer would attract more proteins making the material fouling. On the other hand, at high temperature, since the nanogels are deswollen, the hydrophilic PEG cross-linker can phase separate, as suggested by preliminary results from our group, and possibly hinder cell adhesion making the material non-fouling, as suggested by several other studies done on PEG-grafted SAMs.[26-28] We were also motivated to better understand the reason behind the non-fouling behavior of PEG cross-linked nanogels, and to answer questions such as: i) Whether the phase separation of PEG is important in the non-fouling response of the material? ii) Or does making the material more hydrophilic provide more effective non-fouling behavior? For these studies, we synthesized pNIPMAm based nanogels with PEG 700 as cross-linker and studied them *in vitro.* The pNIPMAm nanogels have LCST around 44 °C in aqueous media and will be swollen and hydrophilic at cell culture temperatures. Thus, the cell adhesion results on these nanogels will help understand the importance of PEG phase separation and hydrophilicity in making a material non-fouling.

To add functionalities to the base pNIPAm nanogels, non-interfering multiple chemoligation strategies can be employed on the engineered surface to conjugate specific bio-ligands. With this aim, pNIPAm nanogels containing PEG-575 as cross-linker and HEMA and AAc as comonomers (therefore providing useful handles for conjugation) were synthesized and studied for their non-fouling behavior. Since in core-shell architecture the functional groups are concentrated on the surface, as desired for chemoligations, pNIPAm-HEMA shells cross-linked with PEG-575 were synthesized on PEG-575 cross-linked pNIPAm cores.

8.2 Experimental Section

7.2.1 Materials

Most materials used in this chapter were described in Chapter 6.

7.2.2 Nanogel Synthesis

The nanogels used in this chapter were synthesized based on the precipitation polymerization strategy discussed in Chapter 2. The synthetic procedure is described in brief here.

pNIPAm-AAc Nanogels:

The synthesis for the pNIPAm-AAc nanogel particles (100 mM total monomer concentration) with 2 mol % poly (ethylene glycol) (PEG) diacrylate (MW 575) cross-linker was performed as per Chapter 6.

pNIPMAm-AAc Nanogels:

Poly(N-isopropylmethacrylamide) (pNIPMAm) nanogel particles (100 mM total monomer concentration) were synthesized with 2 mol % poly (ethylene glycol) (PEG) diacrylate (MW 700) by a free radical precipitation polymerization method. For incorporating functional groups that could be modified later, the nanogel particles were synthesized with 10 mol % acrylic acid as a co-monomer. Briefly, 0.5679 g of NIPMAm monomer, 0.0876 g of cross-linker PEG-diacrylate (MW 700), and 0.0025 g of surfactant sodium dodecyl sulfate (SDS) were dissolved in 49 mL distilled, deionized (DI) water, and filtered through a 0.2 μm filter. The solution was transferred to and stirred in a three-neck, round-bottom flask, and heated to 70 °C while purging with N_2 gas. After reaching 70 °C and purging for 1 h, 34.3 μL of acrylic acid was added, followed by the addition of

0.0114 g (dissolved in 1 mL DI water) of ammonium persulfate (APS) to initiate the reaction. The reaction was kept at 70 °C for 4 h. The synthesized nanogels were then filtered and purified by five cycles of centrifugation at 15,422 × g for 45 min. The supernatant was removed, and the particles were redispersed in DI water. Following a similar procedure pNIPMAm-AAc nanogels with 5 mol % PEG cross-linker were prepared.

pNIPAm-HEMA Nanogels:

Poly(NIPAm-HEMA) nanogel particles (100 mM total monomer concentration) were synthesized with 2 mol % poly (ethylene glycol) (PEG) diacrylate (MW 575) by a free radical precipitation polymerization method described in chapter 2. For incorporating functional groups that could be modified later, the nanogel particles were synthesized with 10 mol % HEMA as a co-monomer. Briefly, 0.5088 g of NIPAm monomer, 0.0701 g of cross-linker PEG-diacrylate, and 0.0025 g of surfactant sodium dodecyl sulfate (SDS) were dissolved in 49 mL distilled, deionized (DI) water, and filtered through a 0.2 μm filter. The solution was transferred to and stirred in a three-neck, round-bottom flask, and heated to 70 °C while purging with N_2 gas. After reaching 70 °C and purging for 1 h, 45 μL of HEMA was added, followed by the addition of 0.0114 g (dissolved in 1 mL DI water) of ammonium persulfate (APS) to initiate the reaction. The reaction was kept at 70 °C for 4 h. The synthesized nanogels were then filtered and purified by five cycles of centrifugation at 15,422 × g for 45 min.

pNIPAm-HEMA Shell on pNIPAm Cores:

Poly(NIPAm-HEMA) shells were added to pNIPAm-BIS core nanogels prepared by precipitation polymerization. The total monomer concentration of shell was 40 mM with 2 mol % poly (ethylene glycol) (PEG) diacrylate (MW 575). Briefly, 0.5088 g of NIPAm monomer, 0.0701 g of cross-linker PEG-diacrylate, and 0.0025 g of surfactant sodium dodecyl sulfate (SDS) were dissolved in 49 mL distilled, deionized (DI) water, and filtered through a 0.2 μm filter. The solution was transferred to and stirred in a three-neck, round-bottom flask, and heated to 70 °C while purging with N_2 gas. After reaching 70 °C and purging for 1 h, 45 μL of HEMA was added, followed by the addition of 0.0114 g (dissolved in 1 mL DI water) of ammonium persulfate (APS) to initiate the reaction. The reaction was kept at 70 °C for 4 h. The synthesized nanogels were then filtered and purified by five cycles of centrifugation at 15,422 × *g* for 45 min.

pNIPMAm-HEMA-AAc Nanogels:

Poly(NIPAm-HEMA-AAc) nanogel particles (100 mM total monomer concentration) were synthesized with 2 mol % poly (ethylene glycol) (PEG) diacrylate (MW 575) by a free radical precipitation polymerization method described in chapter 2. For incorporating functional groups that could be modified later, the nanogel particles were synthesized with 2 mol % acrylic acid and 10 mol % HEMA as a co-monomer. Briefly, 0.4901 g of NIPAm monomer, 0.0701 g of cross-linker PEG-diacrylate, and 0.0025 g of surfactant sodium dodecyl sulfate (SDS) were dissolved in 49 mL distilled, deionized (DI) water, and filtered through a 0.2 μm filter. The solution was transferred to and stirred in a three-neck, round-bottom flask, and heated to 70 °C while purging with

N$_2$ gas. After reaching 70 °C and purging for 1 h, 6.86 µL of acrylic acid and 60.76 µL of HEMA was added, followed by the addition of 0.0114 g (dissolved in 1 mL DI water) of ammonium persulfate (APS) to initiate the reaction. The reaction was kept at 70 °C for 4 h. The synthesized nanogels were then filtered and purified by five cycles of centrifugation at 15,422 × g for 45 min.

7.2.3 PET Film Functionalization

PET films were functionalized with pAAc and then with ABP based on the procedure described in Chapter 6.

7.2.4 Surface characterization via XPS and AFM

XPS was performed at Georgia Institute of Technology's Microelectronics Research Center on a Surface Science Laboratories X-100 spectrometer (Mountain View, CA) using the x-ray gun at 3 eV. AFM images were obtained in AC mode on an Asylum Research MFP-3D atomic force microscope. The details of the setup can be found in Chapter 6.

7.2.5 Sample preparation for Biological Studies

All samples were rinsed in 70% ethanol on a rocker plate for four consecutive days, changing the solution daily to sterilize the surface and remove endotoxin contaminates and were then stored in fresh 70% ethanol until use. Prior to use, samples were rinsed 3 times in sterile PBS and allowed to rehydrate for at least 1 hour.

7.2.6 Protein Adsorption Studies

The amount of adsorbed protein (fibrinogen) on different surfaces was determined using radiolabeled fibrinogen. Nanogel-coated and unmodified PET disks were incubated

for 1 h in a mixture of ^{125}I-labeled human fibrinogen (stock specific activity of 0.86 µCi/µg, MP Biomedicals, Irvine, CA) and unlabeled human fibrinogen (Sigma Aldrich). Gold-coated glass coverslips and EG$_3$ self-assembled monolayers grafted onto gold-coated glass coverslips were used as additional controls. Samples were then rinsed three times with PBS to remove excess radiolabel and were incubated for 30 min in a 1% solution of BSA to block background. After rinsing three times in PBS again to remove unbound protein, radioactivity was measured using a Cobra II auto gamma counter. After correcting for background, the amount of protein adsorbed on each sample was calculated as the radioactivity divided by the surface area, dilution with unlabeled protein, and specific activity.

7.2.7 Monocyte Isolation and Culture

Peripheral human whole blood was obtained from healthy voluntary donors by nursing staff at the Georgia Institute of Technology Student Health Center in accordance to an approved Institute Review Board protocol. Unless otherwise specified, all supplies were from Becton Dickinson. Blood (240 mL) was obtained from each donor in 60 mL Leur-Lok syringes, half of which contained 1 mL of sodium heparin as an anticoagulant.

Autologous human serum was obtained from the non-heparinized portion of blood. Briefly, the blood was centrifuged, and the resultant plasma layer was collected and transferred to sterile conicals and allowed to coagulate at room temperature for 1.5 h. After another centrifugation, the fibrin mesh was displaced and the liquid serum layer was collected and sterile filtered.

Human monocytes were isolated from the heparinized whole blood immediately after collection. Briefly, the blood was transferred to polystyrene bottles (Corning),

diluted 1:1 with sterile PBS without calcium/magnesium, and gently swirled to mix. This mixture was then layered over Lymphocyte Separation Medium (Cellgro/Mediatech, Herndon, VA) and centrifuged. An 18 G needle was then used to aspirate the cell layer, the cells were transferred to containing PBS without calcium/magnesium, and were centrifuged. The cell pellets were then resuspended in lysis buffer (155 mM NH_4Cl, 10 mM $KHCO_3$, 0.1 mM EDTA) to eliminate erythrocyte contaminates and centrifuged. The resultant cell pellets were then rinsed and centrifuged with PBS to remove the lysis buffer.

Human monocytes were resuspended at a concentration of 5×10^6 cells/mL in RPMI 1640 supplemented with 25% autologous human serum and penicillin/streptomycin, plated in a volume of 10 mL on 100×20 mm^2 Primaria-treated culture plates, and incubated at 37 °C and 5% CO_2. After 2 h, nonadherent monocytes were removed by rinsing the plates three times with warm media. The serum was heat-inactivated (56 °C for 1 hr) on day 3, and media changes occurred on days 3 and 6 of culture. A 10 d culture period was selected based on previous results showing it to be sufficient for macrophage maturation.

7.2.8 Evaluation of Macrophage Adhesion in vitro

Following a 10 d culture of the primary human monocytes, adherent cells were removed from the culture plates using warm trypsin and reseeded on both nanogel-coated PET and unmodified PET controls in 24-well Primaria-treated culture plates. Cells were maintained in RPMI supplemented with 25% autologous human serum and penicillin/streptomycin at 37 °C and 5% CO_2. After 48 hrs in culture, samples were rinsed three times with sterile PBS to remove loosely adherent cells. The adherent cells

were then visualized fluorescently via live/dead stain using calcein-AM and ethidium homodimer-1, respectively. Images using 10× objective were taken at five representative areas on each sample, and software was used to count the adherent cells and obtain measurements of area for individual cells. Results shown represent 5 samples per treatment group.

7.2.9 Intraperitoneal Implantation

Sterile samples (2 per mouse) were implanted in the IP cavity of male C57BL mice anesthetized by isofluorane for 48 h. Sham surgeries were performed on additional mice to be used as controls. The IP cavity was injected with 3 mL of sterile PBS. The abdomen was then massaged briefly, the IP lavage fluid was collected, and disks were retrieved for analysis. One sample was used for immunofluorescent staining of adherent cells, and the second was used to harvest adherent cells to be analyzed by flow cytometry. Animals were sacrificed using a CO_2 chamber.

7.2.10 Immunofluorescent Staining of Adherent Cells

Taking care not to disrupt the adherent cell monolayer, the first disk was removed from the IP cavity of each mouse and stored briefly in PBS until completion of the removal surgery. Samples were then rinsed three times in PBS and fixed with 10 % neutral buffered formalin. Adherent cells were then permeabilized using 0.1% Triton-X 100. 5% fetal bovine serum was used to block non-specific protein binding. Explants were then incubated at room temperature in a primary antibody against murine macrophage CD68 (Abcam, Cambridge, MA). After rinsing to remove excess antibody, explants were incubated in a secondary antibody of goat anti-mouse conjugated to AlexaFluor 488 and counterstained with rhodamine phalloidin and Hoechst to stain actin

filaments and nuclei, respectively. Antibodies were diluted 1:200 in the blocking reagent, and all reagents were used at 4 °C. Samples were then rinsed five times in PBS and once in deionized H_2O, mounted on glass slides with coverslips, and stored in the dark at 4 °C until imaged. Images were taken with 20× objectives, and software was used to count the adherent cells. Results shown represent 6 animals per treatment group from a single implantation experiment.

7.2.11 Intracellular Cytokine Staining and Flow Cytometry

The second disk was carefully explanted from each mouse and rinsed briefly in PBS. These samples were quickly transferred to a 24-well plate, and 1 mL of warm Brefeldin A solution (eBioscience, San Diego, CA) was added to inhibit the extracellular release of proteins. The culture plate was then incubated (37 °C and 5% CO_2) for 5 h, allowing ample time for cytokines to accumulate intracellularly. The solution was then discarded and samples were rinsed three times in cold PBS without calcium/magnesium. Adherent cells were then removed from the disk using warm trypsin, transferred to microcentrifuge tubes, and centrifuged to obtain a cell pellet. The cell pellet was resuspended in 1 mL of 10% neutral buffered formalin, and tubes were shaken at low speed. A series of three rinse-and-centrifuge cycles were used to remove excess fixative, and cell pellets were resuspended in a combined permeabilization/blocking buffer and replaced on the shaker plate. Three fluorescently-conjugated primary antibodies (APC anti-mouse TNF-α, FITC anti-mouse IL-1β, and PE anti-mouse MCP-1; eBioscience, San Diego, CA) were added directly to the microcentrifuge tubes at the manufacturer's recommended dilutions, and cells were shaken in the dark. Cells were then subjected to another series of three rinse-and-centrifuge cycles to remove excess antibody and were

resuspended in PBS. A BD LSR flow cytometer was used to measure the fluorescently-labeled intracellular cytokines, and FlowJo software v7 (Ashland, OR) was used to analyze the data. Results shown represent 6 animals per treatment group from a single implantation experiment, and 10,000 events were counted per sample.

7.3 Results and Discussion

The surface of the PET films before and after deposition of the nanogels was characterized by XPS and AFM to confirm the deposition of a stable uniform nanogel coating. The details of the AFM imaging are discussed in Chapter 6. We used XPS to probe the chemical changes occurring on the surface after the deposition. A wide scan elemental survey obtained from XPS is shown in Figure 7.1. The nanogel coated PETs revealed the presence of nitrogen on the surface, which is attributed to be from the amides in the polymer network. High resolution carbon 1s data for determining individual carbon bonds (data not shown) also suggested the presence of amides on the PET surface after nanogel deposition. These characterization studies confirmed the deposition of nanogels on the PET substrate. The PET controls without nanogel deposition did not show the nitrogen peak in the elemental scan.
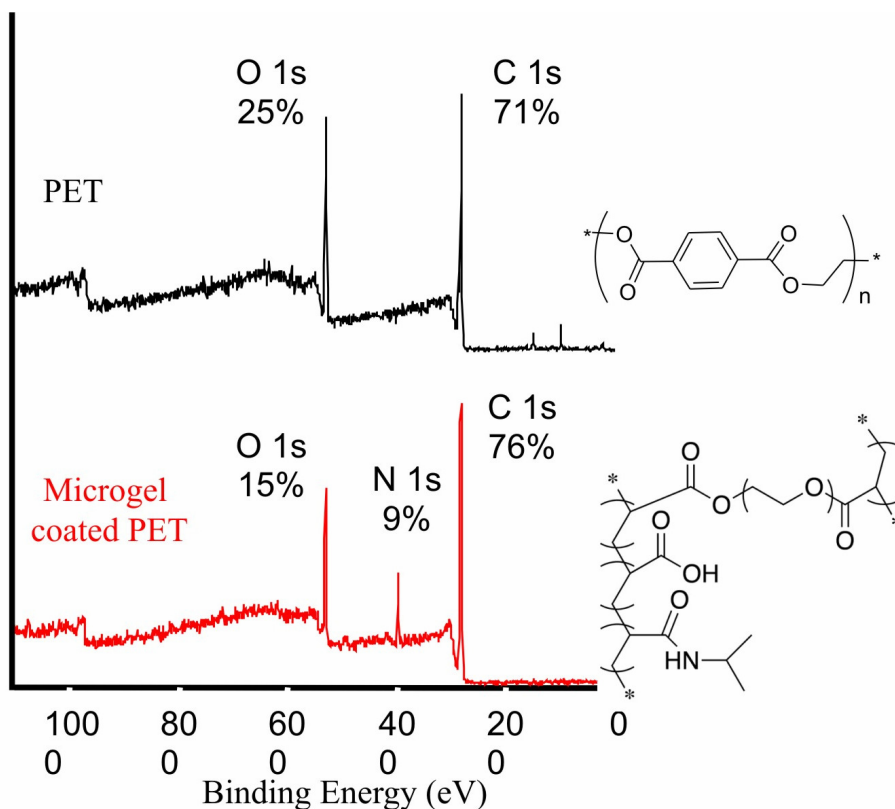
Figure 7.1. XPS scans for unmodified PET and nanogel-coated PET. The nanogel coated PETs show the presence of nitrogen on the surface, attributed to be from the amides in the polymer network. The PET controls without nanogel deposition did not show the nitrogen peak in the elemental scan.

The pNIPMAm-based nanogels having PEG-700 diacrylate (henceforth known as PEG-700) as cross-linker were also synthesized and studied for their cell adhesion response to macrophages *in vitro*. We used the relatively higher MW PEG-700 as the cross-linker, because a smaller MW PEG is most likely buried and inaccessible in the swollen state of the nanogels.[26,27,29] Nanogels with two different cross-linker densities (2 mol% and 5 mol%) of PEG-700 were tested. The pNIPMAm-AAc nanogels were assembled onto PETs using the procedure described in Chapter 6. Following this, IC-21 macrophages were plated onto the substrates in culture media containing 10% serum.

This provides a rigorous test for the non-fouling behavior as cell adhesive proteins present in serum rapidly adsorb onto synthetic surfaces and initiate cell adhesion and spreading. Figure 7.2 shows the cell adhesion results obtained by microscopy of cells stained with calcein-AM. As seen in the figure, bare PET and the control TCPS both showed high levels of cell adhesion and spreading as compared to nanogel-coated PETs. When comparing the pNIPAm *vs* pNIPMAm nanogels, the pNIPAm-coated PETs showed significantly reduced or no macrophage adhesion over the 48 h test period, whereas the pNIPMAm coated PETs show comparatively more cell adhesion and spreading for both cross-linker densities. These observations indicate the important role of nanogel deswelling and exposure of the PEG due to phase separation at high temperature in the pNIPAm nanogels, as shown previously by Gan and Nolan.[29,28]
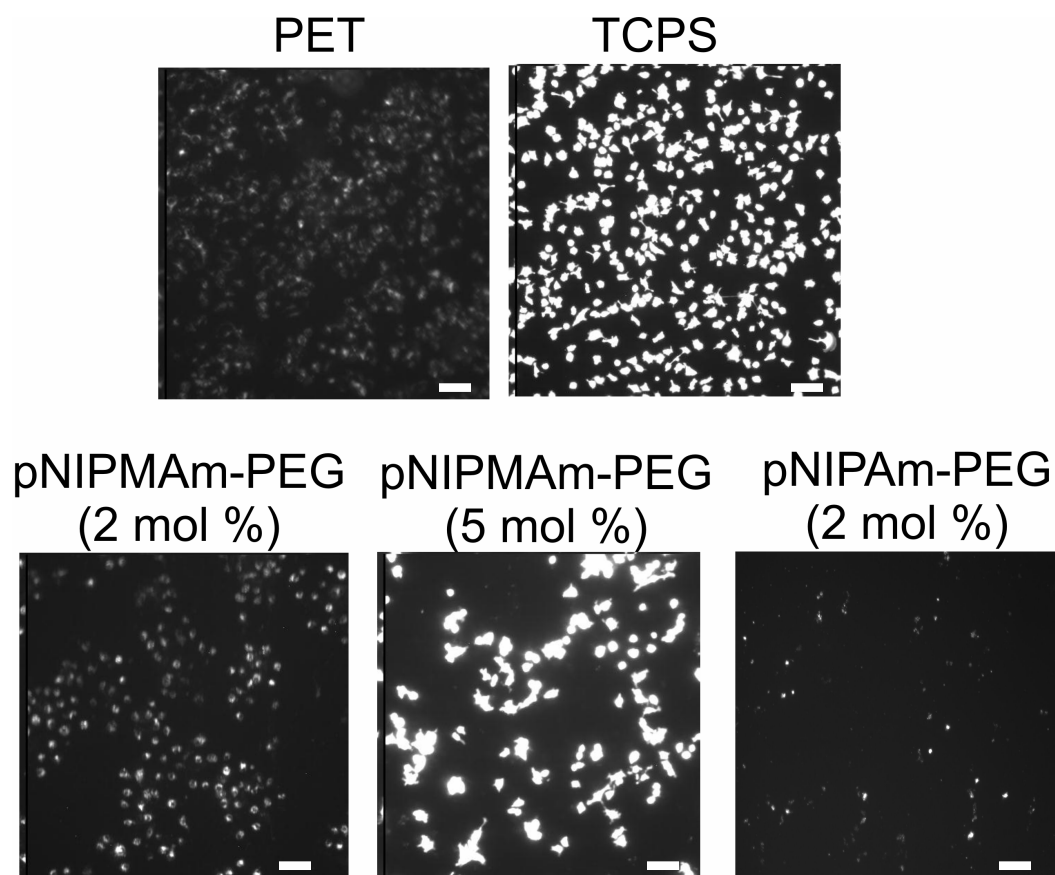
Figure 7.2. Comparison of macrophage adhesion on pNIPAm and pNIPMAm functionalized by nanogels. Adherent cells were stained with calcein-AM, which stains live cells (green). Scale bar = 100 μm.

Adsorption of the plasma protein fibrinogen from physiological fluids onto synthetic materials is known to mediate leukocyte adhesion and subsequent inflammation.[30-32] Since the pNIPAm-AAc nanogels were found to be better than pNIPMAm-AAc, we tested the performance of the former in resisting protein adsorption by radiolabeling. To determine the relative levels of fibrinogen protein adsorption on the nanogel coated PETs, samples were incubated in ^{125}I-radiolabeled human fibrinogen, and radiation levels were detected using a gamma counter. Nanogel-coated PET exhibited 7-

fold lower levels of fibrinogen adsorption compared to unmodified PET (Figure 7.3).

Furthermore, nanogel coatings had lower adsorbed fibrinogen levels than the most non-

fouling material in the literature, tri(ethylene glycol)-terminated self-assembled

monolayers (EG$_3$ SAMs). Thus, the nanogels outperform the EG$_3$ SAMs. [33,34]
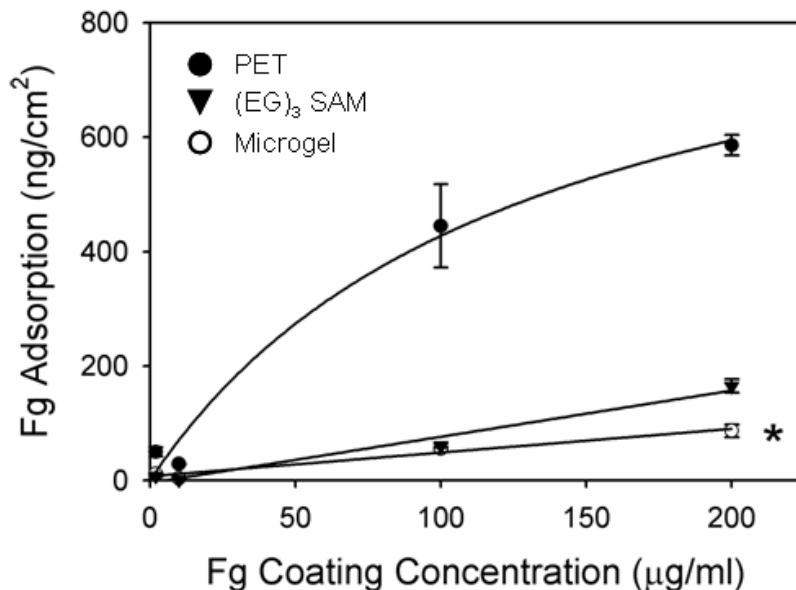
Figure 7.3. Fibrinogen adsorption profiles on biomaterial surfaces. pNIPAm-AAc nanogel-coated PET surfaces adsorb 10-fold lower levels of human fibrinogen than unmodified PET controls, and also display superior performance to tri(ethylene glycol)-terminated self-assembled monolayers on gold.

To further explore the potential of the PEG-575 cross-linked pNIPAm-AAc

nanogels, we studied their response to primary human monocytes. Primary human

monocytes cultured for 48 h on the PETs modified with pNIPAm-AAc nanogel were

analyzed for adhesion and spreading using a protocol well established in the literature.[35]

Significantly less monocytes were adherent on nanogel-coated samples, as compared to

unmodified PET controls (Figure 7.4) in accordance with the results obtained previously with the IC-21 macrophages. Moreover, monocytes exhibited fewer cell extensions and were significantly less spread on nanogel-coated surfaces than on bare PET.
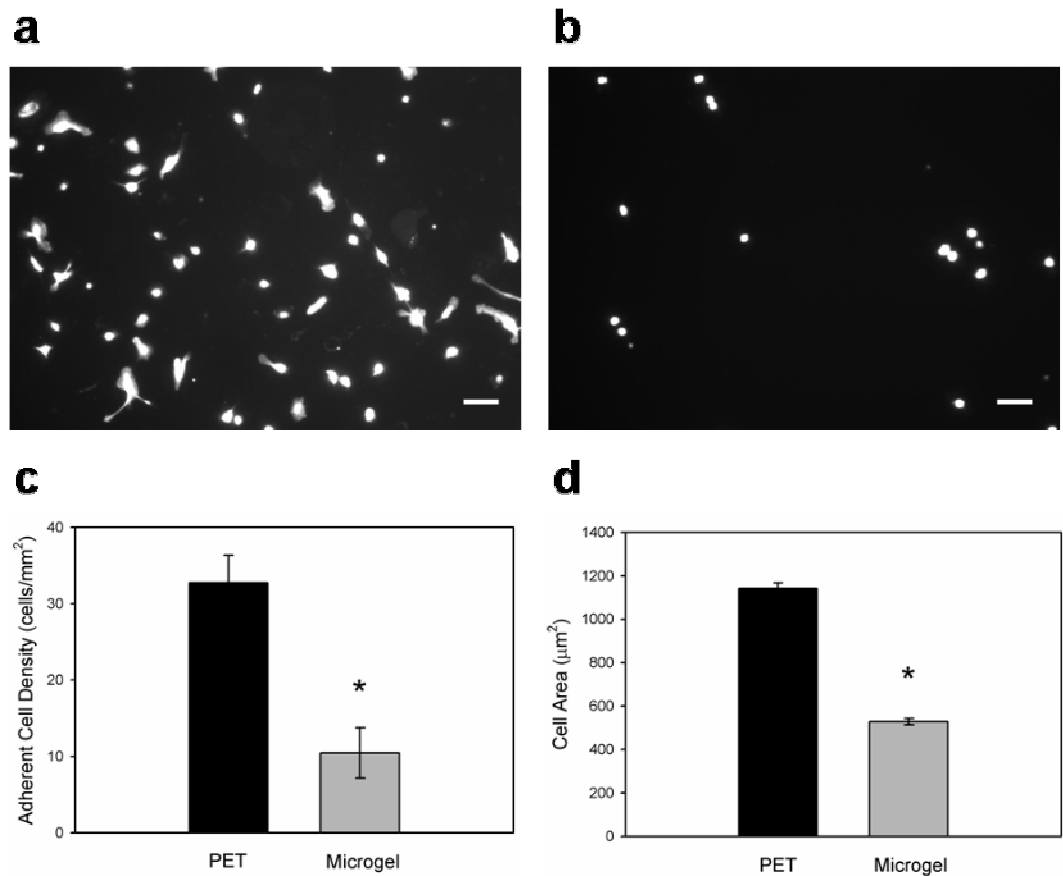
Figure 7.4. *In vitro* primary macrophage adhesion to biomaterial surfaces. Adherent cells were scored for viability, and cell density and area were quantified. Compared to unmodified PET substrates (a), nanogel coatings (b) reduce macrophage adhesion to biomaterial surfaces. (c) Nanogel coatings elicit a 3-fold reduction in cell adhesion compared to unmodified PET surfaces, * $p < 1.1 \times 10^{-4}$. d) Adherent macrophages also exhibited more cell extensions and 2-fold larger surface areas on unmodified PET controls than on nanogel-coated surfaces, * $p < 9.5 \times 10^{-7}$. Data is presented as the average value ± standard error of the mean. Scale bar is 100 μm.

To evaluate leukocyte behavior *in vivo* during acute inflammation, samples were implanted in the intraperitoneal (IP) cavity of mice for 48 h based on a murine intraperitoneal implantation model that is extensively used in the literature to characterize.[30] Explanted disks were stained for the macrophage marker CD68 (anti-CD68), actin (phalloidin), and DNA (Hoechst), and analyzed for cell adhesion and spreading. In addition, cells were harvested from explants, stained intracellularly with antibodies against inflammatory cytokines, and analyzed by flow cytometry to quantify the levels of intracellular cytokines. Nanogel-coated PET exhibited 4-fold lower levels of leukocyte adhesion (* $p < 1.1 \times 10^{-5}$) and also reduced cell spreading compared to unmodified PET implants after 48 h in the IP cavity of mice (Figure 7.5). In addition, fewer macrophages were observed on nanogel-coated samples. Cells harvested from IP explants were stained with antibodies against inflammatory cytokines and analyzed by flow cytometry. When compared with non-functionalized PET, cells associated with nanogel-coated disks displayed significantly lower levels of pro-inflammatory intracellular cytokines (Figure 7.6) like TNF-a, MCP-1 (Figure 7.6a, $p < 1.5 \times 10^{-5}$) and IL-1β. It is important to note that these levels of cytokine expression were similar to the sham controls. Thus, these results demonstrate that the nanogel coatings significantly reduced the pro-inflammatory leukocyte expression and activation compared to PET substrates *in vivo*.
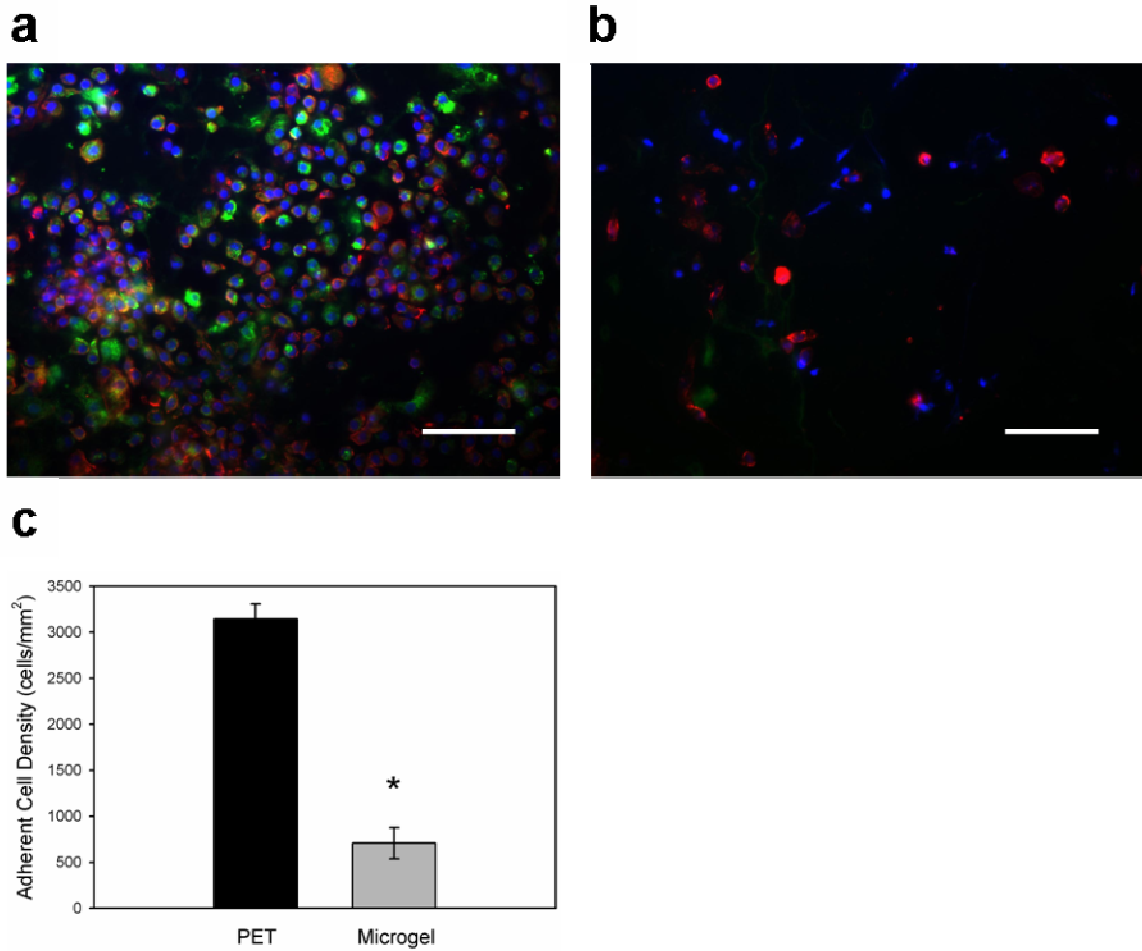
Figure 7.5. Leukocyte adhesion to biomaterials in the intraperitoneal cavity of mice. Explants were stained immunofluorescently for macrophage marker CD68 (green), actin (red), and DNA (blue). In contrast to unmodified PET controls (a), nanogel-coated disks (b) effectively reduced leukocyte adhesion on these implants by a factor of 4.4 as quantified in (c), * $p < 1.1 \times 10^{-5}$. In addition, fewer macrophages were observed on nanogel-coated surfaces than on controls. Data is represented as the average value ± standard error of the mean. Scale bar is 50 µm.
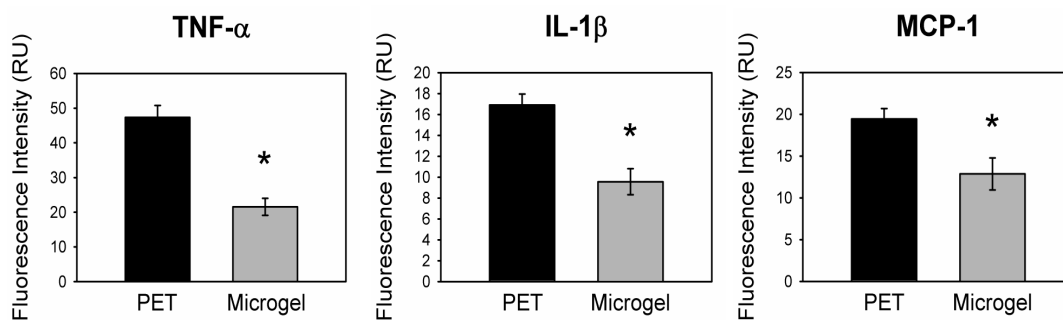
Figure 7.6. Quantification of *in vivo* intracellular cytokine expression by flow cytometric analysis. Data is presented as the unbiased geometric means of the populations ± standard error of the mean using n = 4 or more samples per treatment group.

Since PEG-575 cross-linked pNIPAm-based nanogels were the most protein adsorption resistant, it was used as the primary polymer composition for designing more functional nanogels onto which multiple "on-substrate" post-polymerization modifications could be carried out. Hydroxyl functional groups were incorporated on the pNIPAm nanogels to enable conjugation of peptide or other inflammatory ligands using simple and versatile click chemistry. This was achieved by copolymerizing the hydroxyl group-containing monomer HEMA with NIPAm and PEG 575 diacrylate yielding pNIPAm-HEMA core nanogels. Since, core/shell architecture provides more functional groups on the surface for bioconjugation, pNIPAm-HEMA shells on pNIPAm core nanogels were synthesized. Both HEMA-containing cores and shells were deposited onto the PETs and tested for possible non-fouling behavior. As seen from Figure 7.7, the nanogels are uniformly deposited similar to the pNIPAm-AAc nanogels, suggesting that incorporation of HEMA does not change the nanogel interaction with the PET substrate. The PET films coated with pNIPAm-HEMA core nanogels and pNIPAm-HEMA shell

nanogels were subjected to *in vitro* macrophage adhesion studies similar to those with other nanogels discussed before. Figure 7.8 shows the representative images of the cell adhesion studies. All of the nanogel-coated PET films have less cell adhesion than the uncoated PET and TCPS (positive controls). The HEMA-containing pNIPAm nanogels appear to be equally non-fouling as the pNIPAm-AAc nanogels. Thus, these nanogels could be further developed with additional complexity in terms of their chemical composition and surface functionalities. Towards that goal, another flavor of nanogels with both HEMA (hydroxyl functional group) and AAc (carboxyl functional group) as comonomers were synthesized and studied for their non-fouling behavior.
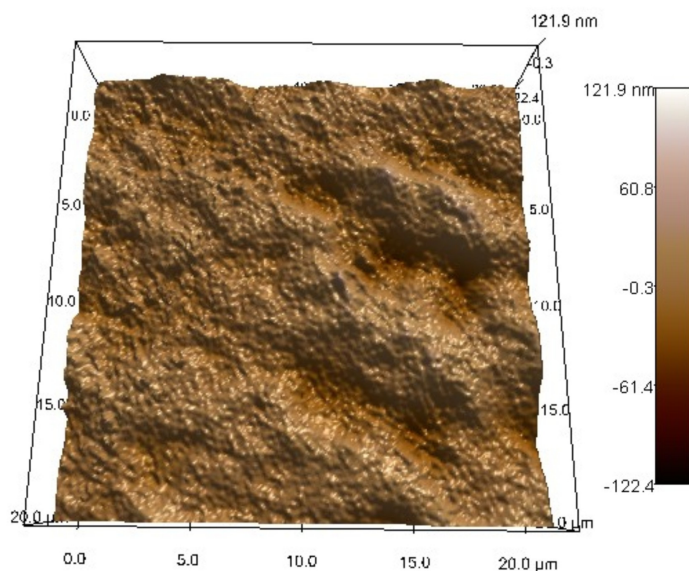
Figure 7.7. AFM image of PET film functionalized with pNIPAm-HEMA core nanogels.

Figure 7.9 shows the results of the cell adhesion studies for PET films coated with the PEG-575 cross-linked pNIPAm-HEMA-AAc nanogels. As expected, the nanogels are

non-fouling and can be used as the base nanogel for developing coatings, which can direct inflammation. The advantage of these nanogels is that since they have two functional groups, multiple ligands can be conjugated onto a single nanoparticles surface. Simple carbodiimide chemistry in solution or on substrate can be done using the carboxyl group. The hydroxyl group can be later used to conjugate another biomolecule *via* click chemistry. This strategy could thus provide base nanogels, which can be conjugated with multiple ligands (using orthogonal chemistries) for making bioactive substrates that present inflammatory and therapeutic ligands for directing inflammation.
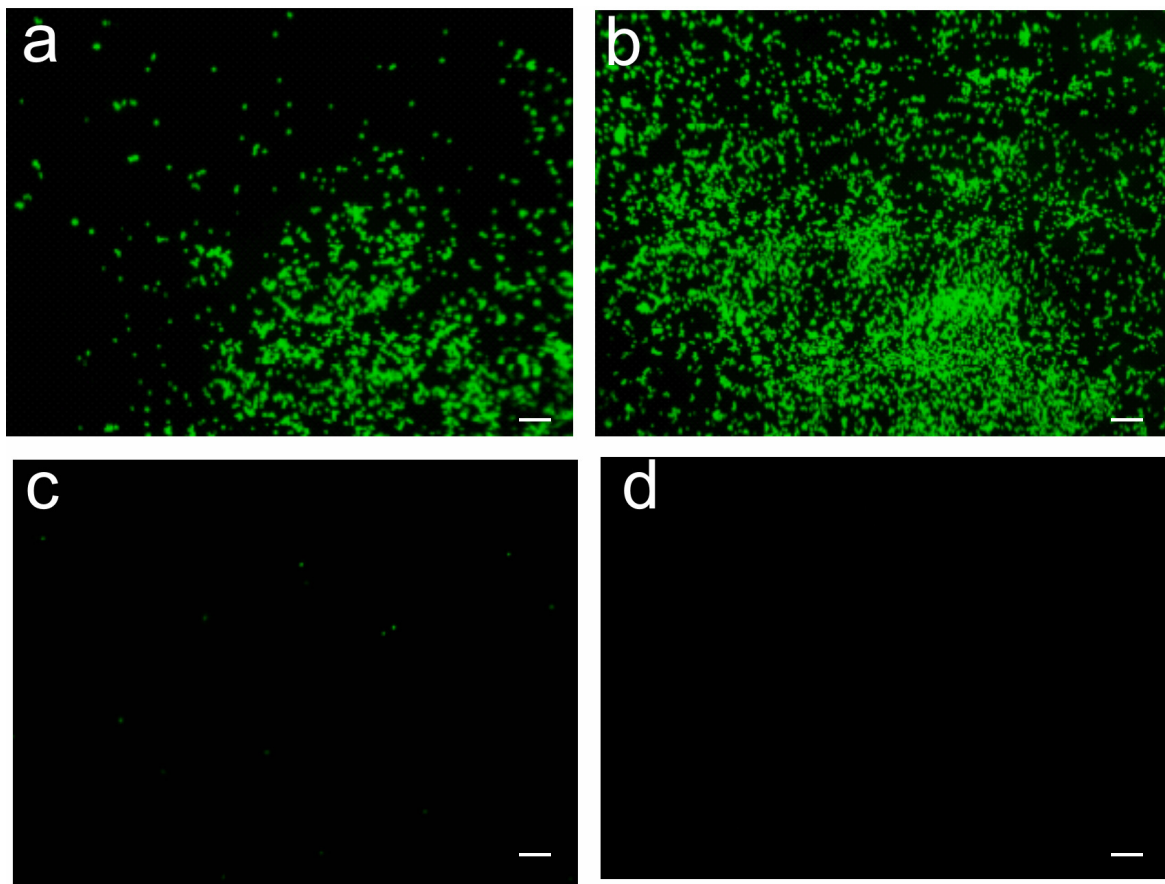
Figure 7.8. Macrophage adhesion on (a) bare PET, (b) TCPS, PET covalently functionalized by (c) pNIPAm-HEMA core nanogels and (d) pNIPAm-HEMA shell nanogels. Adherent cells were stained with calcein-AM, which stains live cells (green). Scale bar = 100 μm.
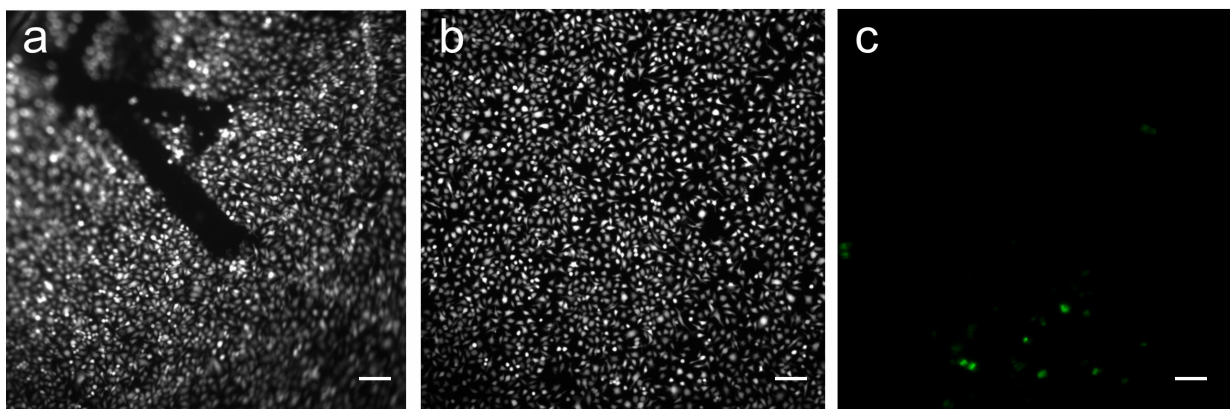
Figure 7.9. Macrophage adhesion on (a) bare PET, (b) TCPS, PET covalently functionalized by (c) pNIPAm-HEMA-AAc nanogels. Adherent cells were stained with calcein-AM, which stains live cells (green). Scale bar = 100 μm.

7.4 Conclusions

These results demonstrate that PEG-cross-linked pNIPAm-based nanogel coatings render biomaterials resistant to protein adsorption and subsequent leukocyte adhesion and spreading. Importantly, these coatings also showed reduced leukocyte activity *in vivo*. Further, pNIPAm-HEMA nanogels and pNIPAm-HEMA-AAc nanogels both were found to be effective in reducing the macrophage adhesion and spreading *in vitro*. This provides opportunity to make non-fouling coatings using nanogels with different composition to customize the coating for diverse applications. The successful development of non-fouling nanogels of different compositions each having unique functionality also allows us to develop coatings with spatial diversity on a single biomaterial substrate. This unique and versatile nanogel technology has great potential to modulate inflammatory responses associated with biomedical and biotechnological applications. We are also developing nanogel-based coatings functionalized with bioadhesive ligands such as the peptide

sequence RGD, which will provide the ability to modulate specific cell-material interactions.

7.5 References and Notes

[1]   Gorbet, M. B.; Sefton, M. V. Biomaterial-associated thrombosis: roles of coagulation factors, complement, platelets and leukocytes. *Biomaterials* **2004**, *25*, 5681-5703.

[2]   Kottke-Marchant, K.; Anderson, J. M.; Umemura, Y.; Marchant, R. E. Effect of albumin coating on the in vitro blood compatibility of Dacron arterial prostheses. *Biomaterials* **1989**, *10*, 147-155.

[3]   Sutherland, K.; Mahoney, J. R., 2nd; Coury, A. J.; Eaton, J. W. Degradation of biomaterials by phagocyte-derived oxidants. *J. Clin. Invest.* **1993**, *92*, 2360-2367.

[4]   Zhao, Q.; Topham, N.; Anderson, J. M.; Hiltner, A.; Lodoen, G.; Payet, C. R. Foreign-body giant cells and polyurethane biostability: in vivo correlation of cell adhesion and surface cracking. *J. Biomed. Mater. Res.* **1991**, *25*, 177-183.

[5]   Wisniewski, N.; Moussy, F.; Reichert, W. M. Characterization of implantable biosensor membrane biofouling. *Fresen. J. Anal. Chem.* **2000**, *366*, 611-621.

[6]   Destouet, J. M.; Monsees, B. S.; Oser, R. F.; Nemecek, J. R.; Young, V. L.; Pilgram, T. K. Screening mammography in 350 women with breast implants: prevalence and findings of implant complications. *Am. J. Roentgenol.* **1992**, *159*, 973-978; discussion 979-981.

[7]   Ambrose, C. G.; Clanton, T. O. Bioabsorbable implants: review of clinical experience in orthopedic surgery. *Ann. Biomed. Eng.* **2004**, *32*, 171-177.

[8]   Voronov, I.; Santerre, J. P.; Hinek, A.; Callahan, J. W.; Sandhu, J.; Boynton, E. L. Macrophage phagocytosis of polyethylene particulate in vitro. *J. Biomed. Mater. Res.* **1998**, *39*, 40-51.

[9]   Sun, D. H.; Trindade, M. C.; Nakashima, Y.; Maloney, W. J.; Goodman, S. B.; Schurman, D. J.; Smith, R. L. Human serum opsonization of orthopedic biomaterial particles: protein-binding and monocyte/macrophage activation in vitro. *J. Biomed. Mater. Res. A* **2003**, *65*, 290-298.

[10]   Anderson, J. M. Biological responses to materials. *Annu. Rev. Mater. Res.* **2001**, *31*, 81-110.

[11]   Thomsen, P., Gretzer, C. Macrophage interactions with modified material surfaces. *Current Opinion in Solid State and Materials Science* **2001**, *5*, 163-176.

[12]   Shen, M.; Garcia, I.; Maier, R. V.; Horbett, T. A. Effects of adsorbed proteins and surface chemistry on foreign body giant cell formation, tumor necrosis factor alpha release and procoagulant activity of monocytes. *J. Biomed. Mater. Res. A* **2004**, *70*, 533-541.

[13]   Tang, L.; Wu, Y.; Timmons, R. B. Fibrinogen adsorption and host tissue responses to plasma functionalized surfaces. *J. Biomed. Mater. Res.* **1998**, *42*, 156-163.

[14]   Collier, T. O.; Anderson, J. M. Protein and surface effects on monocyte and macrophage adhesion, maturation, and survival. *J. Biomed. Mater. Res.* **2002**, *60*, 487-496.

[15]   Hynes, R. O. Integrins: bidirectional, allosteric signaling machines. *Cell* **2002**, *110*, 673-687.

[16]   McNally, A. K.; Anderson, J. M. Beta1 and beta2 integrins mediate adhesion during macrophage fusion and multinucleated foreign body giant cell formation. *Am. J. Pathol.* **2002**, *160*, 621-630.

[17]   Brodbeck, W. G.; Patel, J.; Voskerician, G.; Christenson, E.; Shive, M. S.; Nakayama, Y.; Matsuda, T.; Ziats, N. P.; Anderson, J. M. Biomaterial adherent macrophage apoptosis is increased by hydrophilic and anionic substrates in vivo. *Proc. Nat. Acad. Sci. U.S.A.* **2002**, *99*, 10287-10292.

[18]   Xu, H. Y.; Kaar, J. L.; Russell, A. J.; Wagner, W. R. Characterizing the modification of surface proteins with poly(ethylene glycol) to interrupt platelet adhesion. *Biomaterials* **2006**, *27*, 3125-3135.

[19]   DeFife, K. M.; Shive, M. S.; Hagen, K. M.; Clapper, D. L.; Anderson, J. M. Effects of photochemically immobilized polymer coatings on protein adsorption, cell adhesion, and the foreign body reaction to silicone rubber. *J. Biomed. Mater. Res.* **1999**, *44*, 298-307.

[20]   Moro, T.; Takatori, Y.; Ishihara, K.; Konno, T.; Takigawa, Y.; Matsushita, T.; Chung, U. I.; Nakamura, K.; Kawaguchi, H. Surface grafting of artificial joints

with a biocompatible polymer for preventing periprosthetic osteolysis. *Nat. Mater.* **2004**, *3*, 829-836.

[21]   Cao, L.; Chang, M.; Lee, C. Y.; Castner, D. G.; Sukavaneshvar, S.; Ratner, B. D.; Horbett, T. A. Plasma-deposited tetraglyme surfaces greatly reduce total blood protein adsorption, contact activation, platelet adhesion, platelet procoagulant activity, and in vitro thrombus deposition. *J. Biomed. Mater. Res. A* **2007**, *81*, 827-837.

[22]   Norton, L. W.; Koschwanez, H. E.; Wisniewski, N. A.; Klitzman, B.; Reichert, W. M. Vascular endothelial growth factor and dexamethasone release from nonfouling sensor coatings affect the foreign body response. *J. Biomed. Mater. Res. A* **2007**, *81*, 858-869.

[23]   Hoffmann, J.; Groll, J.; Heuts, J.; Rong, H. T.; Klee, D.; Ziemer, G.; Moeller, M.; Wendel, H. P. Blood cell and plasma protein repellent properties of Star-PEG-modified surfaces. *J. Biomater. Sci., Polym. Ed.* **2006**, *17*, 985-996.

[24]   Shen, M. C.; Martinson, L.; Wagner, M. S.; Castner, D. G.; Ratner, B. D.; Horbett, T. A. PEO-like plasma polymerized tetraglyme surface interactions with leukocytes and proteins: in vitro and in vivo studies. *J. Biomater. Sci., Polym. Ed.* **2002**, *13*, 367-390.

[25]   Shimizu, T.; Yamato, M.; Isoi, Y.; Akutsu, T.; Setomaru, T.; Abe, K.; Kikuchi, A.; Umezu, M.; Okano, T. Fabrication of pulsatile cardiac tissue grafts using a novel 3-dimensional cell sheet manipulation technique and temperature-responsive cell culture surfaces. *Circ. Res.* **2002**, *90*, E40-E48.

[26]   Owens, D. E.; Peppas, N. A. Opsonization, biodistribution, and pharmacokinetics of polymeric nanoparticles. *Int. J. Pharm.* **2006**, *307*, 93-102.

[27]   Malmsten, M.; Emoto, K.; Van Alstine, J. M. Effect of chain density on inhibition of protein adsorption by poly(ethylene glycol) based coatings. *J. Colloid Interface Sci.* **1998**, *202*, 507-517.

[28]   Gan, D. J.; Lyon, L. A. Synthesis and protein adsorption resistance of PEG-modified poly(N-isopropylacrylamide) core/shell microgels. *Macromolecules* **2002**, *35*, 9634-9639.

[29]   Nolan, C. M.; Reyes, C. D.; Debord, J. D.; Garcia, A. J.; Lyon, L. A. Phase transition behavior, protein adsorption, and cell adhesion resistance of poly(ethylene glycol) cross-linked microgel particles. *Biomacromolecules* **2005**, *6*, 2032-2039.

[30]   Hu, W. J.; Eaton, J. W.; Ugarova, T. P.; Tang, L. Molecular basis of biomaterial-mediated foreign body reactions. *Blood* **2001**, *98*, 1231-1238.

[31]   Wu, Y.; Simonovsky, F. I.; Ratner, B. D.; Horbett, T. A. The role of adsorbed fibrinogen in platelet adhesion to polyurethane surfaces: a comparison of surface hydrophobicity, protein adsorption, monoclonal antibody binding, and platelet adhesion. *J. Biomed. Mater. Res. A* **2005**, *74*, 722-738.

[32]   Flick, M. J.; Du, X.; Witte, D. P.; Jirouskova, M.; Soloviev, D. A.; Busuttil, S. J.; Plow, E. F.; Degen, J. L. Leukocyte engagement of fibrinogen via the integrin receptor alphaMbeta2/Mac-1 is critical for host inflammatory response in vivo. *J. Clin. Invest.* **2004**, *113*, 1596-1606.

[33]   Feldman, K., Hahner, G., Spencer, N.D., Harder, P., Grunze, M. Probing resistance to protein adsorption of oligo(ethylene glycol)-terminated self-assembled monolayers by scanning force microscopy. *J. Am. Chem. Soc.* **1999**, *121*, 10134-10141.

[34]   Mrksich, M.; Chen, C. S.; Xia, Y.; Dike, L. E.; Ingber, D. E.; Whitesides, G. M. Controlling cell attachment on contoured surfaces with self-assembled monolayers of alkanethiolates on gold. *Proc. Natl. Acad. Sci. U. S. A.* **1996**, *93*, 10775-10778.

[35]   McNally, A. K.; Anderson, J. M. Complement C3 participation in monocyte adhesion to different surfaces. *Proc. Natl. Acad. Sci. U. S. A.* **1994**, *91*, 10119-10123.

CHAPTER 8

SPATIALLY CONTROLLED IMMOBILIZATION OF

MACROMOLECULES IN HYDROGEL NANOCAPSULES

A simple synthetic method towards pNIPAm-based nanocapsules for biomolecular encapsulation is described in this Chapter. Nanogels with periodate cleavable cross-links (through scission at a vicinal diol) were synthesized followed by addition of a thin shell of pNIPAm-AAc to yield a core/shell nanoparticle. The core was then degraded by sodium periodate, leaving behind aldehydes on the inner surface of the hollow nanocapsule. Aldehydes represent a convenient handle for chemoligation, and were used to covalently immobilize biomolecules at the inner surface of the nanocapsule using reductive amination. Various proteins of different molecular weights as well as small ligands were encapsulated, showing the generality of the nano-encapsulation scheme. Biotin immobilized in the nanocapsule was used to encapsulate a horseradish peroxidase-avidin conjugate via strong biotin-avidin association. The enzyme encapsulated in this way displayed activity comparable to free enzyme in solution. Protease degradation studies on the encapsulated enzyme showed that even after 8 days of proteolytic digestion, a significant amount of enzymatic activity was retained in the

nanocapsule construct relative to free enzyme. The nanocapsule is therefore suggested to offer a protective environment with respect to proteolytic enzymes.

8.1 Introduction

There is an increasing interest in the design of hydrogel nanoparticles (nanogels) that have biofunctionality for applications in cell targeting, drug delivery and biomedicine.[1] In such applications, it is desirable to chemically modify nanogels to further tailor their functionality. Thus, there is an ever-increasing need to identify chemoligation strategies for the facile incorporation of bioactive moieties, including proteins, ligands, and nucleic acids, in a general manner and without causing drastic changes to the intrinsic physicochemical properties of the nanogels (e.g. hydrophilicity and stimuli responsiveness).

Here we describe a simple and general method for covalently immobilizing biomolecules on the inner surface of hydrogel nanocapsules. To achieve this, poly(*N*-isopropylacrylamide) (pNIPAm)-based nanogels possessing a degradable core and a non-degradable shell were first synthesized. Similar particles have been described previously by our group, wherein a cross-linker possessing a vicinal diol is used to create a periodate degradable nanogel core.[2] Following degradation of this core, the resultant low molecular weight polymer chains are removed from the core/shell construct by centrifugation, resulting in essentially a hollow shell, or hydrogel nanocapsule. Previous studies of core/shell particles have illustrated that strong covalent and/or mechanical interactions exist between the shell and core polymer chains at the interface.[3-6] Based on these studies, we hypothesized that after core degradation, remnant polymer chains from the core

182

would remain at the inner surface of the non-degradable shell. Furthermore, since the degradation product associated with diol cleavage is an aldehyde, this remnant polymer should provide convenient chemical handles. Such chemoligation sites could be used to decorate the inner surface of the nanocapsule with a variety of biomolecules, via coupling reactions with functional groups such as hydrazides, amino-oxy groups, and amines using simple chemistry such as reductive amination.[7-10] We illustrate this concept in Schemes 8.1 and 8.2.
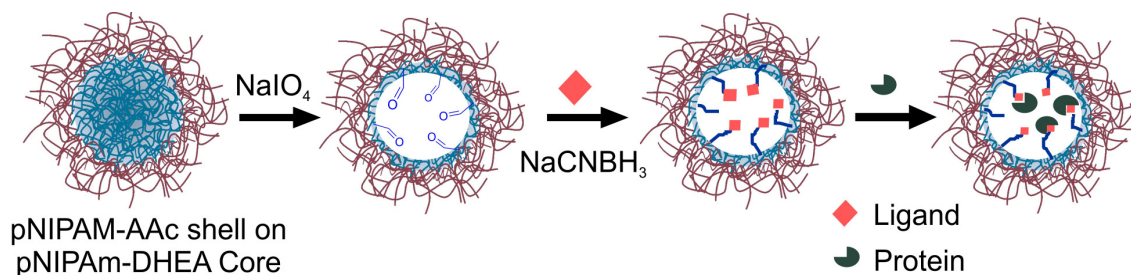
Scheme 8.1. Immobilization of macromolecules in pNIPAm nanocapsules.
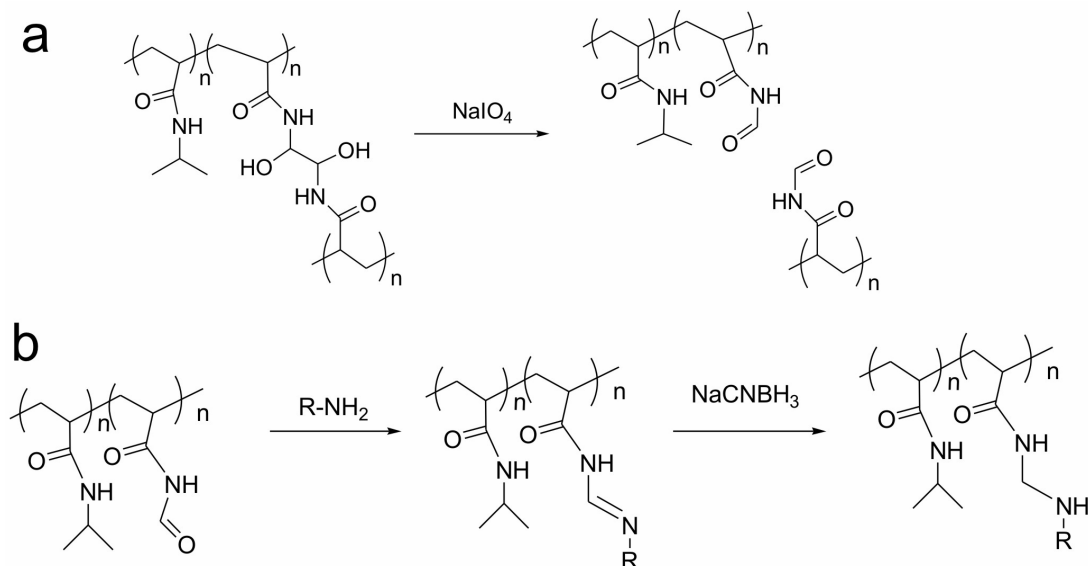
Scheme 8.2. (a) Cleavage of the diol crosslinker with sodium periodate. (b) Reductive amination of the remanant aldehydes on the inner surface of the polymer nanocapsule.

8.2 Experimental Section

8.2.1 Materials

All chemicals were purchased from Sigma-Aldrich unless otherwise noted. All chemicals were used as received except *N*-isopropylacrylamide (NIPAm), which was recrystallized from hexane (J. T. Baker) before use. Biotin hydrazide, avidin, and 2-(4'-hydroxyazobenzene) benzoic acid (HABA) were purchased from Pierce. Horseradish peroxidase-Avidin conjugate (HRP-Avidin) was purchased from Invitrogen. Fluorescein-labeled bovine serum albumin (FITC-BSA, ~7 mol dye per mol protein), human IgG (FITC-IgG) and Protien G (FITC-Protein G, 33 µg dye per mg solid) were purchased from Sigma-Aldrich. Pyrogallol was purchased from TCI America. Horseradish

peroxidase (HRP) was purchased from Biochemika. Phosphate buffers (PBS) were prepared from 0.01 M NaH_2PO_4 solution, and HCl or NaOH solution was added to obtain the desired pH. Water used in all experiments was distilled and then purified using a Barnstead E-Pure system operating at a resistance of 18 MΩ. A 0.2 µm filter was incorporated into this system to remove particulate matter.

8.2.2 Nanogel Synthesis

Synthesis of pNIPAm-DHEA Core Nanogels 1

Hydrogel nanoparticles were synthesized by aqueous free radical precipitation polymerization. For the synthesis of 100 mM (total monomer concentration) pNIPAM-DHEA core nanogels **1**, 1.0180 g (90 mol%) of NIPAm, 0.2024 g (10 mol%) of cross-linker *N,N'*-(1,2-dihydroxyethylene) bisacrylamide (DHEA) and 0.248 g of surfactant sodium dodecyl sulfate (SDS) were dissolved in 100 mL deionized (DI) water and filtered through 0.2 mm membrane filter. This reaction solution was then transferred to a three neck round bottom flask and heated to 70 °C while purging with N_2. After keeping the solution at 70 °C for 1 h, 0.0224 g of ammonium persulfate (APS) dissolved in 1 mL of water was added to initiate the reaction. The reaction was allowed to proceed for 4 h at 70 °C, then cooled down and stirred overnight at room temperature. The nanogel solution was filtered through Whatman filter paper (No.2) the following day. The filtered solution of **1** was further used for addition of a shell without further purification. The photon correlation spectroscopy (PCS) measured hydrodynamic radius (R_h) determined for **1** was 150 ± 5 nm at 25 °C.

Synthesis of pNIPAm-AAc Shell (1)/2.

The detailed procedure of the shell addition onto core nanoparticles is described elsewhere.[1] In brief, for the synthesis of a 40 mM pNIPAm-AAc shell **2** on the pNIPAm-DHEA core **1**, a three-necked round bottom flask was filled with 25 mL of **1**. To this flask an aqueous filtered solution of 0.1148 g (88 mol%) of NIPAm, 0.0311 g (2 mol%) of *N,N'*-methylenebis(acrylamide) (BIS) and 0.0060 g of SDS dissolved in 175 mL of DI water was added. The reaction solution was then heated to 70 °C under nitrogen. After 1 h of temperature stabilization, 68.6 µL (10 mol%) of AAc was added to the reaction flask, which was immediately followed by initiation of the reaction by injection of 0.0094 g APS dissolved in 1 mL DI water. The reaction was allowed to proceed for 4 h at 70 °C and then was cooled and stirred overnight followed by filtration through Whatman filter paper (No.2). The synthesized nanogels were then filtered and purified by five cycles of centrifugation at 15 422 × *g* for 45 minutes. The supernatant was removed and the particles were redispersed in DI water for further use. The PCS measured R_h value for **(1)/2** was 158 ± 1 nm at 25 °C.

8.2.3 Core Degradation

The amount of DHEA in the core to be degraded was calculated from the amount of DHEA added in the reaction solution. Approximately 0.8 mg of **(1)/2** nanogels (~0.05 mmol DHEA, 1 equiv) dispersed in DI water was degraded by adding 0.023 g (0.1 mmol, ~2 equiv) sodium periodate ($NaIO_4$). The solution was kept on the shaker table overnight and the polymer chains from the degradation of the core was removed from the nanogel solution by five centrifugation cycles at 15 422 × *g* for 45 minutes at 32 °C. The clean, hollow **(1)/2** nanocapsules, denoted as **(0)/2** were freeze dried overnight before further

use. Approximately 0.3 mg of polymer was obtained after the degradation, suggesting a loss of 63% of the polymer mass from the **(1)/2** nanogels.

8.2.4 Immobilization of Biomolecules in (0)/2 nanocapsules by Reductive Amination

For immobilization of small molecules into **(0)/2**, a fresh solution of sodium cyanoborohydride prepared by dissolving 0.1527 g of $NaCNBH_3$ in 0.5 mL, 1 N NaOH (to prevent decomposition) was used for each reaction.

Conjugation of FITC-BSA to (0)/2

Fluorescently labeled protein, FITC-BSA (350 µL of a solution prepared from 150 mg of protein dissolved in 1 mL pH 7.0 PBS buffer) was added to 0.4 mg of **(0)/2** and allowed to react for 2 h at 4 °C on a shaker table. Freshly prepared $NaCNBH_3$ solution (200 µL) was added to the reaction vial and further allowed to react overnight at 4 °C. The conjugated nanogels were purified via five centrifugation cycles at 15 422 × g for 30 minutes at 32 °C. The supernatant was replaced with DI water after each centrifugation cycle.

Conjugation of FITC-IgG to (0)/2

Fluorescently labeled antibody, FITC-IgG (350 µL of a solution prepared from 4 mg of antibody dissolved in 1 mL pH 7.0 PBS buffer) was added to 0.3 mg of **(0)/2** and allowed to react for 2 h at 4 °C on a shaker table. Freshly prepared $NaCNBH_3$ solution (200 µL) was added to the reaction vial and further allowed to react overnight at 4 °C. The conjugated nanogels were purified via five centrifugation cycles at 15 422 × g for 30 minutes at 32 °C. The supernatant was replaced with DI water after each centrifugation cycle.

Conjugation of FITC-Protein G to (0)/2

Fluorescently labeled antibody binding protein, FITC-Protein G (350 µL of a solution prepared from 0.25 mg of protein dissolved in 1 mL pH 7.0 PBS buffer) was added to 0.6 mg of **(0)/2** and allowed to react for 2 h at 4 °C on a shaker table. Freshly prepared $NaCNBH_3$ solution (200 µL) was added to the reaction vial and further allowed to react overnight at 4 °C. The conjugated nanogels were purified via five centrifugation cycles at 15 422 × *g* for 30 minutes at 32 °C. The supernatant was replaced with DI water after each centrifugation cycle.

Conjugation of Biotin Hydrazide to (0)/2

Biotin hydrazide (5 mg) was added to 1 mg of **(0)/2** and allowed to react for 2 h at 4 °C on a shaker table. Freshly prepared $NaCNBH_3$ solution (200 µL) was added and further allowed to react overnight at 4 °C. The conjugated nanogels were purified via five centrifugation cycles at 15 422 × *g* for 45 minutes at 32 °C. The supernatant was replaced with DI water after each centrifugation cycle. The biotin conjugated **(0)/2** nanogels are denoted as **(0-bt)/2**.

Immobilization of HRP-Avidin in (0-bt)/2

To 125 µL of **(0-bt)/2** (1 mg dispersed in 1 mL pH 7.0 PBS buffer) HRP-Avidin (100 µL of 2.5 mg/mL) was added and incubated overnight at 4 °C to yield **(0-HRP)/2**. The nanogel solution was then diluted to 0.5 mL and centrifuged five times at 15 422 × *g* for 10 minutes at 32 °C. The pellet of **(0-HRP)/2** obtained was redispersed in DI water after each centrifugation cycle.

8.2.5 Detection of Biotin in (0-bt)/2 using the HABA Assay

To characterize the immobilization of biotin in **(0-bt)/2**, we used the colorimetric assay for biotin-avidin binding, which is based on the displacement of HABA from a HABA-Avidin complex (λ_{max} = 500 nm).[2,3] The HABA-Avidin solution was prepared by dissolving 5 mg of avidin in 8 mL of 0.1 M, pH 7.0 PBS followed by the addition of 364 µL of HABA solution (2 mg dissolved in 1 mL 0.1 M, pH 7.0 PBS). Finally, the total volume was made up to 10 mL by further addition of 0.1 M, pH 7.0 PBS. For the assay, 375 µL of the HABA-Avidin solution was added to 125 µL of a **(0-bt)/2** solution (1 mg/mL) and the change in the absorbance of the complex at 500 nm was monitored via UV-vis spectroscopy.

8.2.6 UV-vis Spectroscopy for Enzyme Load Detection

UV-vis absorbance spectra of all samples were obtained using a Shimadzu UV 1601 spectrophotometer. After cleaning via centrifugation, 0.25 mg particles/mL solution was prepared with a total volume of 0.5 mL. A comparable amount of free HRP-Avidin in 0.5 mL water was also prepared (40 µL of stock solution) for comparison.

8.2.7 Fluorescence Spectroscopy

Fluorescence spectra were recorded on a steady-state fluorescence spectrophotometer (Photon Technology International), equipped with a Model 814 PMT photon-counting detector. The slits were set to achieve a spectral bandwidth of 2 nm, and the spectra were recorded with a step size of 1 nm and an integration time of 1 second.

8.2.8 Pyragallol Assay for Detection of Enzyme (HRP-Avidin) Activity

An assay procedure, provided by Sigma-Aldrich, was used and scaled down for activity measurements.[14] Fresh solutions of hydrogen peroxide (H_2O_2) and pyrogallol were prepared each time for the assay. A 0.05% (w/w) solution of H_2O_2 was prepared from a 30% (w/w) H_2O_2 solution. A 0.5% (w/v) pyrogallol solution was prepared by dissolving 0.10 g of pyrogallol in 20 mL of DI water. For the activity assay, 350 µL of DI water, 53 µL of 100 mM PBS buffer pH 6.0, 27 µL of 0.05% (w/w) H_2O_2 solution, and 53 µL of 0.5% (w/v) of pyrogallol solution were dispensed into a quartz cuvette. To the solution in the cuvette, 17 µL of each sample (diluted 10-fold from loading experiment to 0.025 mg particles/mL solution) was added, briefly mixed and the change in absorbance at 420 nm was monitored for 5 minutes at room temperature. Activity was monitored in triplicate for each sample over a time-span of one week. Samples were kept on a shaker table at approximately 4 °C between activity measurements. Prior to measurements the samples were allowed to equilibrate to room temperature for 15 min.

The activity of each sample was also monitored in the presence of trypsin and proteinase K. Approximately 13 units (0.96 µg) and 1.3 units (39.4 µg) of trypsin and proteinase K, respectively, were added to 1 mL of 0.025 mg particles/mL solution. Activity was monitored in same fashion as above.

8.3 Results and Discussion

Poly(NIPAm)-based core nanogels **1** (hydrodynamic radius (R_h) of 150 ± 5 nm at 25 °C) having *N,N'*-(1,2-dihydroxyethylene) bisacrylamide (DHEA) as a cross-linker were synthesized using precipitation polymerization as previously described by our

group.[2]   Onto **1**, a thin (40 mM total monomer concentration) pNIPAm-AAc shell **2** containing the nondegradable cross-linker *N,N'*-methylenebis(acrylamide) (BIS) was added to yield core/shell nanogel **(1)/2** with R_h of 158 ± 1 nm at 25 °C. Core/shell nanogel synthesis was accomplished using a 'seed and feed' precipitation polymerization method used extensively in our group.[11] The core nanoparticles containing the DHEA cross-links underwent diol cleavage by stoichiometric amounts of sodium periodate (Scheme 2a), thus degrading the core and leaving behind residual aldhehydes at the inner surface of the nanocapsule. The hollow nanocapsule is designated as **(0)/2**. The remnant aldehydes were used for chemical conjugation and therefore spatially controlled covalent immobilization of biomolecules containing amines and hydrazide functional groups as shown in Scheme 8.2b.

Small molecules including 5-aminofluorescein and biotin hydrazide as well as proteins such as bovine serum albumin (BSA), IgG and protein-G (Figures 8.1a and 8.1b) were conjugated to the nanocapsule. The biotin conjugation was characterized using the common colorimetric assay for biotin-avidin binding, which is based on the displacement of 2-(4'-hydroxyazobenzene) benzoic acid (HABA) from a HABA-Avidin complex (λ_{max}=500 nm).[12] As seen in Figure 1b, the addition of biotin-conjugated nanocapsules (**(0-bt)/2**) results in a loss of the HABA-Avidin complex absorption due to the competitive binding of the avidin to biotin present in the nanocapsules. The successful encapsulation of proteins of different sizes (BSA, ~66 kDa; IgG ~150 kDa; Protein G, ~30 kDa) indicates the high porosity of the loosely cross-linked (2 mol%) shell polymer network as illustrated previously.[13] This porosity can be tuned by changing the chemical composition, thickness and the cross-linker density of the shell polymer network.
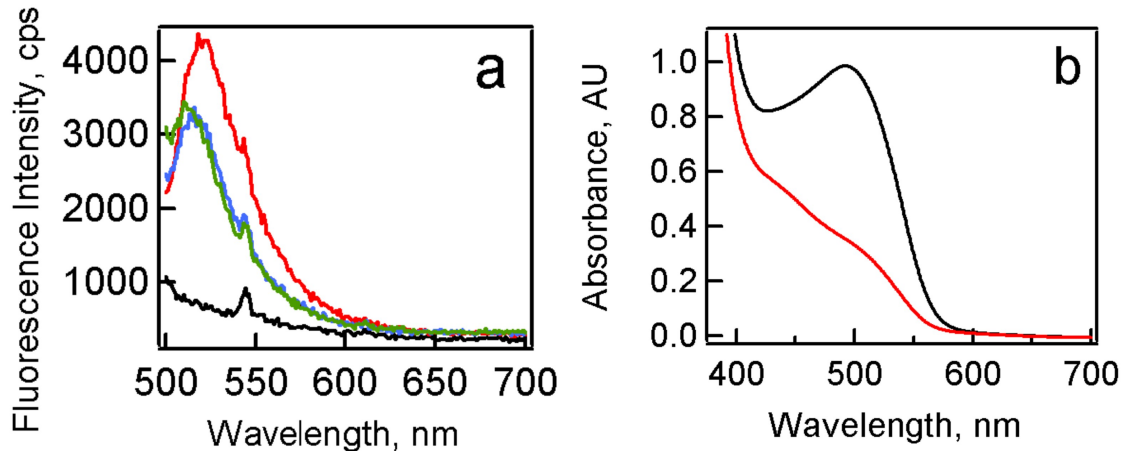
Figure 8.1. Encapsulation of biomolecules in **(0)/2**). (a) Fluoresence spectra of FITC labeled BSA (red), IgG (blue) and Protein G (green) covalently encapsulated in the nanocapsules. No immobilization for FITC-BSA was observed without core degradation (black). (b) Absorption spectra for HABA-Avidin complex before (black) and after the addition of **(0)/2** with encapsulated biotin (denoted as **(0-bt)/2**).

The covalent immobilization of biotin inside the nanocapsules is of special value in the development of a universal immobilization technique, since it provides a functionality to encapsulate enzymes and other active biomolecules non-covalently. We investigated the encapsulation of horseradish peroxidase (HRP) using this construct by incubating **(0-bt)/2** with HRP-Avidin. The HRP becomes encapsulated in the nanocapsule due to the strong, non-covalent biotin-avidin interaction to yield **(0-HRP)/2**. In Figure 8.2a this nanocapsule shows a strong absorption band at 403 nm, which is typical of HRP (black line in Figure 8.2a). The slight difference in the absorption spectra between the encapsulated and free HRP can be attributed to light scattering from the nanocapsules.

Following encapsulation, we investigated the activity of the enzyme. The enzymatic activity of the encapsulated HRP was measured using a spectrohotometric pyragallol assay, which measures the oxidation of pyrogallol to purpurogallin (absorbance at 420 nm) by H_2O_2 catalyzed by HRP.[14] The catalytic oxidation of pyragallol can be determined from the initial slope of the time-dependent absorbance of the oxidized product.

As seen in Figure 8.2b, the encapsulated enzyme has an activity similar to the free enzyme when compared at the same concentrations in aqueous buffer. This is a significant advance over other methods of enzyme immobilization, which typically result in a partial loss of activity as compared to the free enzyme.[15,16] The similarity in the catalytic activity shown here suggests that the enzyme, even after encapsulation, has similar spatial accessibility to that of the free enzyme in aqueous buffer, thus suggesting its location in the hollow interior space of the capsule rather than being entrapped within the polymer network.
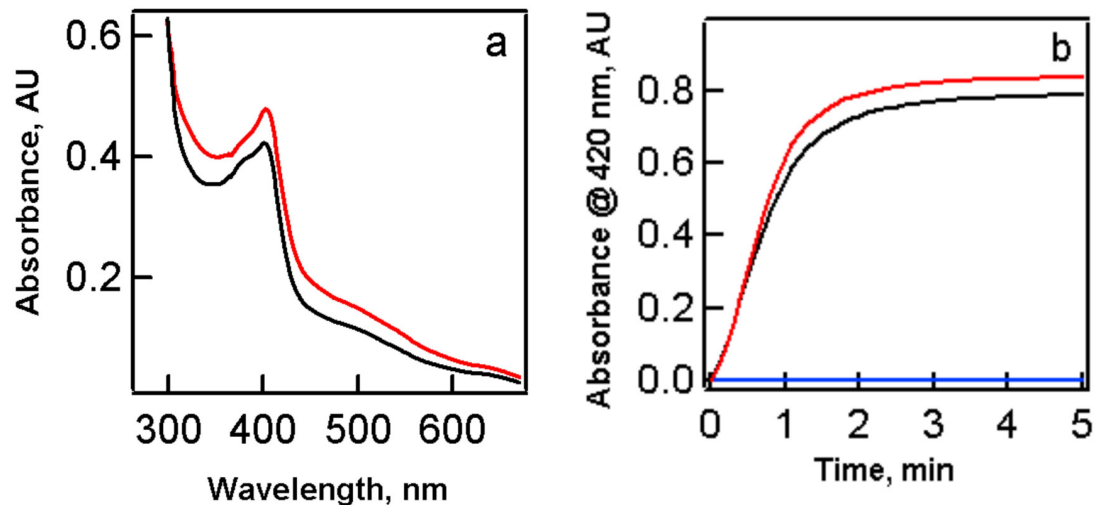
Figure 8.2. Characterization of HRP encapsulation. (a) Absorption spectra of free HRP-Avidin (black) and **(0-HRP)/2** (red). (b) Time-dependent absorbance of the oxidized product in the HRP catalyzed oxidation of pyragallol in the presence of free HRP-Avidin (black), **(0-HRP)/2** (red), and in enzyme free buffer (blue).

In order to further verify that the HRP is contained in the hollow volume of the nanocapsule, we studied the protection of the enzyme from proteolytic digestion. Free HRP-Avidin and **(0-HRP)/2** were incubated with a mixture of the proteases trypsin and proteinase K, which are known to catalyze the hydrolysis of peptide bonds in HRP.[17] The results of these studies are shown in Figure 8.3, where it can be seen that after 8 days of incubation with the protease mixture, there is a substantial decrease in activity (~68 %) for the solution containing free enzyme as compared to the smaller activity loss (~37 %) associated with enzymes immobilized inside the nanocapsules. The better protection of the immobilized HRP clearly suggests that the enzyme is confined within the cavity in the nanocapsule or located in an environment inaccessible to proteolytic digestion, rather than on the outer surface of the nanocapsule. It is interesting that even though the

nanocapsule shell is very thin and permits the passage of various proteins into the capsule

interior, it still provides protection against the proteases in solution.
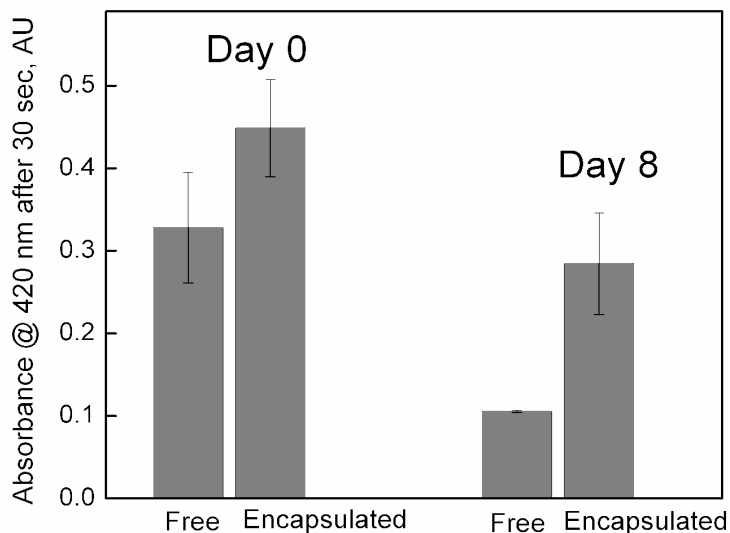
Figure 8.3. Effect of proteases on free and encapsulated HRP. The graph shows a comparison of the production of purpurogallin on day 0 and day 8 by free HRP and the encapsulated HRP in a solution containing trypsin and proteinase K.

8.4 Conclusions

In summary, we have demonstrated a rapid, simple, and potentially universal scheme for the robust encapsulation of small molecules and proteins in responsive pNIPAm nanogels without adversely affecting the activity of the encapsulated molecule. It is also likely that the AAc moieties on our nanogels can help tune the permeability of small molecules by allowing pH-dependent variation of the shell porosity. The AAc groups can also provide a chemical handle for carrying out chemoligation on the surface of the nanocapsules to make nanoparticles with site-specific functionalities on both inner

and outer surfaces. Such complex nanoparticles, due to their utility in highly controlled

biofunctionalization have great potential for the creation of nanomaterials for applications

in biological sensing, biomolecular seperations, biocatalysis, and controlled drug

delivery.

8.5 References and Notes

[1]   Nayak, S.; Lyon, L. A. Soft nanotechnology with soft nanoparticles. *Angew. Chem., Int. Ed.* 2005, *44*, 7686-7708.

[2]   Nayak, S.; Gan, D.; Serpe Michael, J.; Lyon, L. A. Hollow thermoresponsive microgels. *Small* 2005, *1*, 416-421.

[3]   Berndt, I.; Pedersen, J. S.; Richtering, W. Temperature-sensitive core-shell microgel particles with dense shell. *Angew. Chem., Int. Ed.* 2006, *45*, 1737-1741.

[4]   Gan, D.; Lyon, L. A. Interfacial nonradiative energy transfer in responsive core-shell hydrogel nanoparticles. *J. Am. Chem. Soc.* 2001, *123*, 8203-8209.

[5]   Gan, D.; Lyon, L. A. Tunable swelling kinetics in core--shell hydrogel nanoparticles. *J. Am. Chem. Soc.* 2001, *123*, 7511-7517.

[6]   Jones, C. D.; McGrath, J. G.; Lyon, L. A. Characterization of Cyanine Dye-Labeled Poly(N-isopropylacrylamide) Core/Shell Microgels Using Fluorescence Resonance Energy Transfer. *J. Phys. Chem. B* 2004, *108*, 12652-12657.

[7]   Heredia, K. L.; Tolstyka, Z. P.; Maynard, H. D. Aminooxy end-functionalized polymers synthesized by ATRP for chemoselective conjugation to proteins. *Macromolecules* 2007, *40*, 4772-4779.

[8]   Hermanson, G. T. *Bioconjugate Techniques*; Academic Press: San Diego, 1996.

[9]   Plunkett, K. N.; Chatterjee, A. N.; Aluru, N. R.; Moore, J. S. Surface-Modified Hydrogels for Chemoselective Bioconjugation. *Macromolecules* 2003, *36*, 8846-8852.

[10]   Turner, J. L.; Chen, Z. Y.; Wooley, K. L. Regiochemical functionalization of a nanoscale cage-like structure: Robust core-shell nanostructures crafted as vessels for selective uptake and release of small and large guests. *J. Controlled Release* 2005, *109*, 189-202.

[11]   Jones, C. D.; Lyon, L. A. Synthesis and Characterization of Multiresponsive Core-Shell Microgels. *Macromolecules* 2000, *33*, 8301-8306.

[12]   Green, N. M. A Spectrophotometric Assay for Avidin and Biotin Based on Binding of Dyes by Avidin. *Biochem. J.* 1965, *94*, 23c-24c.

[13]   Nayak, S.; Lyon, L. A. Ligand-functionalized core/shell microgels with permselective shells. *Angew. Chem., Int. Ed.* 2004, *43*, 6706-6709.

[14]   http://www.sigmaaldrich.com/img/assets/18160/Peroxidase.pdf. 12/03/07.

[15]   Miller, S. A.; Hong, E. D.; Wright, D. Rapid and efficient enzyme encapsulation in a dendrimer silica nanocomposite. *Macromol. Biosci.* 2006, *6*, 839-845.

[16]   Sun, Y.-M.; Chen, J.-P.; Chu, D.-H. Preparation and characterization of alpha - amylase-immobilized thermal-responsive composite hydrogel membranes. *J. Biomed. Mater. Res.* 1999, *45*, 125-132.

[17]   Grzywnowicz, K.; Greppin, H.; Brzyska, M.; Lobarzewski, J. Changes in activity of soluble and immobilized peroxidases after treatment by various proteases and some metal ions. *J. Mol. Catal.* 1993, *80*, 117-125.

CHAPTER 9

FUTURE OUTLOOK

▪ The nanogels synthesized in Chapter 3 can potentially be used for cancer targeting. The gold nanoparticles in the nanogels before core etching can act as cellular tracking labels as well as laser photothermal agents. The pNIPAm shell can be used to load drugs and the carboxyl groups on the shell can be conjugated to targeting ligands. After, core dissolution the hollow cavity can be used to encapsulate therapeutics or any biomolecule of interest to be delivered. Again, the shell provides chemical handles for chemoligation of targeting ligands and the fluorescence due to AFA gained after gold core etching now acts as the cellular tracking label. Thus, the construct designed is truly a multi-faceted nanoparticle that has potential as a delivery vehicle and therefore deserves further investigation by the means of *in-vitro* cellular studies.

▪ The gold core nanogels synthesized in Chapter 3 can be studied for developing nano-thermometers that can be used to determine the surface temperature around the gold nuclei on laser heating. This can be achieved by synthesizing a polymer shell of pNIPAm containing NIPMAm as comonomer as described in chapter 2. The variation of the amount of NIPMAm in the polymer compostion can result in variation of the LCST of the copolymer. PolyNIPAm-NIPMAm copolymer shell with different LCST temperatures can be synthesized. The gold core can be heated with a laser of particular power. This will photothermally heat-up the gold

nanoparticles and the polymer around it can respond to the local temperature increase arising from the dissipation of heat from the gold nanoparticle. Depending upon the LCST of the polymer it will undergo refractive index changes if that temperature is reached. The change in refractive index around gold nanoparticles can then be easily observed from the changes in the absorption spectrum of gold nanoparticles, which is very sensitive to the changes in the surrounding medium.

- The colloidal crystalline film made and discussed in Chapter 5 using benzophenone-based crosslinking can be studied for use in drug-releasing thin films. The technique can be employed to hollow nanogels synthesized in Chapter 8 by cleaving the DHEA cross-linker to make hollow and stable crosslinked thin films. The thin film made of hollow nanogels can be loaded with drug molecules and their release profiles could be studied.

- Another interesting study on the crystalline cross-linked films based on DHEA nanogels could be aimed towards understanding the changes in the optical properties of the crystalline film after core dissolution. Since, the nanogels become softer after core dissolution the interactions between neighboring nanoparticles in the film can change. In a very preliminary study (not reported in the dissertation), the film appeared to have gained more order after core dissolution. This could be because the softness of the nanoparticles makes them easy to rearrange to some extent. Also since the film is crosslinked the nanoparticles after core dissolution can swell to a certain degree to make all the

nanoparticle to be of similar size, thus reducing polydispersity of the nanogels, which can also enhance the optical properties of the film.

- The synthesis of nanogels based on the Fmoc protection and deprotection of amines technique, can be used to synthesize nanogels with three functional groups such as alcohol (by incorporating HEMA comonomer), protected amines (Fmoc-PEG comonomer) and carboxyl (AAc comonomer). This could give more chemical handles on the surface for ligation. The presence of alcohol groups can provide with handles to convert the nanogel into a clickable azide to perform click chemistry on the nanogels.

VITA

NEETU SINGH

Neetu Singh was born in Gorakhpur, India. She went to Kendriya Vidyalaya IIT-Powai, Mumbai for her high school education. She graduated from S.I.E.S. College (University of Mumbai) in Mumbai, India with a B.Sc. degree in Chemistry in the year 1999 and M.Sc. degree in Organic Chemistry in 2001. After her M. Sc. she joined the lab of Prof. S.V. Bhatt at the Indian Institute of Technology, Bombay, India to do research in antimalarial drug synthesis. She joined the School of Chemistry and Biochemistry at Georgia Institute of Technology in 2003 to pursue her Ph.D. in materials chemistry with Prof. L. Andrew Lyon. Neetu has been recipient of the second prize amongst oral presentations at the Georgia Tech Graduate Technical Symosium in 2007 and the second prize at the Graduate Student Awards Symposium of the School of Chemistry and Biochemistry held in 2007. Apart from research, she enjoys painting and ceramic arts.